Photofragmentations, State Interactions and Energetics of Rydberg and Ion-pair States: 2D REMPI of Halogen Containing Compounds

Jingming Long

Faculty of Physical Sciences
School of Engineering and Natural Sciences
University of Iceland
2013

Photofragmentations, State Interactions and Energetics of Rydberg and Ion-pair States: 2D REMPI of Halogen Containing Compounds

Jingming Long

Dissertation submitted in partial fulfillment of a
Philosophiae Doctor degree in Physical Chemistry

Advisor
Ágúst Kvaran

Co-advisor
Huasheng Wang

PhD Committee
Ari Ólafsson
Andras Bodi
Gísli Hólmar Jóhannesson

Opponents
Hans-Peter Loock
Ragnar Jóhannsson

Faculty of Physical Sciences
School of Engineering and Natural Sciences
University of Iceland
Reykjavík, June 2013

Photofragmentations, State Interactions and Energetic of Rydberg and Ion-pair States: 2D REMPI of Halogen Containing Compounds

Dissertation submitted in partial fulfillment of a *Philosophiae Doctor* degree in Physical Chemistry

Faculty of Physical Sciences
School of Engineering and Natural Sciences
University of Iceland
Dunhagi 3
107, Reykjavik
Iceland

Telephone: 525 4000

Bibliographic information:
Jingming Long,
Photofragmentations, State Interactions and Energetics of Rydberg and Ion-pair States: 2D REMPI of Halogen Containing Compounds, PhD dissertation, Faculty of Physical Sciences, University of Iceland, 2013.

ISBN 978-9935-9146-1-3

Printing: Háskólaprent ehf., Fálkagötu 2, 107 Reykjavík
Reykjavík, Iceland, June 2013

Abstract

The main work of my Ph.D project was to explore and study photofragmentation processes of halogen containing compounds. Molecular photofragmentation channels, involving photodissociations, photoionizations and predissociations play an important role in the photochemistry and photophysics of the atmosphere and in interstellar space. The major experimental method used here is the two-dimensional (2D) (2+n) resonance enhanced multiphoton ionization (REMPI) technique coupled with a time of flight (TOF) mass spectrometry. Experiments, based on this technique were performed to obtain mass spectra as a function of two-photon excitation energies to obtain 2D REMPI data for HCl, HBr, CF_3Br and CH_2Br_2. New states were assigned and photoionization and photodissociation processes of the molecules were studied.

The largest emphasis was laid on studies of the hydrogen halides, HX; X=Cl, Br. Relative ion signal intensities, line-shifts and line-width broadenings due to interactions between Rydberg and ion-pair states were studied quantitatively. Simulations of ion signal intensity ratios ($I(X^+)/I(HX^+)$) were performed to obtain interaction strengths and to estimate the importance of Rydberg state predissociatiion process. Relevant analysis techniques were modified and improved. A deperturbation method, based on analysis of spectral line positions for Rydberg and ion-pair state spectra, was applied to achieve unperturbed spectroscopic constants as well as interaction strengths. REMPI studies and perturbation analyses due to interactions between Rydberg and ion-pair states provide important information relevant to photofragmentation processes for the hydrogen halides.

Útdráttur

Aðal vinnan að baki þessarar doktorsritgerðar fólst í að skoða og greina ljósrofsferla (e. photfragmentation processes) halógen-haldandi efna. Ferli ljóssundrunar (e. photofragmentation channels), sem felast í tengjarofum og jónunum skipta miklu máli í ljósefnafræði og ljóseðlisfræði andrúmsloftsins og í geimsefnafræði (e. astrochemistry). Helsta tilraunaaðferðin sem notuð var nefnist ,“tvívíð (2D) fjölljóseindajónun“ (e. resonance enhanced multiphoton ionization / REMPI) ásamt flugtímamassagreiningum (e. time of flight mass spectrometry/ TOF-MS). Tilraunir fólust í mælingum á massarófum sem fall af tveggja ljóseinda örvunarorku til að fá 2D REMPI gögn fyrir HCl, HBr, CF_3Br og CH_2Br_2. Ný ástönd voru litrófsgreind og ljóssundrunarferlar sameindanna rannsakaðir.

Stærstur hluti verkefnisins var tileinkaður vetnishalíðunum, HX; X = Cl, Br. Styrkir jónaútslaga, hliðranir litrófslína, og breidd litrófslína vegna víxlverkana á milli Rydberg og jón-para-ástanda var kannað magnbundið. Hermanir á afstæðum jónstyrkjum ($I(X^+)/I(HX^+)$) voru framkvæmdar til að meta styrkleika víxlverkana og til að áætla vægi rofferla fyrir Rydberg ástönd. Greiningar- og mæli-aðferðir voru betrumbættar. Aftruflunarreikningar (e. deperturbation calculations), byggðir á greiningum á staðsetningum litrófslína fyrir Rydberg ástönd og jón-para-litróf, voru framkvæmdir til að finna litrófsstuðla orkuríkra ástanda sem og víxlverkunarstyrki. REMPI greiningar og truflanagreiningar vegna víxlverkana Rydberg og jónpara-ástanda leiddu í ljós mikilvægar upplýsingar varðandi ljóssundrunarferla vetnishalíða.

To my wife Fuhui Chen, and to my parents

Table of Contents

List of Figures

List of Tables

List of Publications

Original articles

- Jingming Long, Huasheng Wang, Ágúst Kvaran, ***Photofragmentations, state interactions, and energetics of Rydberg and ion-pair states: Resonance enhanced multiphoton ionization via E and V (B) states of HCl and HBr.*** J. Chem. Phys. , 2013. **138**: p. 044308.

- Jingming Long, Helgi Rafn Hróðmarsson, Huasheng Wang, Ágúst Kvaran, ***Photofragmentations, State Interactions and Energetics of Rydberg and Ion-pair states Two Dimensional Resonance Enhanced Multiphoton Ionization of HBr via Singlet-, Triplet-, $\Omega = 0$ and 2 states***. J. Chem. Phys., 2012. **136**: p. 214315.

- Jingming Long, Huasheng Wang, Ágúst Kvaran, ***Rydberg and Ion-pair states of HBr: New REMPI observations and analysis***. Journal of Molecular Spectroscopy, 2012. **282** p. 20–26.

- Ágúst Kvaran, Kári Sveinbjörnsson, Jingming Long, Huasheng Wang, ***Two-dimensional REMPI of CF_3Br: Rydberg states and photofragmentation channels.*** Chemical Physics Letters, 2011. **516**(1-3): p. 12-16.

- Kristján Matthíasson, Jingming Long, Huasheng Wang, Ágúst Kvaran, ***Two-dimensional resonance enhanced multiphoton ionization of H^iCl; i = 35, 37: State interactions, photofragmentations and energetics of high energy Rydberg states***. The Journal of Chemical Physics, 2011. **134**(16): p. 164302.

- Jingming Long, Huasheng Wang, Ágúst Kvaran, ***REMPI spectra of HCl: Analysis of $F^1\Delta_2$ Spectral Perturbation***. Acta Phy. Sin., 2013. **62** (16) p. 163302

Talks

- Spectral Perturbations in Photorupture Progress of Hydrogen Halides, and What is Expected to be Observed in Velocity Map Imaging. Max-Born Institute. 15, May. **2013**. Jingming Long. Berlin, Germany.
- Mysterious Perturbations in Molecular Spectra: Interpretations and Analysis of REMPI Spectra for Halogen Containing Compounds. Faculty of Physical Sciences, University of Iceland. 08. Mars, **2013**. Jingming Long. Reykjavík, Iceland.

Posters

- Two-Dimensional (2+n) REMPI Spectroscopy: State Interactions, Photofragmentations and Energetics of the Hydrogen Halides. Ráðstefna Efnís (Efnafræðifélags Íslands), Efnafræðirannsóknir Á Íslandi - Tengsl Grunnrannsókna Og Atvinnulífs, Á Hótel Sögur, , 19. Nov., **2011**. Jingming Long, Huasheng Wang and Ágúst Kvaran. Reykjavík, Iceland.
- Two-Dimensional (2+n) REMPI Spectroscopy of CH_3Br and CF_3Br: Rydberg States and Photofragmentation Channels. Ráðstefna Efnís (Efnafræðifélags Íslands), Efnafræðirannsóknir Á Íslandi - Tengsl Grunnrannsókna Og Atvinnulífs, Á Hótel Sögur, , 19. Nov., **2011**. Huasheng Wang, Jingming Long and Ágúst Kvaran. Reykjavík, Iceland.
- Two-Dimensional (2+n) REMPI Spectroscopy: Perturbations Due To E -V State Interactions in the Hydrogen Halides. The 22nd Colloquium on High Resolution Molecular Spectroscopy, 29.08.-

02.09. **2011**. Jingming Long, Huasheng Wang, Ágúst Kvaran. Djon, France.

- Two-Dimensional (2+ n) REMPI Spectroscopy: State Interactions, Photofragmentations and Energetics of the Hydrogen Halides. The 22nd Colloquium on High Resolution Molecular Spectroscopy, 29.08.-02.09. **2011**. Jingming Long, Huasheng Wang, Kristjan Matthiasson And Agust Kvaran. Djon, France.
- Two-Dimensional (2+n) REMPI Spectroscopy Of CH_3Br And CF_3Br: Rydberg States and Photofragmentation Channels. The 22nd Colloquium On High Resolution Molecular Spectroscopy, 29.08.-02.09. **2011**. Huasheng Wang, Jingming Long, Agust Kvaran. Djon, France
- Multiphoton Absorption and Ionization of Molecules: Technical Improvements on Data Sampling. Rannsóknarþing VoN Háskóli Íslands, 08-09. Oct., **2010**, Jingming Long, Huasheng Wang and Ágúst Kvaran. Reykjavík, Iceland.
- Two-photon Absorption Followed by n-photon Ionization of Molecules: (2+n) REMPI of CF_3Br. Rannsóknarþing VoN Háskóli Íslands, 08-09. Oct., **2010**, Kári Sveinbjörnsson, Jingming Long, Huasheng Wang and Ágúst Kvaran. Reykjavík, Iceland.

List of Abbreviations

REMPI	Resonance enhanced multiphoton ionization
TOF	Time of flight
2D	Two dimensional
MO	Molecular orbital
FCF	Franck-Condon factor
MCP	Micro-channel plate
CCD	Charge coupled device
SHG	Second harmonic generation
KDP	KH_2PO_4 or potassium dihydrogen phosphate
BBO	Beta-BaB_2O_4 or beta barium borate
VMI	Velocity map imaging
DLD	Delay line detector
IR	Intensity ratio
FWHM	Full width at half maximum
BW	Bandwidth
LS	Line-shift
VUV	Vacuum ultraviolet
PES	Potential energy surface

NRI	Near-resonance interaction
ORI	Off-resonance interaction

T	Temperature
Ω	The projection of total angular momentum of electrons Ω=Λ+Σ
J	Total angular momentum of molecule
v’	Vibrational quantum number
Ψ	Wavefunction
δ	Quantum defect
Bv’	Rotational constant
Dv’	Centrifugal distortion constant

Acknowledgements

I have clearly remembered that day when I first arrived at Iceland from China. My supervisor Prof. Ágúst Kvaran and co-advisor Dr. Huasheng Wang picked up me at the Keflavik airport in the cold evening. I never forget the happy time during my PhD project in such beautiful place named *Ísland*, which is far away from my hometown.

Now it is close to my graduation time. First of all, I would like to express my heartfelt thanks to my supervisor Prof. Ágúst Kvaran. Because this thesis wouldn't be finished without his instruction, continued support and encouragement. I am also very grateful to his wife Ólöf Þorsteinsdóttir for her help with my tax refund in Iceland, which saved me a lot of time to focus on my study.

I also sincerely thank my co-advisor Dr. Huasheng Wang for his instruction and assistant on experiments, and his wife Jianhua Yan for their consideration of my wife and me in Iceland. Without their help, we would not adapt to live in Iceland very quickly and finish our study successfully.

Many thanks go to Ágúst Kvaran and Ólöf Þorsteinsdóttir, Huasheng Wang and Jianhua Yan again, that's because they treated us like parent to children more than teacher to student.

I would like to thank Prof. Christof Maul, who arranged two-month exchange study in Physical and Theoretical Chemistry Institute, Technical University of Braunschweig. I also thank Michael Schiller, Misha Poretskiy for their help in Germany.

I am grateful to my Ph.D committee members for their valuable instruction. They are Prof. Ari Ólafsson, Dr. Andras Bodi, Dr. Gísli Hólmar Jóhannesson.

I also would like to thank my wife and parents' understanding and supporting during my studying. Since I started my PhD study, I haven't been with them together for Chinese spring festival for four years, which is the most important member-united day for Chinese people.

The finance support of the University Research fund, University of Iceland and the Icelandic Science foundation (Rannis), Deutsche Forschungsgemeinschaft (DFG) funds for exchange study in Germany for two months is gratefully acknowledged.

1 Introduction

Investigations of atoms and molecules, involving absorption of photons, provide insight into fundamental physical and chemical phenomena, such as photoionization and photodissociation. These phenomena are common, for example in atmospheric chemistry, photochemistry and astrochemistry due to the effect of UV/VUV radiation, which can cause a release of bounded electrons from atoms and molecules, and/or a breakage of molecular bonds. To understand the nature of inter- and intra-molecular photoelectron dynamics in detail is an ultimate goal of photochemists.

Photofragmentation of molecules (involving ions, and/or radical formations) is the main context of photochemical reactions and relevant dynamics, which can provide important information about interactions between different molecular states, and molecular fragmentations following bond breaking. Spectra obtained by different spectroscopic techniques have proved to be important to study and understand the detailed principles behind photofragmentation phenomena.

Spectra due to optical absorptions or emissions because of transitions between different states in atoms/molecules typically show regular electronic structures. Molecules also show characteristic vibrational structures and rotational structures. As is known, in an absorption or an emission of one photon its frequency v can be derived by the relationship $hv=E_1-E_2$, where h is the Planck constant and E_1 and E_2 are the quantum energy levels involved. To obtain the relevant spectra, many different types of spectroscopic techniques are used such as traditional absorption spectroscopy[1-5], laser induced fluorescence (LIF) spectroscopy[6], and resonance enhanced multiphoton ionization (REMPI) spectroscopy[7-24] to name a few. These different techniques have been employed to study molecular energetic and photoionization/photodissociation dynamics. Besides the use of a large number of spectroscopic techniques, many theoretical studies, such as *ab initio* calculations [25-35], have been performed to predict or to explain spectral structures.

REMPI TOF (time of flight) is a popular technique to study photofragmentations, photoionization and photodissocation processes, state-to-state interactions and so on. During a REMPI process, one of the electrons in a molecule is excited from the ground state to an excited state by absorbing two or more photons simultaneously. By absorbing additional photons the molecule loses an electron to form an ion if the photon energy is sufficient. Small molecules typically have ionization energies of about 8-15 eV, which corresponds to an absorption of about three UV photons. If photofragmentation (photodissociation and photoionization) processes occur, free electrons and ions (parent molecular or fragment ions) will be formed. All the ions could be detected in the experiment. Expressions 1.1- 1.3 show examples of what could happen if a diatomic molecule is resonantly excited by two photons.

In expression 1.1 a molecule AB is excited by two-photon absorption to form AB*. By consequent absorption of one more photon the molecule could form the AB^+ molecular/parent ion and a free electron or transfer to a superexcited state followed by dissociation into two neutral fragments, one of which could be in an excited state. Alternatively AB* also may dissociate into two neutral fragments directly.

$$AB \xrightarrow{2h\nu} AB^* \xrightarrow{1h\nu} AB^+ + e^- \quad \text{Resonant excitation and photoionization (1.1)}$$

$$\rightarrow A + B^*/A^* + B$$

Photodissocation (1.2)

$$\rightarrow AB^* \rightarrow A/A^*_{so} + B$$

Predissociation or photodissociation (1.3)

In my PhD work all spectral data were obtained by REMPI-TOF technique, which is a high resolution and sensitive spectroscopic technique. It involved both state- and mass- resolution. REMPI spectra for different ion masses such as H^+, $^{35}Cl^+$, $H^{35}Cl^+$, $^{37}Cl^+$, $H^{37}Cl^+$ for HCl, were recorded simultaneously in one REMPI experiment. The spectral data involving ion signals for different masses and excitation wavenumbers could be displayed graphically as two dimensional (2D)

plots named 2D REMPI spectra [11,16,36-44]. This kind of spectral data are informative about electronic, vibrational and rotational structures of the molecule, as well as about state interaction and lifetime from peak positions, line intensities and linewidths [3,8,21-23,38,43,44]. Abnormal deviations of spectral features from regular predictable trends (spectral perturbations) are informative about state-to-state interactions. The state interactions are grouped into homogeneous ($\Delta\Omega=0$) and heterogeneous interactions ($\Delta\Omega\neq0$) [37,42,45]. The perturbations due to electronic, vibrational, rotational and spin-orbit interactions[45] are different based on the properties of the states involved. To analyze spectral perturbation in diatomic molecules, a deperturbation method has been developed by Lefebvre-Brion and Field *et al.* [45-49].

Hydrogen halides such as HCl and HBr are ideal molecules for fundamental studies in spectroscopy. These diatomic molecules have been regarded as prototypes of heteronuclear diatomics, which have been studied experimentally [7,12,21,36,39,40,50-53] as well as theoretically [26,32,33,35,54,55] for decades. Many spectral data have been obtained for HCl [7,8,21,29,41,43,52,53,56-62] and HBr [11,12,14,24,38,42,63]. For example, absorption spectra and (2+1) REMPI studies carried out for HCl by Ginter [3] *et al.* and Green *et al.* [8,22,23], in particular, have revealed a number of spectra due to transitions to Rydberg and ion-pair states. Similarly, work by Callaghan and Gordon [24] obtained for the spectral range of 74000 - 85000cm^{-1} for HBr, shown many interesting and informative spectral features.

REMPI combined with the 3D velocity map imaging (VMI) technique also has been employed to analyze different velocity and angular distribution of photoelectron and photoions depending on different excited states [7,52,53,64-70]. In addition to a REMPI setup, a velocity map imaging system also consists of a position-sensitive detector followed by a phosphor and charge coupled device (CCD) [52,64,65] or a Medipix/Timepix detector [71,72], or a delay line detector (DLD) [68,69,73,74]. This technique is very useful to study photofragmentation processes via different excited states for hydrogen halides [7,52,64,65].

Although many spectra have been obtained and analysed for the hydrogen halides, there are still a number of "surprising" spectral features which are not yet understood [67]. A large number of phenomena due to interactions between Rydberg and ion-pair states [7,64], have been reported by the

Kvaran's research group [16,29,37-39,41,42,44,75]. Relevant state interactions and photofragmentation processes have been studied for a number of Rydberg states and the $V^1\Sigma^+$ ion-pair state for the hydrogen halides by the one-colour REMPI-TOF technique. Observations can be classified depending on the strengths of Rydberg to ion-pair state interactions as follows:

- Very weak near-resonance interactions (NRI), distinguishable by negligible rotational line shifts but significant alterations in signal line intensities, observed for triplet Rydberg states and $\Omega > 0$ state interactions.
- Weak NRI, distinguishable by localized line shifts, (hence energy level shifts), as well as alterations in signal line intensities, observed for singlet states and $\Omega > 0$ state interactions.
- Medium to strong off-resonance interactions (ORI), distinguishable by large scale line/energy level shifts, as well as alterations in signal intensities observed for triplet and singlet states and $\Omega = 0$ state interactions.

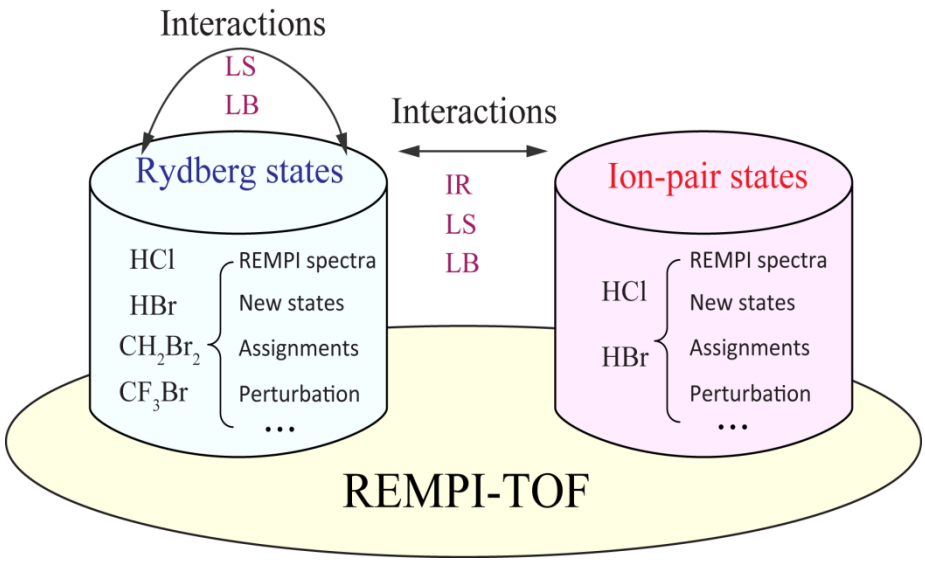

Figure 1.1 Spectral data of HCl, HBr, CH_2Br_2 and CF_3Br were obtained by REMPI-TOF. Intensity ratio (IR), line shift (LS) and linewidth broadening (LB) due to state interactions were studied for Rydberg and ion-pair states.

Figure 1.1 illustrates the main work dealt with in this thesis. All masses and REMPI spectra of HCl, HBr, CH_2Br_2 and CF_3Br were obtained by REMPI-TOF. New spectra found for first time, were assigned to new Rydberg and ion-pair states. State interactions between Rydberg and ion-pair states as well as photofragmentation processes were studied carefully. Signal intensity ratio calculations involving three energy levels were optimized for near-resonance and off-resonance interaction analysis. A deperturbation method was introduced, and performed to analyze perturbations due to state interactions.

2 Theoretical background

Molecular spectra are "windows" to observe molecular structures, properties and dynamics. A spectral peak can contain important information concerning molecules, based on its frequency (or wavenumber), line intensity, line shape and linewidth. In UV-Vis spectroscopy, the spectra are often given in wavenumbers (with a unit of cm^{-1}) rather than frequency or wavelength for the convenience. Based on the physical quantities derived from such information, we can derive various information about molecules on microscopic scale, which normally can't be obtained directly. Thus, for example, a peak position reflects energy properties of a molecule. For molecules, excited states can be separated into electronic states, vibrational states and rotational states. With a known energy structure of the ground state of a molecule, the energy properties of excited states can be easily derived from experimental spectral data. Linewidth, the full width at half maximum (FWHM) of a spectral peak, contains information on the lifetime of the excited state. Rydberg states of atoms and molecules can have long lifetimes due to limited overlap of Rydberg state and core electron wavefunctions. To first approximation the lifetime is proportional to the cube of the principal quantum number *n*.

Potential energy surfaces (PES) (see figure 2.1) based on the Born-Oppenheimer approximation, are a very important concept to help us to understand state properties as well as state to state interactions and state mixing. Many theoretical studies on PES of diatomic molecule such as hydrogen halides (HX, X=F, Cl, Br, I) by using *ab initio* calculation have been performed [25,26,29]. From such PESs spectroscopic constants including band origins v_0, vibrational frequencies ω_e, rotational constants Bv' have been derived and used to compare with or predict experimental data. Thus spectroscopy has benefited from the rapid development of quantum chemical computational techniques in recent years.

2.1 The Born-Oppenheimer approximation

The Born-Oppenheimer approximation states that the motion of nuclei and electrons can be separated due to the large difference in masses. The electrons move much faster than the nuclei. Therefore, the nuclei can be considered to be static, and the wavefunctions of nuclei and electrons can be separated (see equation 2.1) in the Schrödinger equation $\hat{H}\psi = E\psi$. The total wavefunctions are obtained by infinite expansions of the wavefunction solutions based on the Born-Oppenheimer approximation, as shown in equation 2.2. In the Born-Oppenheimer approximation, the adiabatic approximation is applied where the molecules are pictured as a set of nuclei moving on a potential energy surface defined by the electronic energy. This approximation fails in the vicinity of surfaces crossing or almost cross (an avoided crossing). This often happens where a large number of energetically close-lying electronic states are involved. Interactions between two or more potential energy surfaces can be described in terms of two limiting cases: the nonadiabatic and the adiabatic representation.

$$\Psi_{i,v}^{BO} = \Phi_{i,\Lambda,S,\Sigma}(r;R)\chi_v(R,\theta,\phi) \tag{2.1}$$

$$\Psi_i^T = \sum_{i,v}^{\infty} c_i \Psi_{i,v}^{BO} \tag{2.2}$$

The molecular Hamiltonian $\hat{H}$ is divided into electronic and nuclear terms in the Born-Oppenheimer approximation,

$$\hat{H} = \hat{T}^e(r) + V(r,R) + \hat{T}^N(R,\theta,\phi) = \hat{H}^{el}(r,R) + \hat{T}^N(R,\theta,\phi) \tag{2.3}$$

where $\hat{T}^e(r)$ is the electron kinetic energy operator, $V(r, R)$ represents the interelectron repulsion and the electron-nuclear attraction. The total energy of the molecule is expressed as

$$E^{tot} = E^{el} + E^{vib} + E^{rot} \tag{2.4}$$

where E^{el} is electronic energy, which includes the electronic kinetic energy and the potential energy, E^{vib} is the vibrational energy and E^{rot} is the rotational energy[76].

For Rydberg states, E^{el} can be approached by E_n in the Rydberg state equation (2.5) for known ionization energy *IE*.

$$E_n = IE - \frac{R}{(n-\delta)^2} \tag{2.5}$$

n is the principal quantum number and δ is the quantum defect, the value *R* is the Rydberg constant. High Rydberg states have large *n* quantum number. Molecular geometries of Rydberg states are very similar to the ground state of the molecular ion to which the states converge. The vibrational (E^{vib}) and rotational (E^{rot}) energy levels for diatomic molecules are expressed as

$$E^{vib} = \omega_e\left(v+\frac{1}{2}\right)() - \omega_e\chi_e\left(v+\frac{1}{2}\right)^2 + \omega_e y_e\left(v+\frac{1}{2}\right)^3 + ... \tag{2.6}$$

$$E^{rot} = B_v J(J+1) - D_v J^2(J+1)^2 + ... \tag{2.7}$$

where

$$B_v = B_e - \alpha_e\left(v+\frac{1}{2}\right) \tag{2.8}$$

$$D_v = D_e - \beta_e\left(v+\frac{1}{2}\right) \tag{2.9}$$

B_v' and D_v' are the vibrational dependent rotational and the centrifugal distortion constants, respectively.

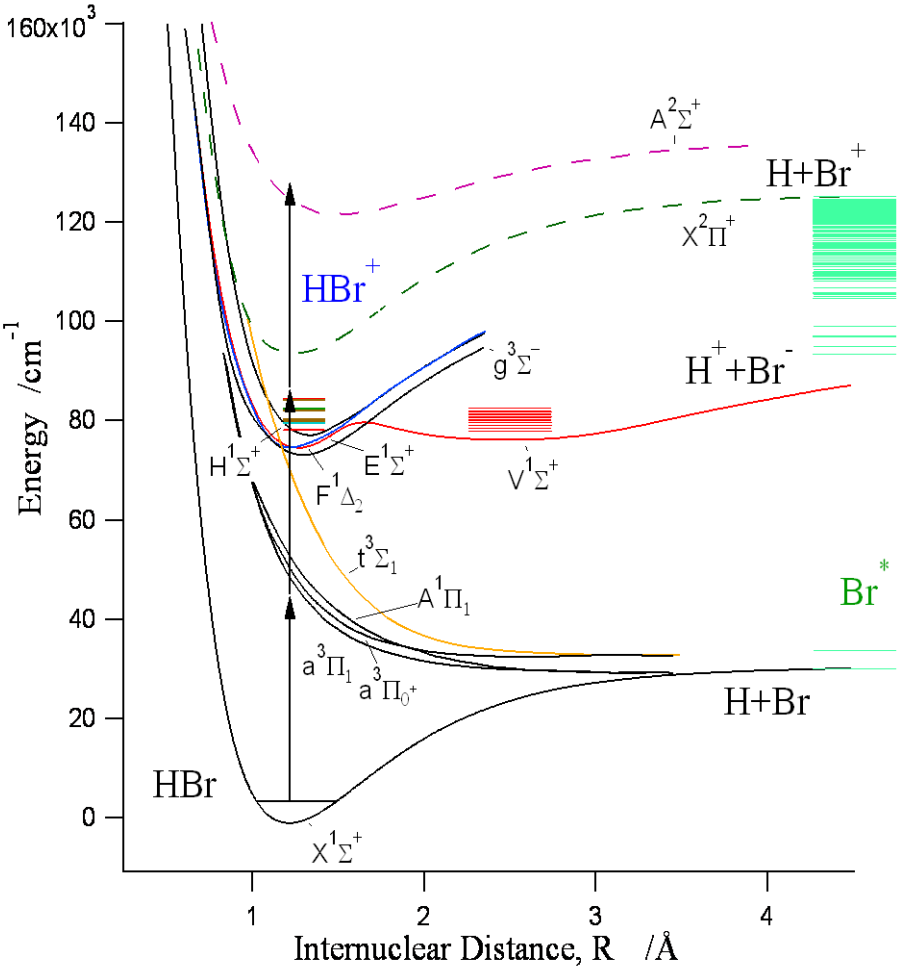

Figure 2.1 Potential energy curves for HBr. The HBr molecule can be excited by two-photon to a Rydberg state or an ion-pair state from the ground state followed by ionization.

2.2 Spectral terms and molecular orbitals

Molecular orbitals can be approximately constructed by performing a linear combination of atomic orbitals (LCAO). Thus, two atomic 1s orbitals will form $1s\sigma_g$ bonding and $1s\sigma_u^*$ antibonding orbitals for homenuclear diatomic molecule such as H_2. Table 2.1 shows the correlation between atomic orbitals and molecular orbitals.

Table 2.1 Correlation between atomic orbitals and bonding molecular orbitals

Atomic orbitals l	**Bonding molecular orbitals** λ
s	$s\sigma$
p	$p\sigma, p\pi$
d	$d\sigma, d\pi, d\delta$
f	$f\sigma,\ f\pi,\ f\delta,\ f\phi$

The total angular momentum without nuclear spin is represented by ***J***. The orbital angular momentum, the spin orbital angular momentum and the nuclear rotational angular momentum are labelled as ***L***, ***S*** and ***R*** respectively. All vectors are shown in figure 2.2. Their projections of ***L***, ***S*** and ***R*** on the molecular axis are Ω, Λ and Σ, respectively. The relationship between those is

$$\Omega = |\Lambda + \Sigma| \tag{2.10}$$

where Λ=0, 1, 2 … is assigned as $\Sigma, \Pi, \Delta\ldots$, terms symbols for a molecule are ${}^{2S+1}\Lambda_\Omega$.

Configuration of the ground state of HCl and HBr at the equilibrium distance is given by $\ldots\sigma^2\pi^4$. Configuration of the ground state of molecular ion is $\ldots\sigma^2\pi^3$. The term symbols of the states which have been

observed and studied, particularly concerned Rydberg states and ion-pair states for HBr were listed in table 2.2 as well as their molecular orbital (MO) configurations. The major work on (2+n) REMPI spectra of HCl and HBr concerns analysis of photofragmentations (photodissociations and photoionizations), state-to-state interactions and spectral perturbations, which involves the Rydberg state $E^1\Sigma^+$, $F^1\Delta_2$ and $g^3\Sigma^+$ as well as ion-pair state $V^1\Sigma^+$.

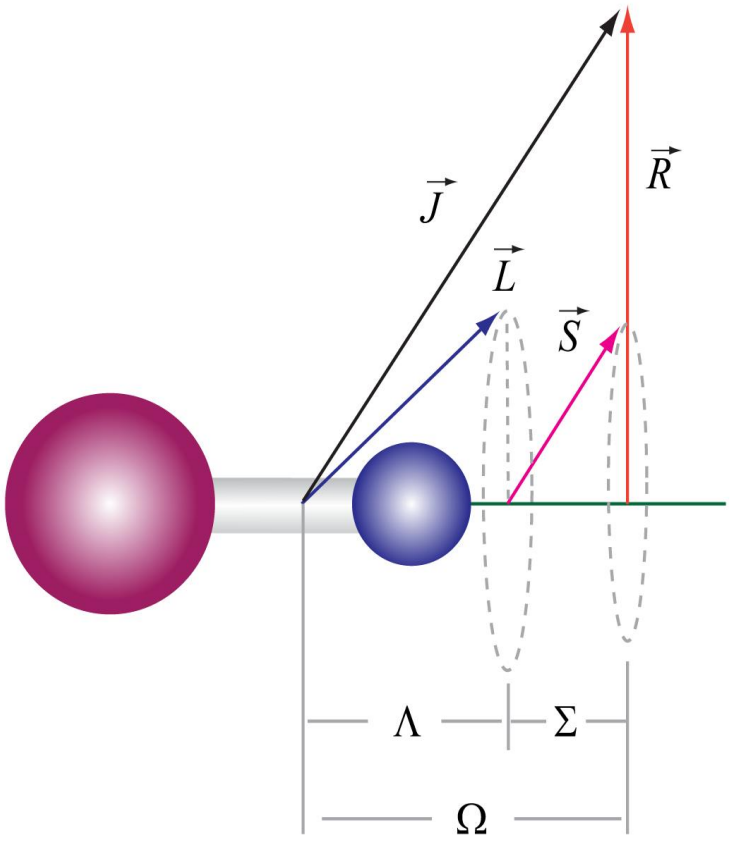

Figure 2.2 Angular momenta in a diatomic molecule

Table 2.2 Molecular orbital configurations and term symbols for HBr and HBr^+ ($^{2S+1}\Lambda_\Omega$, $\Omega=|\Lambda+\Sigma|$). The states $W^1\Sigma^+(0^+)$,$u^3\Delta_2$ are assigned and reported here for the first time.

MO configuration	Term Symbols	MO configuration	Term Symbols
$\sigma^2\pi^3 5d\sigma$	$n^3\Pi(0,1,2)$		
	$N^1\Pi(1)$		
		$\sigma^2\pi^3$	$X^2\Pi(3/2,1/2)$
$\sigma^1\pi^4\sigma*$	$V^1\Sigma^+(0^+)$		
	$t^3\Sigma^+(0^-,1)$	$\sigma^2\pi^3 6p\pi$	$6p\pi^3\Sigma^-$
			$W^1\Sigma^+(0^+)$
$\sigma^2\pi^3 5p\pi$	$f^3\Delta(1,2,3)$		$u^3\Delta_2$
	$F^1\Delta(2)$		
	$g^3\Sigma^-(0^+,1)$	$\sigma^2\pi^3 6p\sigma$	$r\Pi^3(0,1,2)$
	$G^1\Sigma^-(0^-)$		$R^1\Pi(1)$
	$e^3\Sigma^+(0^-,1)$		
	$E^1\Sigma^+(0^+)$	$\sigma^2\pi^3 6s\sigma$	$m^3\Pi(0,1,2)$
			$M^1\Pi(1)$
$\sigma^2\pi^3 5p\sigma$	$d^3\Pi(0,1,2)$		
	$D^1\Pi(1)$	$\sigma^2\pi^3 5d\delta$	$k^3\Pi(0,1,2)$
			$K^1\Pi(1)$
$\sigma^2\pi^3 5s\sigma$	$b^3\Pi(0,1,2)$		
	$C^1\Pi$	$\sigma^2\pi^3 5d\pi$	$i^3\Delta(1,2,3)$
			$I^1\Delta(2)$
$\sigma^2\pi^3\sigma*$	$a\Pi^3(0,1,2)$		$j^3\Sigma^-(0^+,1)$
	$A\Pi^1(1)$		$J^1\Sigma^-(0^-)$
			$h^3\Sigma^+(0^-,1)$
$\sigma^2\pi^4$	$X^1\Sigma^+(0^+)$		$H^1\Sigma^+(0^+)$

2.3 Multiphoton ionization

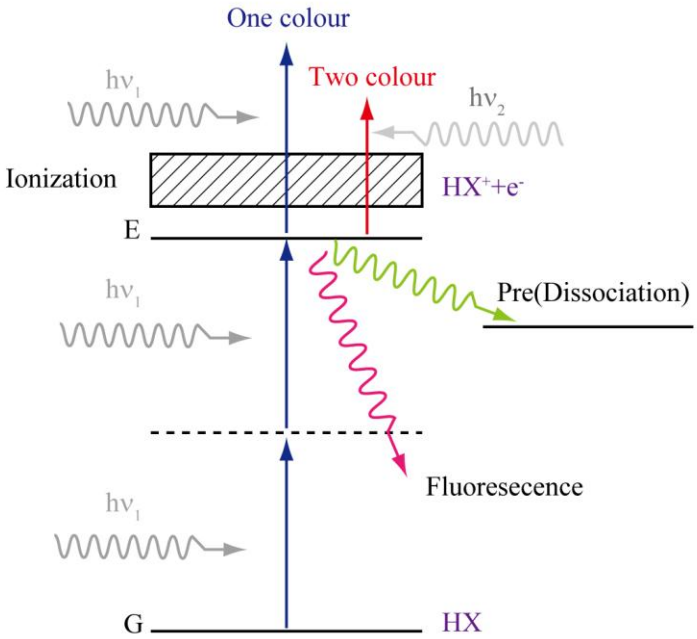

Figure 2.3 One and two-colour (2+1) REMPI processes. The dotted line indicates a virtual state. Three major escape channels for a molecule in an excited state: fluorescence, dissociation and ionization by absorption of an additional photon to form a molecular ion. G: ground state, E: excited state.

Multiphoton absorption involves excitation of an atom or a molecule from the ground state *G* to the excited state *E* by simultaneous absorption of two or more photons (see figure 2.3). By absorbing one more photon the atom or molecule can be ionized, if the photon energy is sufficient to exceed the ionization limit. This process is named resonance enhanced multiphoton ionization (REMPI)[77]. If the light used to ionize (for probe) has the same wavelength as the resonance excitation light (for pump), it is named one-colour REMPI, whereas if the wavelengths are different, then it is named two-colour REMPI. Ions formed can be detected by a time of flight (TOF) mass spectrometry for gas phase species. The TOF mass

spectrometry is composed of an ionization chamber, electrode plates, a flight tube and micro-channel plates (MCP) detector (more detail in chapter 3). Figure 2.3 shows a typical excitation scheme. A molecular excited state could be a Rydberg state or a valence state, which can transit back to the ground state by emitting a photon (fluorescence), or it can result in a dissociation (i.e. photodissociation) directly or indirectly (predissociation). State coupling between a bound and a repulsive state is a prerequisite for a predissociation. Normally, Rydberg states typically have high ionization rates and slow fluorescence rates. Therefore, in case of limited dissociation, these can have long lifetimes and high ionization efficiencies.

REMPI-TOF has been widely used in the field of spectroscopy for decades. The technique has several advantages over more conventional methods such as traditional absorption spectroscopy.

- Visible and near-ultraviolet light can be used to study highly electronically excited states of a molecule.
- A number of molecular excited states can be reached by multi-photon excitation compared to single-photon excitations and therefore provides a chance to study excited states with different symmetry characteristics.
- The method allows high resolution, and high sensitivity signal detections.

The ion intensity can be predicted with ionization rate $W(n)$.

$$W(n) = \sigma_n I^n \tag{2.11}$$

where σ is the absorption cross section for n photons, and I means the laser power. The relationship given by equation 2.11 sometimes can be used to calculate the number of photons involved in the process of photoionization by power dependent REMPI experiments[20].

2.4 State interactions

Perturbations were often observed in REMPI spectra and were manifested as ion intensity ratio variations, line shifts and/or linewidth broadenings. Perturbations can be classified as electrostatic, vibrational, rotational perturbation and spin-orbit perturbation[45]. These can be represented as Hamiltonian off-diagonal matrix elements. In the case of $\Delta\Omega=0$ state interactions, these are customarily named as homogeneous perturbations, otherwise $\Delta\Omega\neq0$ interactions these are referred to as heterogeneous perturbations. Selection rules for different perturbations and the corresponding off-diagonal matrix elements are listed in table 2.3. The *L*-uncouplings and *S*-uncouplings are parts of rotational perturbation, which are found here to be of importance for interactions between those Rydberg states ($\Omega=1$) and ion-pair state $V^1\Sigma^+$ of HCl and HBr molecule.

Table 2.3 Off-diagonal elements of the total Hamiltonian [a]

Neglected terms in the Born-Oppenheimer approximation	Nature of the interactions	Selection rules $\Delta J=0$ and g←/→u			
		$\Delta\Lambda$	$\Delta\Sigma$	ΔS	$\Delta\Omega$
$\langle\Lambda,S,\Sigma,\Omega, v\vert \mathbf{H^{el}} \vert \Lambda',S',\Sigma',\Omega', v'\rangle$	Electronic (Homogeneous)	0	0	0	0
$\langle\Lambda,S,\Sigma,\Omega, v\vert \mathbf{T^{N}} \vert \Lambda',S',\Sigma',\Omega', v'\rangle$	Vibational (Homogeneous)	0	0	0	0
$\langle\Lambda,S,\Sigma,\Omega, v\vert \mathbf{H^{so}} \vert \Lambda',S',\Sigma',\Omega', v'\rangle$	Spin Orbital (Homogeneous)	0 or ±1	0 or ±1	0 or 1	0
$\langle\Lambda,S,\Sigma,\Omega, v\vert -\frac{1}{2uR^2}\mathbf{JL} \vert \Lambda',S',\Sigma',\Omega', v'\rangle$	*L*-uncoupling (Heterogeneous)	±1	0	0	±1
$\langle\Lambda,S,\Sigma,\Omega, v\vert -\frac{1}{2uR^2}\mathbf{JS} \vert \Lambda',S',\Sigma',\Omega', v'\rangle$	*S*-uncoupling (Heterogeneous)	0	±1	0	±1

[a] For more details see reference [45]

Ranking of interaction strength is shown in table 2.4 for Hund cases (a), (b) and (c). The heterogeneous perturbations (H^{rot}) are rotational quantum number *J'* dependant (see equation 2.26). More details can be found in the book written by Field and Lefebvre-Brion[45].

Table 2.4 Relative interaction strengths [45]

Hund case	$\mathbf{H^{el}}$	$\mathbf{H^{so}}$	$\mathbf{H^{rot}}$
(a)	strong	intermediate	weak
(b)	strong	weak	intermediate
(c)	intermediate	strong	weak

Possible state mixing and interactions between bound states and bound states (bound-to-bound interactions including Rydberg and ion pair states) and between bound states and continuum states (bound-to-continuum interactions) for the hydrogen halides are shown as table 2.5. The homogeneous interactions between the Rydberg state $E^1\Sigma^+$ and the ion-pair states $V^1\Sigma^+$ are emphasized in this study. Mixing of bound and continuum states is the cause of predissociative channels, which will result in short lifetimes, hence linewidth broadenings of the excited states.

Table 2.5 Typical interactions between states [a]. E: electrostatic interactions, JL: L-uncoupling interactions, SO: spin- orbit interactions

	Bound states			Continuum states		
	$E^1\Sigma^+$	$V^1\Sigma^+$	$C/D^1\Pi$	$t^3\Sigma_0^+$	$A^1\Pi$	$a^3\Pi_{0,1,2}$
$E^1\Sigma^+$	-	E	JL		JL	SO
$g^3\Sigma_0^-$	SO	SO				JL
$H^1\Sigma^+$	E	E	JL			
$F^1\Delta$		JL	JL			
$f\ ^3\Delta$						SO
$e^3\Sigma_0^+$				E		JL

[a] See reference [78]

2.4.1 Line shift

Spectral line shifts, reflect that energy level shifts more probably due to state interactions. For example, we often found that the Rydberg state $E^1\Sigma^+$ interacts strongly with other Rydberg states and ion- pair states $V^1\Sigma^+$. Figure 2.4 illustrates energy level shifts happen in a Rydberg state and an ion- pair state due to interactions when the two energy levels are close in energy.

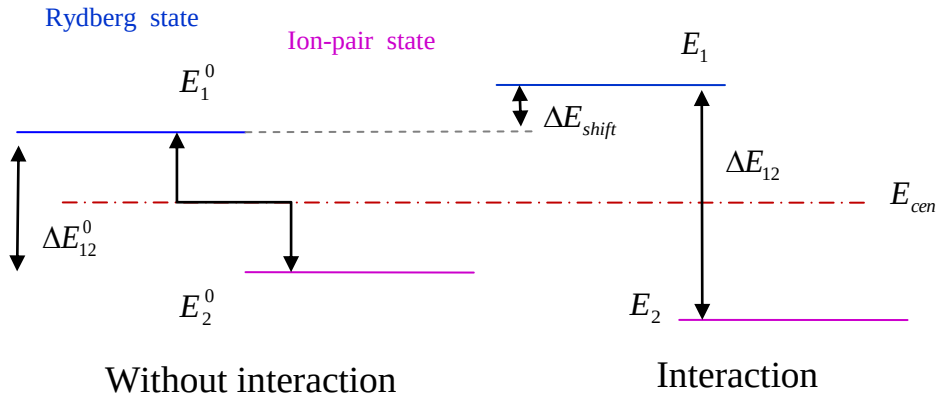

Figure 2.4 Line shifts due to state interactions. On the left is an unperturbed Rydberg state and an ion-pair state with energy difference ΔE^0_{12} and unperturbed energy levels are E^0_1 and E^0_2, respectively. On the right the effect of the interactions is shown, where both energy levels shift by ΔE_{shift} in opposite directions. The energy difference becomes ΔE_{12}

From figure 2.4, we can easily derive the expressions 2.12-2.15, which can be used to calculate ΔE_{shift} for a known interaction strength W and the energy differences between two unperturbed states. Alternatively, we can estimate the interaction strength W by using equation 2.14 to fit experimental energy levels.

$$E_1 = E_{cen} + \frac{1}{2}\sqrt{4|W_{12}|^2 + |E_1^0 - E_2^0|^2} \qquad (2.12)$$

$$E_2 = E_{cen} - \frac{1}{2}\sqrt{4\,|\,W_{12}\,|^2 + |\,E_1^0 - E_2^0\,|^2} \tag{2.13}$$

$$\Delta E_{12} = \sqrt{4\,|\,W_{12}\,|^2 + |\,E_1^0 - E_2^0\,|^2} = \sqrt{4\,|\,W_{12}\,|^2 + \Delta E_{12}^{0\,2}} \tag{2.14}$$

$$\Delta E_{shift} = \frac{1}{2}\left(\Delta E_{12} - \sqrt{\Delta E_{12}{}^2 - 4\,|\,W_{12}\,|^2}\right) \tag{2.15}$$

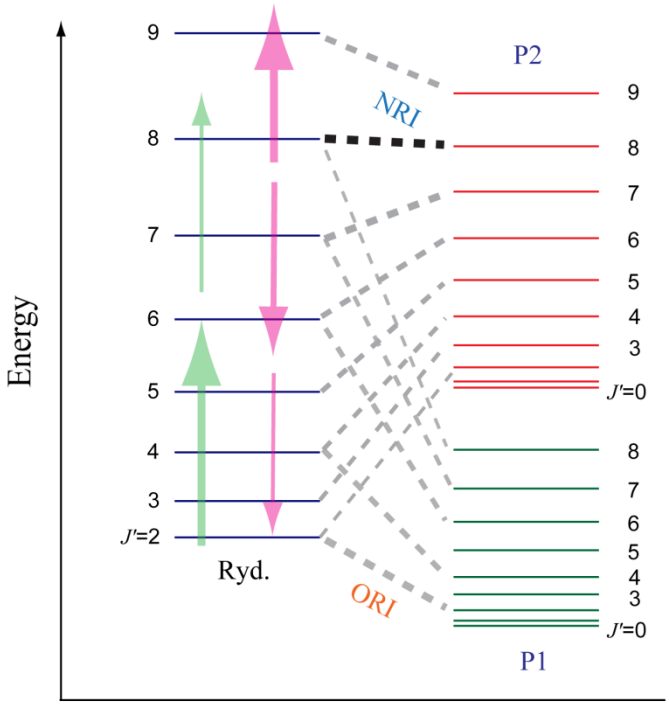

Figure 2.5 Energy levels of a Rydberg state and perturbing states such as ion-pair state. Ryd. Rydberg state, P1: perturbing state 1, P2: perturbing state 2, NRI: near-resonance interaction, ORI: off-resonance interaction.

An example of energy level shifts due to interactions between three states (*Ryd. P1, P2*) is shown in figure 2.5. The interactions between the Rydberg state *J'*=8 and its perturbing state, *P2*, *J'*=8 is classified to a near-resonance interaction (NRI), whereas the interaction between the

Rydberg state and perturbing states for other *J'* are off -resonance interactions (ORI). The arrows indicate that the "effect" directions of the perturbing states *P1* and *P2*.

2.4.2 Linewidth broadening

Lifetime is a characteristic property of an excited state. Spectral linewidth will depend on the natural lifetime, pressure and doppler broadening. Furthermore, it is also strongly influenced by bound-to-continuum state couplings, which causes dissociation. The relaxation of an excited state can be due to radiative as well as non-radiative decays. Predissociation belongs to the latter case. Predissociation is particularly important near energy potential curve crossings for states of analogous symmetries (equal Ω), and when perturbation selection rules are satisfied (see table 2.3). Tunnelling also can affect state lifetime, for example the $E^1\Sigma^+$ state of DBr[79]. In order to determine the lifetime of a short lived electronically excited state properly, an ultrafast system using pump and probe femtosecond or attosecond laser pulses is needed. Thus, lifetimes could be determined from detecting ion signals as a function of delay time between pump and probe laser pulses. Therefore, lifetime of excited state can be estimated by measuring spectral linewidths if the resolution of the laser system is larger than that of the spectrum. Once the spectral peaks are obtained, different shape functions for spectral lines can be used for simulations. Most commonly Lorentzian and Gaussian shape function are used. The previous one is used to estimate homegeneous broadening while the latter one is used for heterogeneous broadening. Two functions are provided as below.

The Lorentzian shape function is

$$\chi(\upsilon,\upsilon_0)=\frac{\Gamma/2\pi}{(\upsilon-\upsilon_0)^2+(\Gamma/2)^2} \tag{2.16}$$

The Gaussian shape function is

$$\chi(\upsilon,\upsilon_0)=\frac{2}{\Gamma}\left(\frac{\ln 2}{\pi}\right)^{1/2} e^{-\left(\frac{4\ln 2(\upsilon-\upsilon_0)^2}{\Gamma^2}\right)} \tag{2.17}$$

In both equation (2.16), (2.17), v_0 is central wavenumber. The linewidth Γ (full width at half maximum, FWHM) can be obtained by a line fitting to give the lifetime $\tau(ps)$ by the equation (2.18).

$$\tau(\text{ps}) = \frac{5.3}{\Gamma(\text{cm}^{-1})} \tag{2.18}$$

2.4.3 Ion signal intensity ratio

The major photofragmentation processes following two-photon excitations from the ground state HX($X^1\Sigma^+$) to an excited rovibrational (v', J') quantum level of a Rydberg state HX^* (R) or an ion pair state HX^* (V) are summarized below. This holds for HX; X= Cl, Br or I, which do have similar energy structures with decreasing energy gaps between states as mass increases. The molecules in the ground state are resonantly excited by two-photon to Rydberg or ion-pair states, followed by state transfers and/or further photon absorption.

$HX(X) \xrightarrow{2h\nu}$

(i) $HX^*(R) \xrightarrow{h\nu} HX^+ + e^-;\ HX^+ \xrightarrow{h\nu} H^+ + X;$

(ii) $HX^*(R) \rightarrow H + X/X^*;\ X/X^* \xrightarrow{3h\nu} X^+ + e^-;$

(iii) $HX^*(R) \xrightarrow{h\nu} H + X^*;\ X^* \xrightarrow{h\nu} X^+ + e^-;$

(iv) $HX^*(V) \xrightarrow{h\nu} HX^+ + e^-;\ HX^+ \xrightarrow{h\nu} H^+ + X;$

(v) $HX^*(V) \xrightarrow{h\nu} H + X^*;\ X^* \xrightarrow{h\nu} X^+ + e^-;$

(vi) $HX^*(V) \xrightarrow{h\nu} H^* + X;\ H^* \xrightarrow{h\nu} H^+ + e^-;$

(vii) $HX^*(V) \xrightarrow{h\nu} H^+ + X^-;$

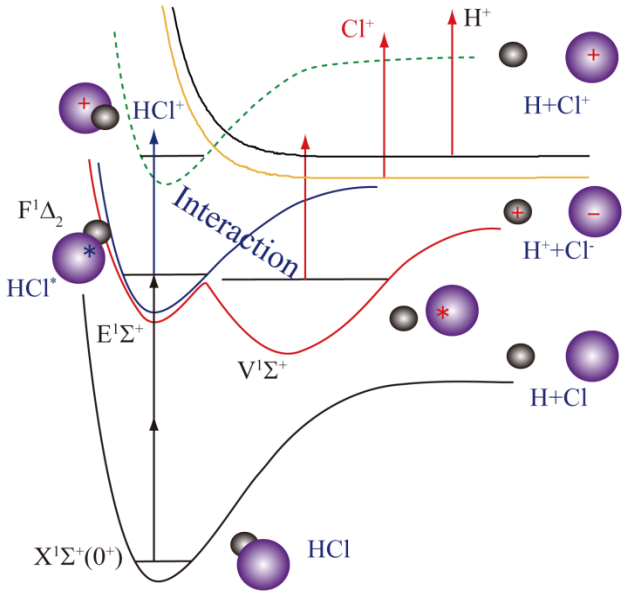

Figure 2.6 Simplified potential energy diagram for HCl, and main channels for parent and fragmental ion formations.

Among these processes (i-vii) molecular ion formation is the chief ionization channel following excitation to a "pure" Rygberg states (i). Due to the larger internuclear distance of the ion-pair state (see $V^1\Sigma^+$ state in the figure 2.6), repulsive states are more accessible by further photon excitation to form neutral fragments, $H^*(n=2)$ +X and H+X^*. Further one-photon absorption can form fragment ions. Due to the large internuclear distance of ion-pair state, the Franck Condon factor for the transition between $V^1\Sigma^+$ state and $X^2\Pi$ state (the ground state of molecular ion) is quite small. Therefore, the possibility of molecular ion formation by this channel is very low, and multiphoton ionization via the ion-pair state will mainly produce atomic ions. The main photoion and photodissociation channels, according to this, are shown by arrows lines in figure 2.6. "Pure" Rydberg and ion-pair states are rarely to be found. Rydberg to ion-pair state interactions occur for most states. Furthermore, Rydberg to Rydberg state interactions also are common. The effect of Rydberg to ion-pair state interactions on relative ion signal intensities (for fragment- vs parent- ions signal), however, is found to be dominant [37,41,42].

Based on the above statements, we proposed a model to estimate the ion intensity ratio, $I(X^+)/I(HX^+)$ to derive the state to state interaction strengths *W*, and fractions of state mixing. The relevant equations are the following.

$$\frac{I(\mathrm{X}^+)}{I(HX^+)}=\alpha_H\frac{\left[\gamma_H+c_{2H}^2(1-\gamma_H)\right]}{(1-c_{2H}^2)}+\alpha_L\frac{\left[\gamma_L+c_{2L}^2(1-\gamma_L)\right]}{(1-c_{2L}^2)} \quad (2.19)$$

where

$$I(^iX^+)=\alpha_{2I}c_{2I}^2+\beta_1c_1^2; \qquad I(H^iX^+)=\alpha_1c_1^2+\beta_{2I}c_{2I}^2; \qquad I=H,L$$

$$\alpha_I=\alpha_{2I}/\alpha_1; \qquad \gamma_I=\beta_1/\alpha_{2I}; \qquad \alpha_I\gamma_I=\beta_1/\alpha_1; \qquad I=H,L$$

Intensity ratios vs. J' have been expressed as a function of fractional contributions to the state mixing, derived for two-level interactions[39]. Assuming, to a first approximation, that the ion intensity ratio is a sum of contributions due to interactions between a Rydberg state (1) and two ion-pair (2) vibrational states (2*H* and 2*L*), such as those between the $E^1\Sigma^+(v')$ ($E(v')$) and the $V^1\Sigma^+(v')$ states closest in energy (V_H and V_L), the following expression is derived,

$$c_{2I}^2=\frac{1}{2}-\frac{\sqrt{(\Delta E_{J'}(1,2I))^2-4(W_I)^2}}{2\,|\,\Delta E_{J'}(1,2I)\,|}; \;\; c_1^2=1-c_{2I}^2; \quad I=H,L \quad (2.20)$$

where c_{2I}^2 (I = H,L) are the fractional contributions of the V_I (I = H,L) state to the state mixing. $\Delta E_{J'}(1, 2H)$ and $\Delta E_{J'}(1, 2L)$ are the energy spacings between levels with the same J' quantum numbers for the 1, 2*H* and 1, 2*L* states respectively, easily derivable from energy levels. W_H and W_L are the corresponding interaction strengths. α_1, β_1, α_{2I}, β_{2I} (I = H,L) are ionization rate coefficients. γ_I and $\alpha_I\gamma_I$ are measures of $^iX^+$ ion formations via dissociation of the Rydberg state, relative to that of the

formations of $^iX^+$ via exciations of the ion-pair state (γ_I) and relative to that of the formations of H^iX^+ via excitation of the Rydberg state ($\alpha_I\gamma_I$). To the first approximation $W_L = W_H = W$, $\alpha_L = \alpha_H = \alpha$ and $\gamma_L = \gamma_H = \gamma$ is assumed[80], which gives a simplified expression.

$$\frac{I(^iX^+)}{I(^iHX^+)} = \alpha\left\{\frac{\left[\gamma + c_{2H}^2(1-\gamma)\right]}{(1-c_{2H}^2)} + \frac{\left[\gamma + c_{2L}^2(1-\gamma)\right]}{(1-c_{2L}^2)}\right\} \qquad (2.21)$$

Fractional mixings of the three states, C_1^2, C_{2L}^2 and C_{2H}^2 are determined as,

$$\begin{aligned} C_1^2 &= 1/(1+k_L+k_H) \\ C_{2L}^2 &= k_L/(1+k_L+k_H) \\ C_{2H}^2 &= k_H/(1+k_L+k_H) \end{aligned} \qquad (2.22)$$

Where $k_L = c^2{}_{2L}/c_1{}^2$, $k_H = c^2{}_{2H}/c_1{}^2$.

2.5 Deperturbation procedure

Deperturbation is an advanced method to analyze spectral perturbations quantitatively. Deperturbation takes account of the non-diagonal matrix elements of the Hamiltonian to derive spectroscopic parameters and interaction strengths from a least-square fitting of experimental spectral data [45,46]. The first step is to construct an effective Hamiltonian matrix such as shown in table 2.6.

The deperturbation procedure was based on the method given by Lefebvre-Brion and Robert Field [45]. It was formulated in the Igor Pro software[81]. We took account of the interactions between different states, are shown in the equation (2.23). The first term on the right side H^{el} is the electrostatic interaction. The next three terms represent rotational interaction. Other terms are relativistic parts of the Hamiltonian.

$$H' = H^{el} + B(R)(L^+S^- + L^-S^+) - B(R)(J^+L^- - J^-L^+) - B(R)(J^+S^- - J^-S^+)$$
$$+ (H^{SO} - A_{S,\Lambda,S',\Lambda'}(R))(L_Z S_Z) + H^{SS} + H^{SR} \tag{2.23}$$

Table 2.6 Effective Hamiltonian matrix elements, Ryd. is Rydberg state. P1 and P2 are Perturbing states. W_{P1} and W_{P2} are the interaction strengths.

	Ryd.	*P1*	*P2*
Ryd.	E^0_{Ryd}	W_{P1}	W_{P2}
P1	W_{P1}	E^0_{P1}	
P2	W_{P2}		E^0_{P2}

The diagonal matrix elements are expressed as

$$E^0_{\mathrm{Ryd}} = \nu_0 + B_{\mathrm{v}}' J'(J'+1) - D_{\mathrm{v}}' J'^2 (J'+1)^2 \tag{2.24}$$

$$E^0_{\mathrm{P}i} = \nu^0_{\mathrm{P}i} + B_{\mathrm{P}i}' J'(J'+1) - D_{\mathrm{P}i}' J'^2 (J'+1)^2 \;; \quad i=1,\ 2 \tag{2.25}$$

Interaction strengths are constant for homogeneous perturbations, whereas for heterogeneous perturbations, these depend on rotational quantum numbers *J'* as

$$W = W' \sqrt{J'(J'+1)} \tag{2.26}$$

where *W'* is a constant. The deperturbation procedure within Igor Pro was named Deperturbation.pxp (part codes in Appendix). It allows an evaluation of the interaction strengths as well as unperturbed spectroscopic parameters for a given spectral data and suitable initial guess values.

3 Experiment and program design

To obtain 2D REMPI spectra for sample gases, we need to combine laser controlling, energy tracking, gas injecting, and data collecting in a compatible mode. A schematic sketch is shown in figure 3.1.

3.1 Laser system and experimental procedure

Ultraviolet and visible laser radiation was generated by an excimer laser pumped dye Laser. The laser beam was focused into a SHG crystal to generate frequency doubling radiation. Its energy output was kept stable by an antotracking device. The lasers involved are listed in table 3.1 along with important parameters.

Table 3.1 Laser and relevant parameters

	Excimer Laser	**Dye Laser**
Name	Compex 205	Scanmate
Manufacturer	Lambda Physics	Lambda Physics
Working wavelength	308 nm	Adjustable
Repetition	1~10 Hz	1~10 Hz
Bandwidth	-	0.095 cm^{-1}
Intensity	1.5 W	10~30 mW
Resolution	-	0.1 cm^{-1}

The experimental setup is shown in Figure 3.1. XeCl, excimer laser radiation was used to pump dye laser to produce pulsed radiation. Normally, the output wavelength was in the visible region at 400 ~ 600 nm. The beam was adjusted in terms of quality before focusing into

Second Harmonic Generator (SHG) for frequency doubling. The SHG is composed of a BBO-2 crystal, a compensator and a detector with a computer-controlled feedback circuit to track the energy variation and to perform power calibrate in real time. After frequency doubling, the laser beam was focused into a vacuum chamber by a lens of 20 cm focal length. The pressure inside the vacuum chamber was usually kept less than 10^{-6} mbar during experiments, by a diffusion pump. A turbo pump was used to evacuate the TOF chamber.

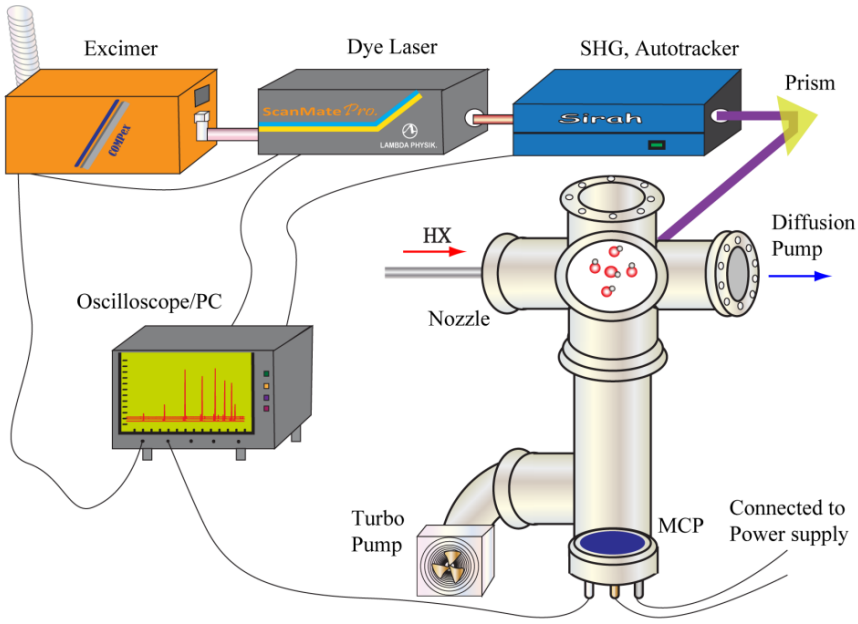

Figure 3.1 2D REMPI- TOF Setup. SHG second harmonic generator; MCP micro-channel plate; PC personal computer.

The gas sample was injected into the chamber through a pulsed nozzle. The nozzle was typically kept open for about 150 ~200 μs. The molecular beam was crossed by a delayed laser beam. Ions formed were extracted into a drift tube, and focused onto a MCP (Micro-Channel Plate) detector. The signal was fed into personal computer, and was processed by a LabVIEW program. The original data were displayed and saved in the oscilloscope/computer (LeCroy WaveSurfer 44MXs-A, 400 MHz) for further handling. Typically, average signals for about 100 pulses were stored.

3.2 Molecular beam

Atomic and molecular beams are fundamental for photochemistry studies. Beam technique formation involves supersonic jet cooling hence preparing of cold molecules (see figure 3.2). The molecular beam was injected into the vacuum chamber (pressure about 10^{-7} mbar) through a pulsed nozzle to create gas pulses. The nozzle diameter was about 500 μm. Backing pressure was typically about 2 bar. Laser pulses were typically delayed about 450~550 μs with respect to the gas pulse to guarantee maximum signals. The repetition rate of gas and laser pulses was typically kept at 10 Hz suitable to avoid overload of vacuum system.

The molecules beam could be further shaped by the use of a skimmer. The molecules in the beam are vibrationally and rotationally cooled with an effective temperature typically, less than about one hundred Kelvin. The number of intermolecular collisions in the beam is near to zero.

The species studied here are HBr, HCl, CH_2Br_2 and CF_3Br.

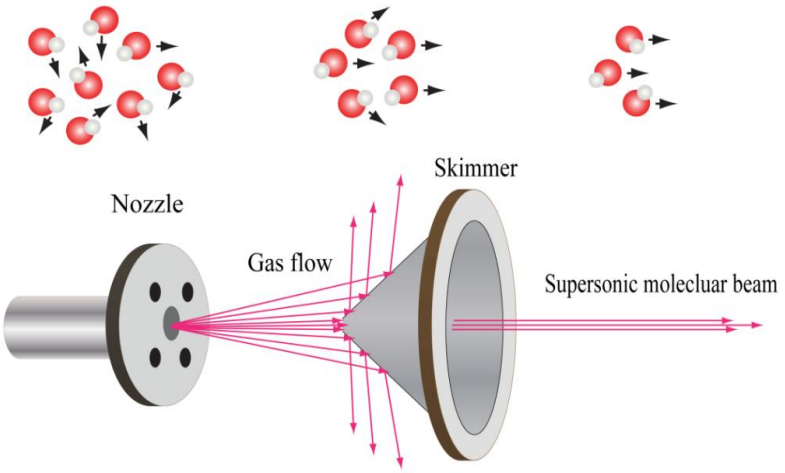

Figure 3.2 Supersonic jet cooling

In all the REMPI experiments, we removed the skimmer to involve rotationally hot molecules as well as in order to detect transitions between high rotational energy levels *J'←←J''*.

3.3 Time of flight

The flight time of an ion in the time of flight (TOF) tube is proportional to the square root of its mass. Thus, the lighter the ion mass is, the earlier it arrives at the MCP detector. The TOF mass spectrometer separates different ions by the difference of arrival time due to the different masses. The ion signal as a function of ion masses is a mass spectrum. In order to find out an unknown masses, normally we can use Equation 3.1 to fit known mass to obtain constant *a* and *b*, then to calculate the mass of unknown ions according to their arrival time using equation 3.2.

$$t = a\sqrt{M} + b \tag{3.1}$$

$$M = \frac{(t-b)^2}{a^2} \tag{3.2}$$

The a and b are constants determined by fitting values of the known masses such H^+, C^+. Here C^+ signal frequently appear due to minor oil impurities in the system. Typically arrival times for some ions along with their masses are listed in table 3.2. As clearly seen in table 3.2, the arrival time increases with mass. An typically assigned mass spectra for HCl is give in figure 3.3

Table 3.2 Time of flight analysis of some ions

Ion	**TOF** (μs)	**M/z** (amu)
H^+	1.71	1
C^+	3.63	12
$^{35}Cl^+$	5.54	35
$H^{35}Cl^+$	5.61	36
$^{37}Cl^+$	5.67	37
$H^{37}Cl^+$	5.73	38

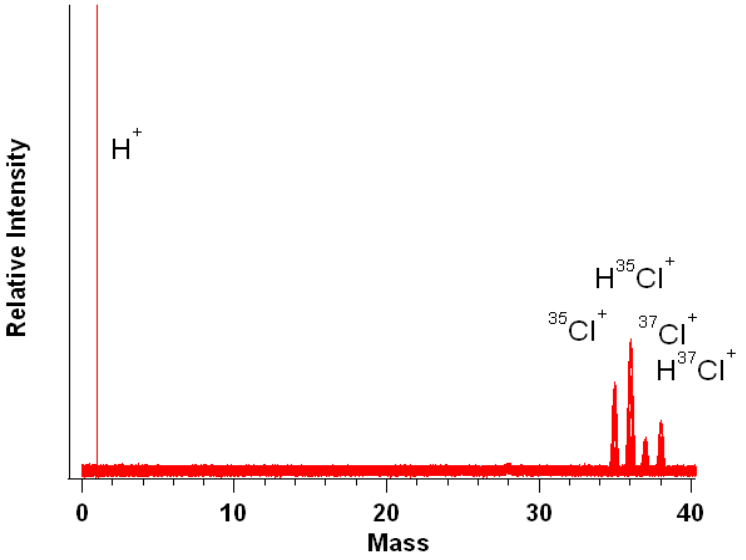

Figure 3.3 Superimposed mass spectra of HCl obtained in (2+n)REMPI

3.4 Equipment control sequences

The experimental control is based on sequences of triggering signals from a computer. According to LabVIEW program, the pulse sequences are shown in figure 3.4. Thus REMPI spectrum could be recorded successfully by scanning the dye laser for specific spectral ranges determined by the dyes.

In the beginning of an experiment, commands are sent to the dye laser to move its grating to a position of the beginning wavelength λ_1, the dye laser generates a chain of 30 or 100 pulses at 10Hz to trigger the opening of the nozzle. Each pulse is delayed and fed to excimer pump laser. After this process, the dye laser changes the wavelength from λ_1 to λ_2 by a specified step size. The above process is repeated until the total wavelength range has been covered. During the scan, the output energy is kept stable at the SHG crystal turned by auto-tracking.

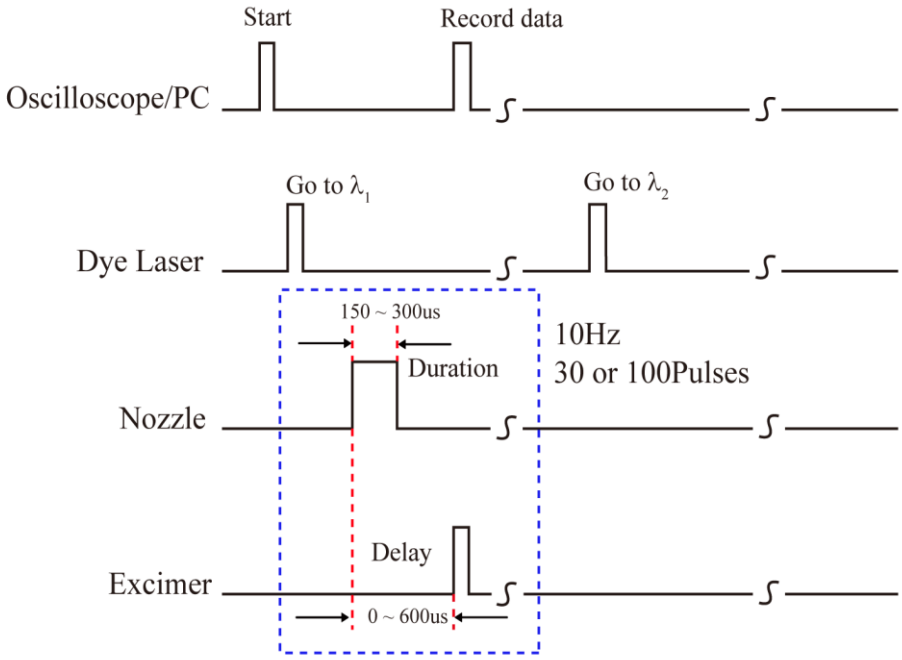

Figure 3.4 Control sequence

3.5 Program design for experiment

Ions formed in the vacuum chamber by laser excitation between a repeller and an extractor plate are directed into a time of flight tube and focused on a MCP detector. The signals are processed by a LabVIEW program in a computerized oscilloscope, which is also used for controlling the laser system and the nozzle.

The program named REMPI.vi designed at the platform of virtual instrument (National Instrument, LabVIEW) is written to control wavelength scanning, as well as to receive and save experimental data. From its control panel, experimental parameters such as the start and end wavelength, scan steps, repeat rate and so on, can be easily set. Raw mass spectral data are saved in a text format on the hard disk for further processing by Igor Pro software. Ion signals as a function of the time of flight, hence masses and laser wavenumbers via two photon excitation are

stored in Igor Pro (see figure 3.3). An procedure 2DREMPIV1.2.ipf is used to integrate signal intensities for different wavenumbers for the various ions such as H^+, $^{35}Cl^+$, $H^{35}Cl^{++}$, $^{37}Cl^+$, $H^{37}Cl^+$ for HCl experiments. Finally REMPI spectra, which show ion signals as a function of excitation wavenumbers can be achieved. Typical REMPI spectra for HCl molecule are shown in figure 3.5.

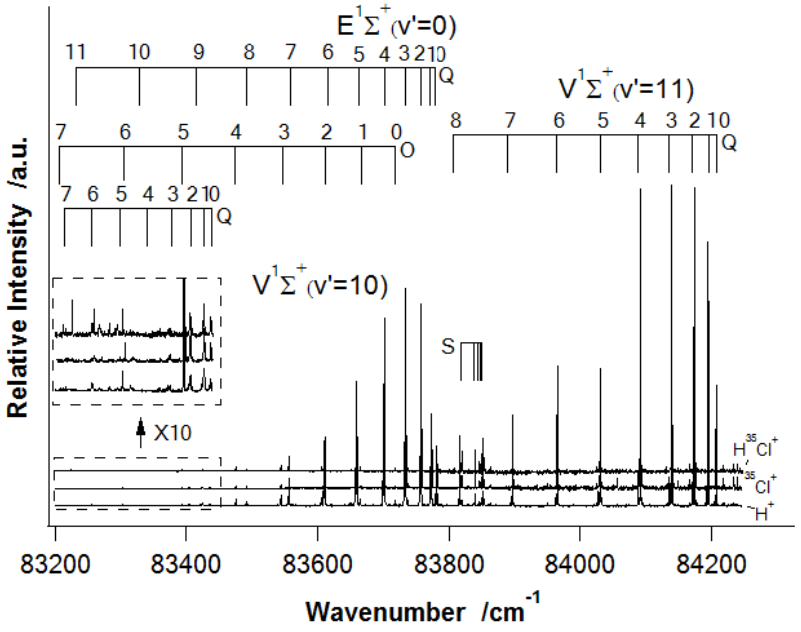

Figure 3.5 (2+n) REMPI spectra for HCl showing resonance exictation to $E^1\Sigma^+(v'=0)$, $V^1\Sigma^+(v'=10,11)$.

4 Analysis

4.1 $F^1\Delta_2$(v'=1) state of HCl

The Rydberg state $F^1\Delta_2$ for HCl and HBr has been studied quite extensively [7,9,36,42,50,51,60,82,83]. (2+n) REMPI spectrum for resonance excitations to the $F^1\Delta_2$(v'=1) and $V^1\Sigma^+$(v'=13,14) states for HCl are shown in figure 4.1. Mass resolved spectra of the $F^1\Delta_2$(v'=1) Q branch are shown in figure 4.2. Near-resonance interaction (NRI) is clearly seen for the J'=8 state of $F^1\Delta_2$(v'=1). This also shows from intensity ratios, $I(^{35}Cl^+)/I(H^{35}Cl^+)$ as a function of J'(see figure 4.3) and alterations in line positions (see figure 4.4) which vary dramatically due to interactions with ion-pair state. Analysis of the ion intensity ratio vs. J' data involving three energy level ($F^1\Delta_2$(v'=1), $V^1\Sigma^+$(v'=13,14)) mixings give an interaction strength W'=0.6 cm^{-1} ($W_H'=W_L'$, given interaction strengths from high and low ion-pair state vibrational energy level have an equal value) and a predissociation constant $\gamma = 0.025$. Deperturbation analysis was also performed. See the summary in table 4.1.

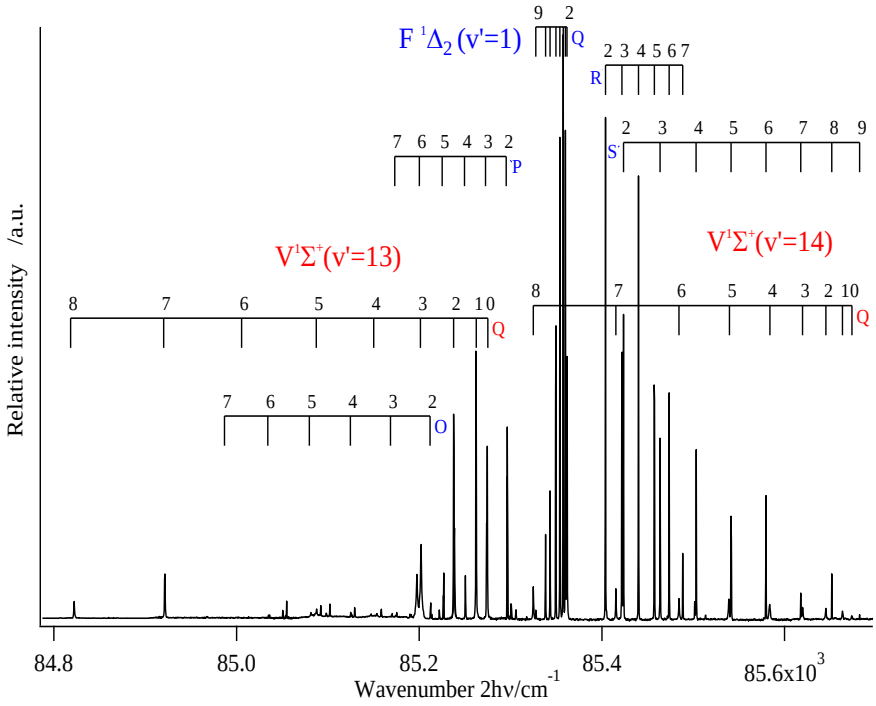

Figure 4.1 (2+n)REMPI spectra for resonance transitions to the HCl $F^1\Delta_2$ (v'=1) and $V^1\Sigma^+$(v'=13、14) states. Figure from reference [84]; Copyright ©2013 Chinese Physical Society.

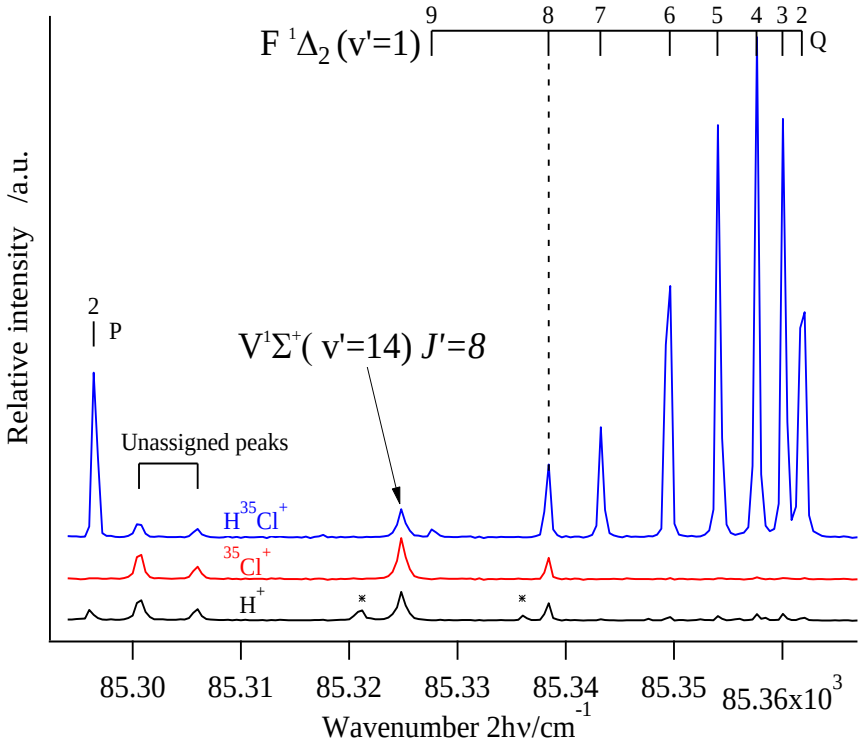

Figure 4.2 Mass-resolved (2+n) REMPI spectra for HCl, $F^1\Delta_2$ (v'=1) Q branch. Figure from reference [84]; Copyright ©2013 Chinese Physical Society.

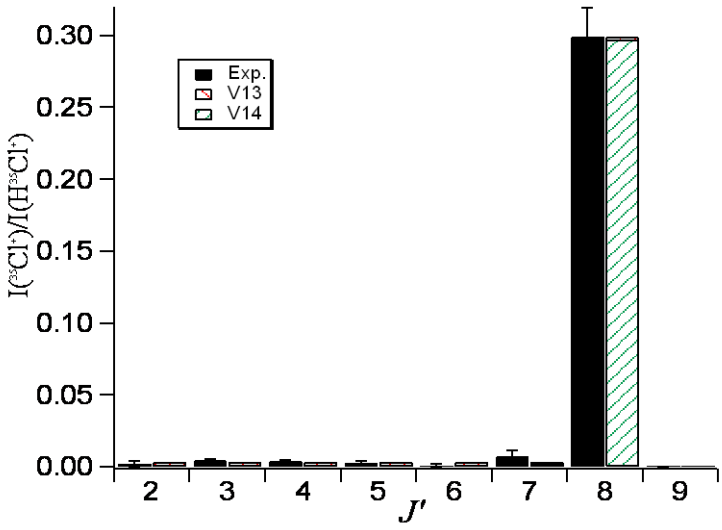

Figure 4.3 Experimental and calculated ion signal intensity ratios for HCl, $F^1\Delta_2(v'=1)$. Figure from reference [84]; Copyright ©2013 Chinese Physical Society.

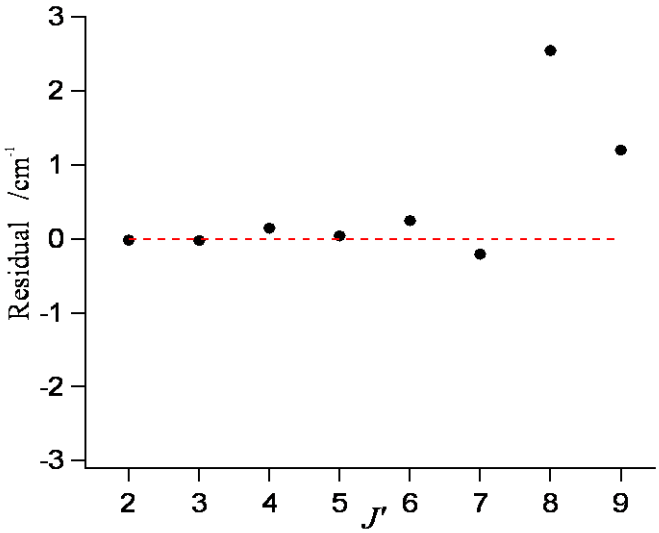

Figure 4.4 The deviation of experimental and unperturbed peak positions for $F^1\Delta_2(v'=1)$. Unperturbed peak postions are simulated by using an ideal rotational constant. The figure taken from reference [84]; Copyright ©2013 Chinese Physical Society.

The nonzero γ value indicates that predissociation is important to $F^1\Delta_2$ state, the evidence of which also was found by Liyanage [9]. Experimental data and its analysis indicates that the majority of the Cl^+ ions formed via the $F^1\Delta_2$(v'=1) J'=8 excitation is attributed to an interaction with the ion-pair state $V^1\Sigma^+$(v'=14).

Table 4.1 Experimental and calculated parameters. All has a unit of cm^{-1} except α and γ.

	$F\ ^1\Delta_2$(v'=1)		
	Exp.	**Intensity ratio**	**Deperturbation**
v_0	85363	-	85363
Bv'	10. 17	-	10. 18
$Dv'\times10^3$	1.9	-	2.2
α	-	0.07	-
γ	-	0.025	-
W_L'	-	0.6	0.9
W_H'	-	0.6/0.65[a]	0.9

[a] Value from reference [36] .

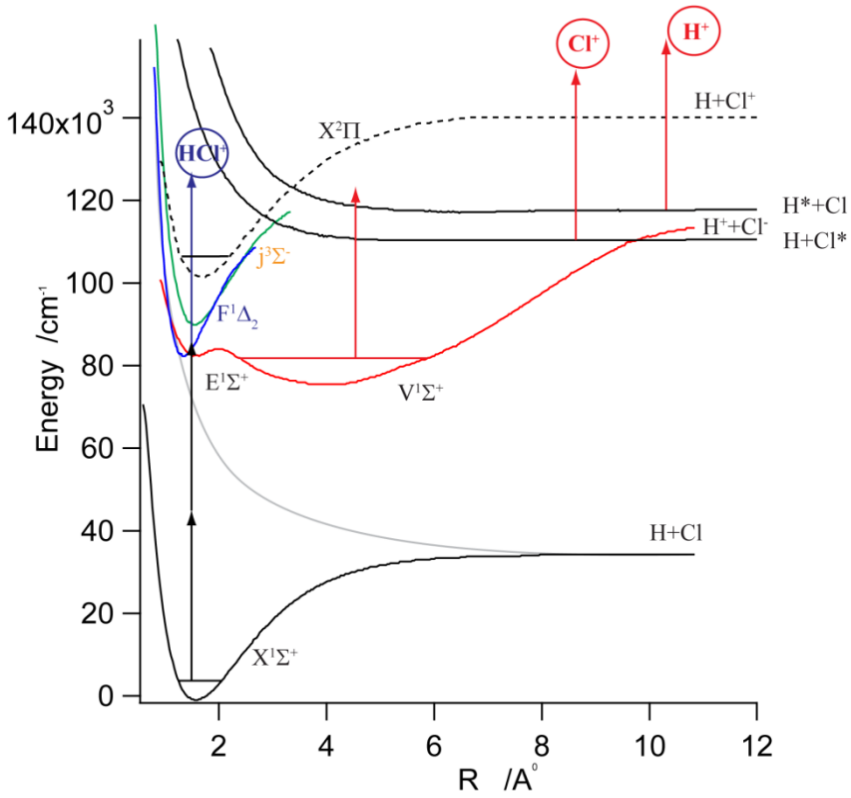

Figure 4.5 Potential energy curves and excitations for HCl. Figure from reference [84]; Copyright ©2013 Chinese Physical Society.

Figure 4.5 shows potential energy curves for HCl and the main photoionization and photodissociation channels via resonance excitation to the Rydberg state $F^1\Delta_2$. Lower probable channels, which may occur, are not shown. Direct ionization of the Rydberg state will give HCl^+ dominantly [42,76], whereas ionization of the ion-pair state will mainly produce the atomic ions, H^+ and Cl^+. Therefore, the majority of the Cl^+ ion formed though $F^1\Delta_2$ state is due to interactions between the Rydberg state $F^1\Delta_2$ and ion-pair state $V^1\Sigma^+$. Fractions of the state mixing as a function of J' are listed in table 4.2.

Table 4.2 Energy differences between $F^1\Delta_2(v'=1)$ and the nearest $V^1\Sigma^+$ ($v'=13$、14) states, interaction strengths W and fraction populations C_F^2, $C_L^2+C_H^2$.

J'	$\Delta E_{F\text{-}L}$ /cm^{-1}	$\Delta E_{H\text{-}F}$ /cm^{-1}	$W_L=W_H$ [a] /cm^{-1}	C_F^2 /%	$C_L^2+C_H^2$ /%
2	121	283.2	1.47	99.98	0.02
3	155.4	259	2.08	99.97	0.03
4	207.6	226.2	2.68	99.97	0.03
5	263.6	185.5	3.29	99.95	0.05
6	336.9	135.1	3.89	99.9	0.1
7	420.3	73.7	4.49	99.62	0.38
8	517.3	-12.7	5.09	79.88	20.12

[a] Derived by Eq.(2.26) for W'=0.6 cm^{-1} listed in table 4.1 from the calculation of ion signal intensity ratios.

4.2 CF_3Br

Absorption and fluorescence spectra of CF_3Br have been studied experimentally [85-88]. We recorded mass spectra of CF_3Br showing the CF_3^+, C^+ and Br^+ ions in (2+1) REMPI for the two-photon resonance excitation region 71320 – 84600 cm^{-1}. CF_3Br was found to be resonantly excited from the ground state (X) to Rydberg states (Ryd.) followed by dissociations to form CF_3/CF_3^* and Br/Br^* (spin-orbit excitation) fragments. (2+1) REMPI of Br and Br* was also detected. Relevant energetics, excitations and photofragmentation processes were presented in reference [18] (see Figure 4.8). The photofragmentation processes are given below (i)-(vi).

(i) $CF_3Br(X) \xrightarrow{2h\nu} CF_3Br^{**}(Ryd.)$

(ii) $CF_3Br^{**}(Ryd.) \rightarrow CF_3 + Br/Br^*$

(iii) $CF_3Br^{**}(Ryd.) \rightarrow CF_3^* + Br/Br^*$

(iv) $Br/Br^{*} \xrightarrow{2h\nu} Br^{**}; Br^{**} \xrightarrow{1h\nu} Br^{+} + e^{-}$

(v) $CF^{*}_{3} \xrightarrow{1h\nu} CF_3^{+} + e^{-}$

(vi) $CF^{*}_{3}Br^{**}(Ryd.) \rightarrow CF_3^{+}Br^{-} \rightarrow CF_3^{+} + Br^{-}$

1D (2+1) REMPI spectra of CF_3^{+} ion is shown and assigned in figure 4.6 along with the absorption spectra of CF_3Br and fluorescence spectra of CF_3^{*}. Br atomic lines due to the transitions Br^{**} ($[^3P]_c$ 5*p*, 6*p*; $[^1D]$, 5*p*)←←Br^{*} ($^2P_{1/2}$), Br^{**}($[^3P]_c$ 5*p*) ←← Br ($4p^2$, $^2P_{3/2}$) are shown in figure 4.7.

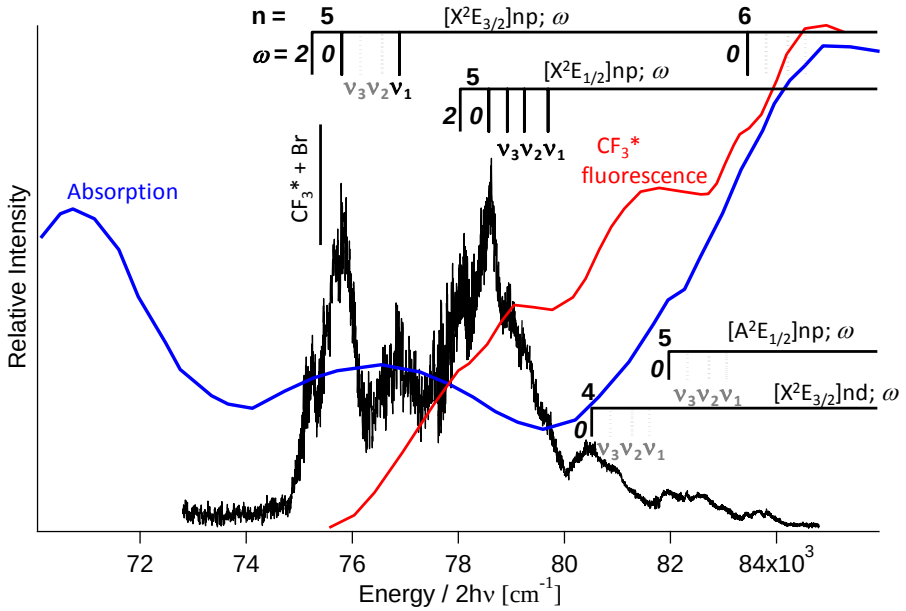

Figure 4.6 CF_3Br: 1D REMPI spectrum of CF_3^{+}, relative absorption spectrum from reference [87] (blue) and fluorescence spectra from reference [86] (red). Threshold for CF_3^{*}+Br formation is marked. Figure taken from reference [18]; Copyright©2011 Elsevier B.V.

The bromine atomic REMPI signals between 70987 - 72012 cm^{-1} are found to be very weak due to insignificant transition to Rydberg states in this region, whereas the bromine signals between 74300 - 84600 cm^{-1} are stronger as a result of medium to strong transitions to *p* and *d* Rydberg states. The Br^{+} ions are formed by (2+1) REMPI of Br/Br^{*} atoms after predissociation of Rydberg states (see channels (ii) - (iv)).

The predissociation channel (ii) is dominant for excitation energies lower than 75332 cm^{-1}. For higher energies channel (vi) competes with (ii) followed by (v) to form CF_3^+ ions. No correlation is found between the 1D REMPI spectra and fluorescence spectrum[86]. Power dependence experiments were performed to obtain consistent slope value of about 2 from log-log plots of CF_3^+ signal intensities as a function of the laser power, suggesting that the CF_3^+ formation only requires two photons. All in all this suggests that the channel (vi) play an important role in the formation of CF_3^+.

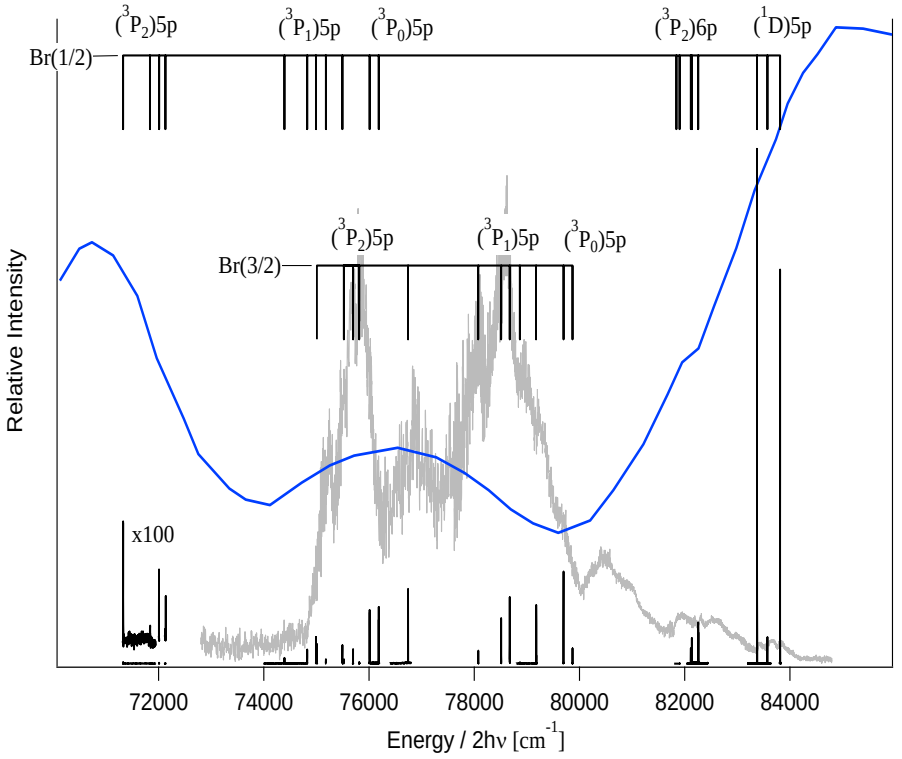

Figure 4.7 CF_3Br: Br^+ 1D REMPI spectrum along with relative absorption spectrum from reference [87](blue). Figure from reference [18]; Copyright©2011 Elsevier B.V.

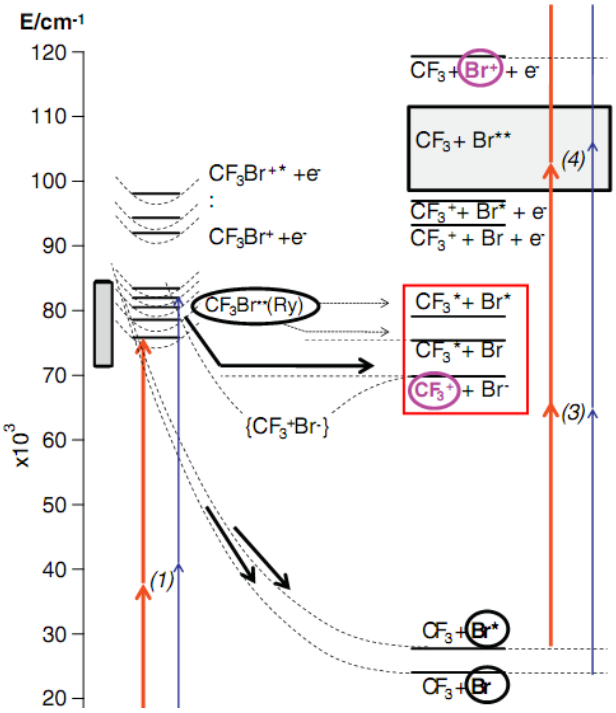

Figure 4.8 CF_3Br: (2+n) REMPI of CF_3Br: energetics, excitations and photofragmentation processes. Figure from reference [18]; Copyright©2011 Elsevier B.V.

4.3 CH_2Br_2

(2 + n) REMPI mass spectra of CH_2Br_2 were recorded for the 71200 - 83680 cm^{-1} resonance excitation range. A typically mass spectrum showing the C^+, CH^+, CH_2^+, $^{79}Br^+$ and $^{81}Br^+$ ions as well as some impurity signals is given in figure 4.9. For excitation larger than 83200 cm^{-1} H_2^+ signals were also found (see figure 4.13). No Br_2^+, CBr^+, CH_2Br^+ and HBr^+ ions were detected. Although a number of experimental and theoretical studies on CH_2Br_2 has been performed [89-95], its spectroscopy and photofragmentation processes are still largely uncertain.

1D (2 + n) REMPI spectra of the ions C^+, CH^+ and CH_2^+ along with the CH_2Br_2 absorption spectrum are shown in figure 4.10. These ions were found for the total scanning region. Particularly large spectral structures in the high energy region (> 79000 cm^{-1}), for example, a broad peak of

C^+ peak, were observed at about 80600 cm^{-1} as well as many sharp CH^+ peaks (see figure 4.11). Analogous broad C^+ peak at 80600 cm^{-1} has also been observed by others [96,97] (see figure 4.11). The sharp CH^+ peaks are assigned to one-photon resonance transitions from the excited state $A^2\Delta(v'=0)$ to the $D^2\Pi(v'=2)$ state. Consequently the excited CH^* ($D^2\Pi$) is ionized to form CH^+ ions by further one-photon absorption [97,98].

Br^+ atomic (2 + 1) REMPI signals due to resonance transitions from the ground state Br ($4p^2$, $^2P_{3/2}$) and spin-orbit excited Br^* ($^2P_{1/2}$) to Br^{**} ($[^3P]_c$ 5*p*; 6*p*) excited states are shown in figure 4.12. Besides these atomic lines, the Br^+ ion spectra also exhibit analogous signal structure as the C^+, CH^+ and CH_2^+ ions. This suggests that all these fragments are formed by photodissociation via the same excited CH_2Br_2 Rydberg states.

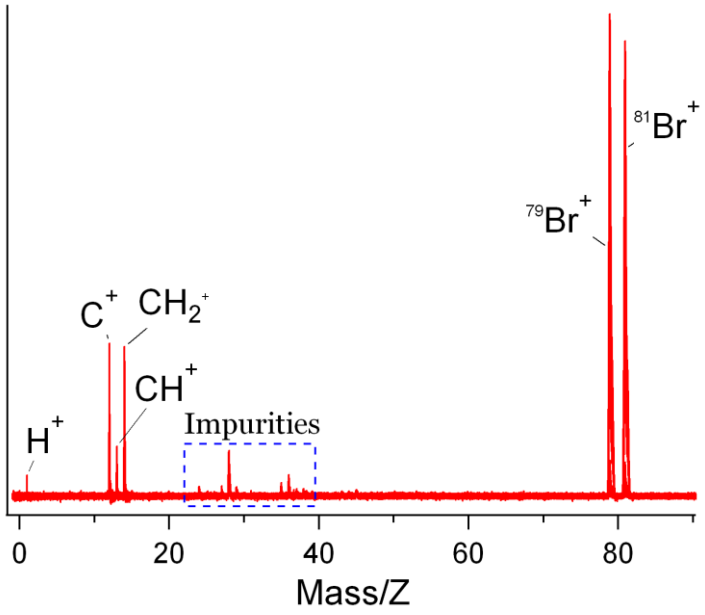

Figure 4.9 1D (2+n) REMPI mass spectra of CH_2Br_2 in the excitation range of 83520-83680 cm^{-1}.

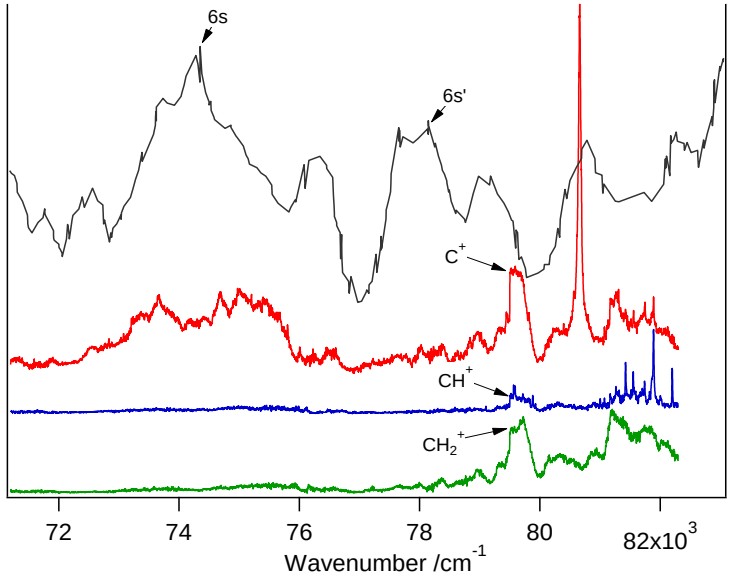

Figure 4.10 CH_2Br_2: C^+, CH^+ and CH_2^+ 1D REMPI spectra along with the absorption spectrum of CH_2Br_2 (the black line) from reference [95].

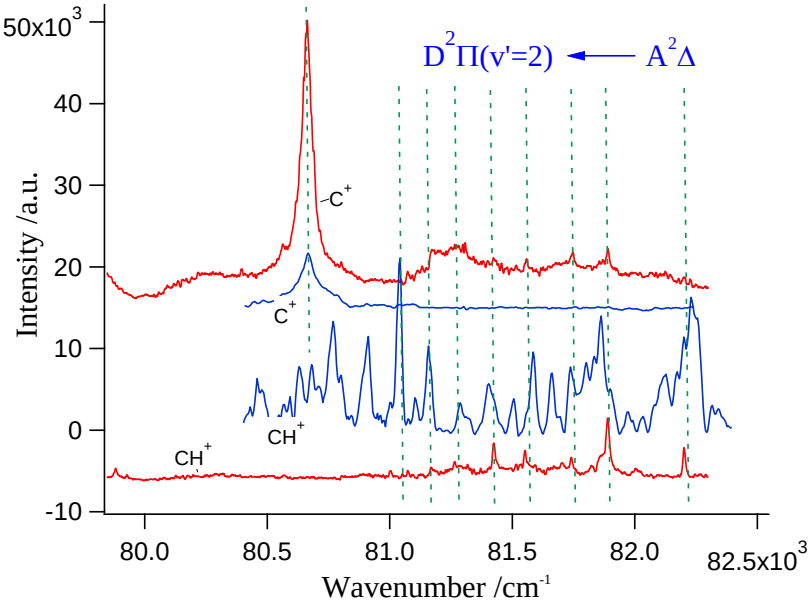

Figure 4.11 One photon ionization of the CH radical formed by photodissocation of CH_2Br_2: Ours (red) and others (blue) [97].

Weak but significant sharp H_2^+ signals were found in the excitation energy region 83200- 83500 cm^{-1} (see figure 4.13). An unusual and a regular H^+ spectrum observed is shown in figure 4.14 (a) and (b), respectively. Analogous "unusual" H^+ spectra, showing different peak structures have also been observed in REMPI spectra of HCl and HBr at 82260 cm^{-1}. The signals at 82260 cm^{-1} primarily corresponded to the H (2+1) REMPI due to the resonance transitions ($^2P_{1/2,\ 3/2}(2p)$; $^2S_{1/2}(2s) \leftarrow\leftarrow {}^2S_{1/2}$ (1s)). However, the regular H^+ spectrum is actually (2+1) REMPI spectra of the impurity HCl molecules in the vacuum chamber.

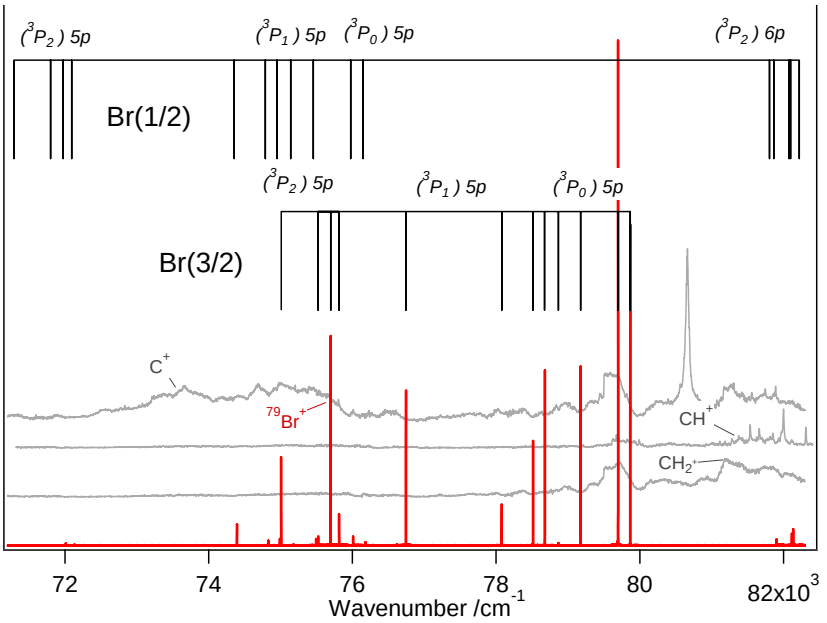

Figure 4.12 CH_2Br_2: Br atomic (2+1) REMPI spectra (red) for the two-photon wavenumber excitation region 71200 – 82300 cm^{-1} along with REMPI spectra of the C, CH^+, CH_2^+ ions (gray). Peaks due to two-photon resonance transitions from Br($4p^5$;$^2P_{1/2}$) (top)and Br($4p^5$;$^2P_{3/2}$) (below)) to ($(^3P_J)_c$; J=2,1,0; 5p, 6p) are marked. $(^3P_J)_c$ are the ion core terms.

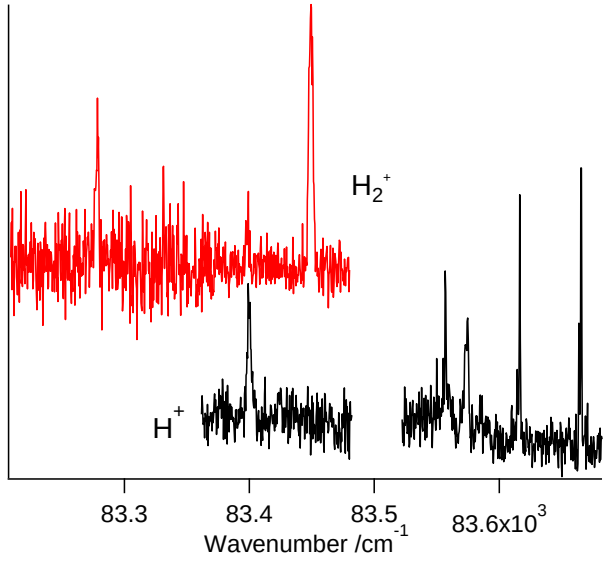

Figure 4.13 CH_2Br_2: H_2^+ (2+n)REMPI spectrum (red) and H^+(2+n)REMPI spectra(black)

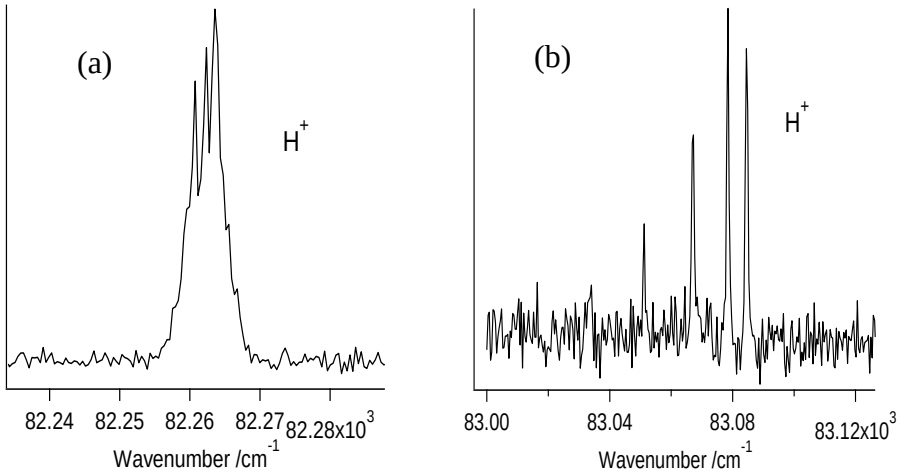

Figure 4.14 CH_2Br_2: H^+ (2+n) REMPI spectra. "Unusual" peak spectral structure in H (2+1)REMPI on the left (a); Regular spectral structure on the right (b).

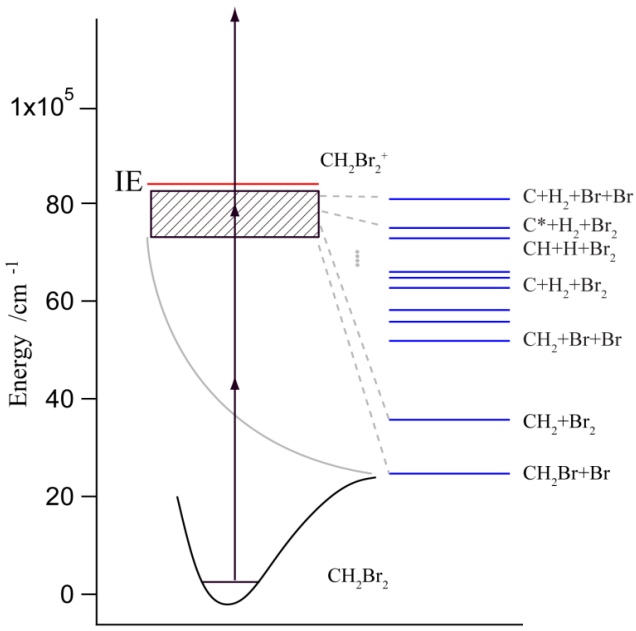

Figure 4.15 CH_2Br_2: (2+n) REMPI of CH_2Br_2: energetics, excitations and fragmentation threshold energies.

Energetics relevant to possible photofragmentation processes are shown in figure 4.15. Based on observed photofragments in our REMPI experiments, the following photofragmentation processes are proposed:

(i) $CH_2Br_2(X) \xrightarrow{1h\nu} CH_2Br + Br/Br^*$

(ii) $CH_2Br_2(X) \xrightarrow{2h\nu} CH_2Br_2{}^{**}(Ryd.)$

(iii) $CH_2Br_2{}^{**}(Ryd.) \rightarrow CH_2 + Br/Br^*$

(iv) $CH_2Br_2{}^{**}(Ryd.) \rightarrow CH^*(A^2\Delta) + Br/Br^*$

(v) $CH^*(A^2\Delta) \xrightarrow{1h\nu} CH^{**}(D^2\Pi) \xrightarrow{1h\nu} CH^+ + e^-$

(vi) $Br/Br^* \xrightarrow{2h\nu} Br^{**}; Br^{**} \xrightarrow{1h\nu} Br^+ + e^-$

(vii) $CH_2Br_2{}^{**}(Ryd.) \rightarrow C^* + H_2 + Br_2$

(viii) $CH_2Br_2{}^{**}(Ryd.) \rightarrow CH + H + Br_2$

(ix) $H \xrightarrow{2h\nu} H^*; H^* \xrightarrow{1h\nu} H^+$

5 Included papers

The papers are included in this thesis:

- Jingming Long, Huasheng Wang, Ágúst Kvaran, ***Photofragmentations, state interactions, and energetics of Rydberg and ion-pair states: Resonance enhanced multiphoton ionization via E and V (B) states of HCl and HBr.*** J. Chem. Phys. , 2013. **138**: p. 044308.

- Jingming Long, Helgi Rafn Hróðmarsson, Huasheng Wang, Ágúst Kvaran, ***Photofragmentations, State Interactions and Energetics of Rydberg and Ion-pair states Two Dimensional Resonance Enhanced Multiphoton Ionization of HBr via Singlet-, Triplet-, Ω = 0 and 2 states***. J. Chem. Phys., 2012. **136**: p. 214315.

- Jingming Long, Huasheng Wang, Ágúst Kvaran, ***Rydberg and Ion-pair states of HBr: New REMPI observations and analysis***. Journal of Molecular Spectroscopy, 2012. **282** p. 20–26.

- Ágúst Kvaran, Kári Sveinbjörnsson, Jingming Long, Huasheng Wang, ***Two-dimensional REMPI of CF_3Br: Rydberg states and photofragmentation channels.*** Chemical Physics Letters, 2011. **516**(1-3): p. 12-16.

- Kristján Matthíasson, Jingming Long, Huasheng Wang, Ágúst Kvaran, ***Two-dimensional resonance enhanced multiphoton ionization of H^iCl; i = 35, 37: State interactions, photofragmentations and energetics of high energy Rydberg states***. The Journal of Chemical Physics, 2011. **134**(16): p. 164302.

Paper I

Jingming Long, Huasheng Wang, Ágúst Kvaran, Photofragmentations, state interactions, and energetics of Rydberg and ion-pair states: Resonance enhanced multiphoton ionization via E and V (B) states of HCl and HBr. J. Chem. Phys., 2013. **138** 044308.

THE JOURNAL OF CHEMICAL PHYSICS **138**, 044308 (2013)

Photofragmentations, state interactions, and energetics of Rydberg and ion-pair states: Resonance enhanced multiphoton ionization via *E* and *V* (B) states of HCl and HBr

Jingming Long, Huasheng Wang, and Ágúst Kvaran[a)]
Science Institute, University of Iceland, Dunhagi 3, 107 Reykjavík, Iceland

(Received 19 November 2012; accepted 2 January 2013; published online 25 January 2013)

$(2 + n)$ resonance enhanced multiphoton ionization mass spectra for resonance excitations to diabatic $E^1\Sigma^+$ (v′) Rydberg and $V\,^1\Sigma^+$ (v′) ion-pair states (adiabatic $B^1\Sigma^+$(v′) states) of H^iCl (i = 35,37) and H^iBr (i = 79,81) were recorded as a function of excitation wavenumber (two-dimensional REMPI). Simulation analyses of ion signal intensities, deperturbation analysis of line shifts and interpretations of line-widths are used to derive qualitative and quantitative information concerning the energetics of the states, off-resonance interactions between the E states and V states, closest in energy as well as on predissociation channels. Spectroscopic parameters for the $E^1\Sigma^+$ (v′)(v′ = 1) for $H^{35}Cl$ and v′ = 0 for $H^{79}Br$ states, interaction strengths for $E - V$ state interactions and parameters relevant to dissociation of the E states are derived. An overall interaction and dynamical scheme, to describe the observations for HBr, is proposed. © *2013 American Institute of Physics*. [http://dx.doi.org/10.1063/1.4776260]

INTRODUCTION

VUV (vacuum ultraviolet)[1,2] and REMPI[3–10] spectroscopic studies of the hydrogen-halides have revealed and led to characterization of large number of electronically excited states. It is customary to group these into valence and Rydberg states. The former group of states consists of low energy repulsive states correlating with the ground atomic and spin-orbit excited halogen species $H + X(^2P_{3/2})/X^*(^2P_{1/2})$ and the ion-pair state $V\,^1\Sigma^+$ which correlates with the ground ionic species $H^+ + X^-$. The dominant configuration of the ion-pair state is $\sigma\pi^4\sigma^*$.[11] The Rydberg states, which have been observed, have ground and/or spin-orbit excited ion cores ($^2\Pi_{3/2,1/2}$) and electronic configurations $\sigma^2\pi^3\,nl\lambda$. Perturbations observed in spectra as line shifts or intensity anomalies[3,4,7,9,12–18] are indicative of state interactions and state mixings which vary largely in nature and magnitude. These are mostly due to Rydberg to repulsive valence state interactions, seen as line-width broadenings due to predissociations or as line shifts and/or intensity alterations due to interactions between Rydberg and ion-pair vibrational states.[3,4,7,9,12–16,18] Rydberg to Rydberg state interactions are also observed.[7,13,18]

The strongest state interactions are observed between the diabatic $E^1\Sigma^+(4p\pi)$ Rydberg states and the diabatic $V\,^1\Sigma^+(\sigma\pi^4\sigma^*)$ ion-pair states which merge together to give the lowest energy $B^1\Sigma^+$ adiabatic potential curves in calculations.[11,19] The B states show double minima closely corresponding to the average internuclear distances of the E and the V states. This shows as dramatic alterations in energy quantum levels, hence vibrational and rotational parameters, from that for unperturbed states.[20] Thus, quantum energy levels of the Rydberg vibrational states are compressed, whereas those for the ion-pair states expand to give lower and higher rotational parameters, respectively.[14] Dynamic studies, by use of photofragment imaging techniques coupled with REMPI for HCl and HBr have revealed various photoionization processes for these states.[21]

Recently, we have used the two-dimensional (2D) REMPI technique to study photofragmentation processes and state interactions for HCl and HBr,[12,15,16,18] which show as signal line shifts, intensity alterations, and line-width broadenings, depending on the total angular momentum quantum numbers (J'). Quantitative analyses based on level-to-level interactions have allowed determinations of interaction strengths and parameters relevant to photofragmentation processes. These analyses revealed that Rydberg states, both interacting with repulsive valence states and ion-pair states, play central role as gateway states for ion-pair state dissociations.[18] Such interaction patterns could be important for molecular photodissociation processes in general. Main emphasis, so far, has been on weak to medium strong near-resonance state interactions between Rydberg and ion-pair states, but stronger off-resonance, homogeneous state interactions, such as those between the $E^1\Sigma^+$ and the $V\,^1\Sigma^+$ states, are likely to be of more importance for fragmentation processes.

In this paper, we present data and analysis relevant to interactions between $E^1\Sigma^+$ and $V\,^1\Sigma^+$ states, predissociation processes involved, as well as energetics of the states, both for HCl and HBr.

EXPERIMENTAL

Following laser excitations ion yield signals were recorded as a function of mass and laser radiation

a)Author to whom correspondence should be addressed. Electronic mail: agust@hi.is. Telephone: +354-525-4694/+354-525-4800. Fax: +354-552-8911.

wavenumber to obtain two-dimensional REMPI data for jet cooled HCl and HBr samples. The apparatus used is similar to that described in Refs. 12, 18, and 22. Experimental parameters are given in the supplementary material.[23] Tunable excitation radiation in the 460–520 nm wavelength region was generated by an excimer laser pumped dye laser system, using a Lambda Physik COMPex 205 excimer laser and a Coherent ScanMatePro dye laser. Frequency doubled radiation was focused into an ionization chamber between a repeller and extractor plates. We operated the jet in conditions that limited cooling in order not to lose transitions from high rotational levels. Thus, undiluted, pure gas samples were used. Ions formed were extracted into a time-of-flight tube and focused onto a MCP detector. Signals were fed into a LeCroy WaveSurfer 44MXs-A, 400 MHz storage oscilloscope and stored as a function of flight time. Average signal levels were evaluated and recorded for a fixed number of laser pulses (typically 100 pulses) to obtain mass spectra. REMPI spectra for certain ions as a function of excitation wavenumber (1D REMPI) were obtained by integrating relevant mass signal intensities. Care was taken to prevent saturation effects as well as power broadening by minimizing laser power. Laser calibration was performed by recording an optogalvanic spectrum, obtained from a built-in neon cell, simultaneously with the recording of the REMPI spectra. Line positions were also compared with the strongest hydrogen chloride rotational lines reported by Green *et al.*[5] The accuracy of the calibration was found to be about $\pm$ 2.0 cm^{-1} on a two-photon wavenumber scale. Intensity drifts during the scan were taken into account, and spectral intensities were corrected accordingly.

RESULT AND ANALYSIS

Spectra and energy levels

Mass-resolved $(2 + n)$ REMPI spectra are shown for the excitation regions 83 200–84 250 cm^{-1} and 85 600–86 440 cm^{-1} for H^{35}Cl in Figs. 1(a) and 1(b), respectively. Peaks due to two-photon resonance transitions from the ground state $X^1\Sigma^+$ to $E^1\Sigma^+(v' = 0, 1)$ (hereafter named $E(0)$ and $E(1)$) and $V\,^1\Sigma^+$ ($v' = 10, 11, 14, 15$) (named $V(10)$–$V(15)$) as well as $g^3\Sigma^-(v' = 1)$ are assigned. The spectra intensities for $V(10)$ and $V(14)$ are noticeably weaker than those for $V(11)$ and $V(15)$. The spectrum for $V(10)$ has been amplified in Fig. 1(a) for clarification. Mass-resolved $(2 + n)$ REMPI spectra are shown for the excitation region 77 540–78 480 cm^{-1} for H^{79}Br in Fig. 1(c). Peaks due to the transitions from the ground state $X^1\Sigma^+$ to $E^1\Sigma^+(v' = 0)$ ($E(0)$) and $V\,^1\Sigma^+$ ($v' = m + 4$, $m + 5$) ($V(m + 4)$ and $V(m + 5)$) are assigned. The spectra intensities for $V(m + 5)$ are noticeably weaker than those for $V(m + 4)$.

Rotational level energies were derived from the line positions and the rotational level energies of the ground state[24,25] (see Fig. 2). When more rotational lines have been observed by others,[2,5,8] these were added to our data. To a first approximation an unperturbed state will show linear behaviour for the energy spacing between neighbour energy levels, $\Delta E_{J',J'-1}$ $(=E(J')-E(J'-1))$, as a function of J' with a slope of $2B_{v'}$, where $B_{v'}$ is the v′-dependent rotational constant. Observed

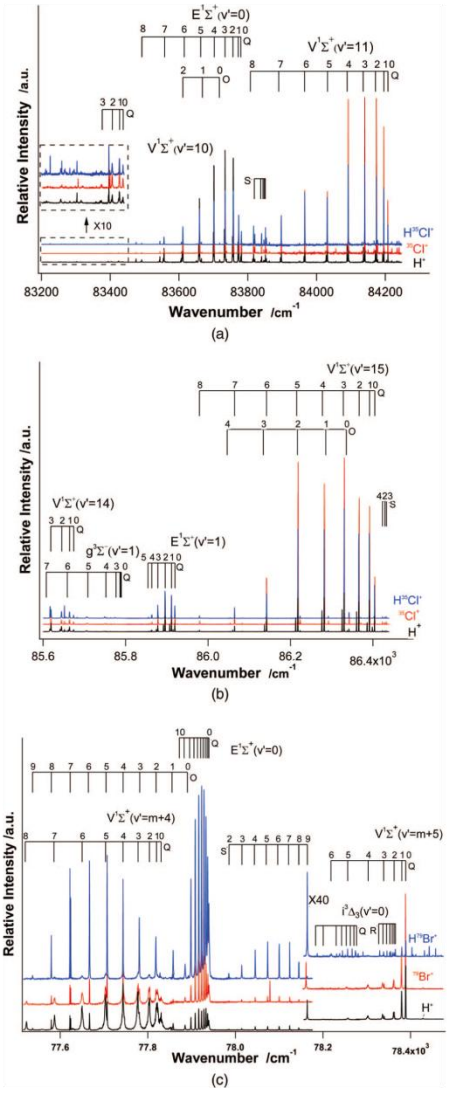

FIG. 1. (a) and (b) HCl: 1D REMPI spectra for H^+, $^{35}Cl^+$, $H^{35}Cl^+$ and J' assignments for rotational peaks corresponding to two-photon resonance excitations to the $E^1\Sigma^+(v' = 0, 1)$, $V^1\Sigma^+(v' = 10, 11, 14, 15)$ and $g^3\Sigma^-(v' = 1)$ states for the excitation regions 83 200–84 250 cm^{-1} (a) and 85 600–86 440 cm^{-1} (b). (c) HBr: 1D REMPI spectra for H^+, $^{79}Br^+$, $H^{79}Br^+$ and J' assignments for rotational peaks corresponding to two-photon resonance excitations to the $E^1\Sigma^+(v' = 0)$, $V^1\Sigma^+(v' = m + 4, m + 5)$ and $i^3\Delta_3(v' = 0)$ states for the excitation region 77 520–78 450 cm^{-1}.

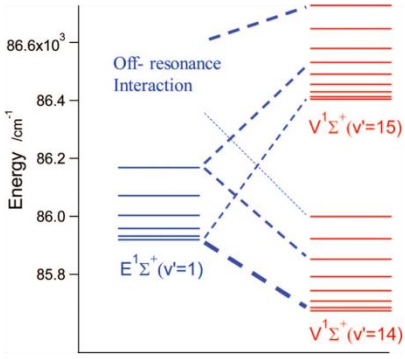

FIG. 2. HCl: Rotational energy levels, derived from the observed REMPI rotational peaks for the $E^1\Sigma^+(v' = 1)$ and $V^1\Sigma^+(v' = 14, 15)$ states. Level-to-level off-resonance interactions between the $V(v')$ ion-pair states and the $E(v')$ Rydberg states are indicated by broken lines. Strength and alterations in state mixings are indicated, roughly, by varying thickness of broken lines.

curvatures or irregular shapes of $\Delta E_{J',J'-1}$ as a function of J' (Fig. 3) indicate strong homogeneous off-resonance state interactions, of which those between the E and the neighbour V states will dominate. The interaction is "repulsive" in nature, showing as an increase in spacing between energy levels with same J' quantum numbers, $\Delta E_{J'}(E, V)$ $(=E_{J'}(E)-E_{J'}(V))$, where $E_{J'}(E)$ and $E_{J'(V)}$ are the energy levels for the E and the V states, respectively (see Table I). The repulsion effect depends on the degree of state mixing which decreases as $\Delta E_{J'}(E, V)$ increases. Therefore, since the spacing between neighbour energy levels ($\Delta E_{J',J'-1}$) in ion-pair states are smaller than the corresponding spacings in Rydberg states, the repulsion effect, hence the mixing, increases with J' for an interaction between a Rydberg state and a higher energy ion-pair state (V_H) but decreases with J' for a corresponding interaction with a lower energy ion-pair state (V_L). This is indicated in Fig. 2 by varying thickness of broken lines in the case of the interactions between $E(1)$ and $V(14)/V(15)$. This effect explains the positive curvatures seen in the $\Delta E_{J',J'-1}$ vs J' plots for the V_H states $V(15)$ and $V(11)$ for HCl and negative curvatures seen for the V_L states $V(14)$ and $V(10)$ for HCl

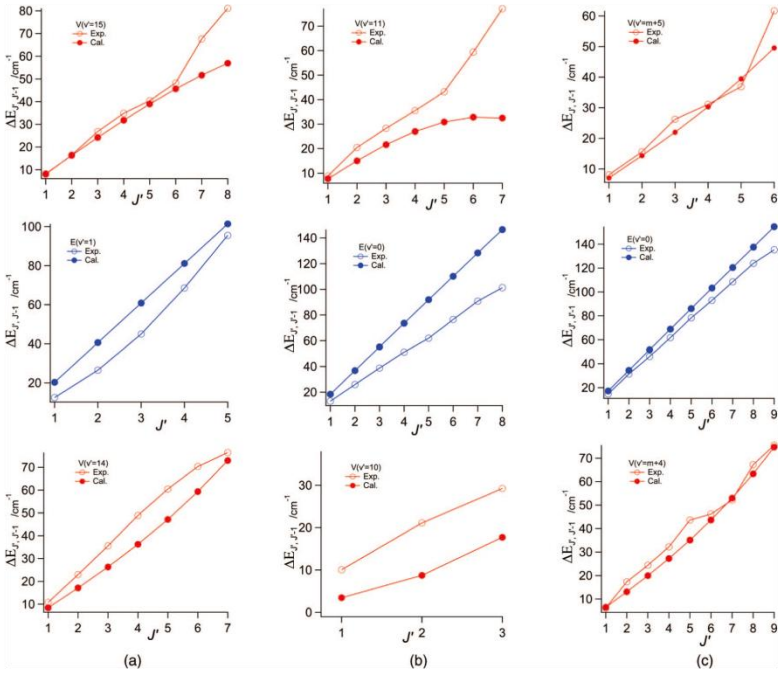

FIG. 3. (a) and (b) $H^{35}Cl$: Spacings between rotational levels ($\Delta E_{J',J'-1}$) as a function of J' for $V^1\Sigma^+(v' = 15)$ ((a), top), $E^1\Sigma^+(v' = 1)$ ((a), middle), $V^1\Sigma^+(v' = 14)$ ((a), bottom), $V^1\Sigma^+(v' = 11)$ ((b), top), $E^1\Sigma^+(v' = 0)$ ((b), middle) and $V^1\Sigma^+(v' = 10)$ ((b), bottom). (c) $H^{79}Br$: Spacings between rotational levels ($\Delta E_{J',J'-1}$) as a function of J' for $V^1\Sigma^+(v' = m + 5)$ ((c), top), $E^1\Sigma^+(v' = 0)$ ((c), middle) and $V^1\Sigma^+(v' = m + 4)$ ((c), bottom). Open circles are derived from observed Q lines (this work and Refs. 2, 5, and 8). Filled circles are derived from deperturbation calculations (see text).

TABLE I. $\Delta E_{J'}$ relevant to off-resonance interactions between $E^1\Sigma^+(v'=1)$ and $V^1\Sigma^+$ ($v'=14,15$) states ($H^{35}Cl$) (left), $E^1\Sigma^+(v'=0)$ and $V^1\Sigma^+$ ($v'=10,11$) states ($H^{35}Cl$) (middle) and $E^1\Sigma^+(v'=0)$ and $V^1\Sigma^+$ ($v'=m+4,m+5$) states (HBr) (right).

	$H^{35}Cl$		$H^{35}Cl$		$H^{79}Br$	
J'	$\Delta E_{J'}(E(1)-V(14))$	$\Delta E_{J'}(V(15)-E(1))$	$\Delta E_{J'}(E(0)-V(10))$	$\Delta E_{J'}(V(11)-E(0))$	$\Delta E_{J'}(E(0)-V(m+4))$	$\Delta E_{J'}(V(m+5)-E(0))$
0	246.0	485.1	346. 4	427.7	110.8	447.8
1	247. 7	480.7	348. 8	423.6	119.3	441.2
2	251.4	470.6	354. 2	418. 1	133.4	425.4
3	260.7	452.5	363.5	407. 7	155.1	405.6
4	280.3	418.8	377.9[a]	392.1	184.6	375.0
5	315.4	363.8	398.2[a]	373.3	219.3	333.5
6			430.8[a]	356.2	266.0	302.2
7			479.0[a]	342.6	322.3	266.0[b]
8			542.9[a]		379.0	235.0[b]
9					438.8	200.0[b]

[a]Values estimated by use of spectroscopic parameters for $V(10)$.
[b]Values estimated by extrapolation.

(Fig. 3). The clear positive curvature seen in the $\Delta E_{J',J'-1}$ vs J' plot for the $E(1)$ state (Fig. 3(a)) is indicative of a larger repulsion interaction (hence larger mixing) with $V(14)$ compared to that with $V(15)$ due to less energy difference (see Table I and Fig. 2). The "close to linear" shape of the $\Delta E_{J',J'-1}$ vs J' plot (Fig. 3(b)) for $E(0)$, on the other hand, suggests that a decreasing repulsion with J' due to mixing with $V(10)$ closely matches an increasing repulsion with J' due to $V(11)$. This is what might be expected from inspection of the energy differences (Table I).

Signal intensities and interpretations

It has been shown that ion signal intensities in one-color REMPI differ largely depending on the resonance excited states of HCl[3,12,15,16] and HBr.[8,18] "Pure" unperturbed Rydberg states mostly result in parent ion signals whereas ion-pair states, mixed with Rydberg states, give both fragment and molecular ions with an increasing contribution of the fragment ion signals as the mixing decreases. Rydberg states mixed with ion-pair states, show fragment ion signals depending on the degree of mixing and interaction strength. Accordingly, ion signal ratios, $I(^iX^+)/I(H^iX^+)$ (X = Cl, Br), are found to vary with J'. In addition, J'-independent contributions to the signal ratios have been found for some Rydberg state excitations. These are believed to be due to dissociation channels.[16]

Figures 4(a) and 4(b) show $I(^{35}Cl^+)/I(H^{35}Cl^+)$ as a function of J' for $H^{35}Cl$, $E(1)$ and $E(0)$, respectively. Similar graphs were obtained for $H^{37}Cl$. The sharply decreasing intensity ratio with J' for $J' \geq 1$, observed for $E(1)$ (Fig. 4(a)) indicates decreasing overall mixing of the $E(1)$ state with ion-pair states as J' increases. This fits with a dominating mixing with the $V(14)$ state in agreement with the conclusion from the energy level shifts, mentioned above. The "close to constant" or "slightly decreasing" intensity ratio vs. J' observed for $E(0)$ (Fig. 4(b)) suggests analogous total mixing of $E(0)$ with $V(10)$ and $V(11)$, also in agreement with the conclusion above. Figure 4(c) shows $I(^{79}Br^+)/I(H^{79}Br^+)$ as a function of J' for $H^{79}Br$, $E(0)$. Similar graph was obtained for $H^{81}Br$. The intensity ratio shows a decrease with J' for J' = 1–5, a minimum near J' = 5–8 and significant increase for J' = 9. This is a clear indication of a decreasing mixing of $E(0)$ with $V(m+4)$ but an increasing mixing with $V(m+5)$ as J' increases.

Intensity ratios vs. J' have been expressed as a function of fractional contributions to the state mixing, derived for two-level interactions.[17] The assumption is made that the ion intensity ratio is a sum of contributions due to interactions between a Rydberg state (1) and two ion-pair vibrational states ($2H$ and $2L$), such as those between the $E(v')$ and the V (V_H and V_L) states. Thus, an expression for $I(X^+)/I(HX^+)$ (X = Cl, Br), depending on the fractional contributions of the V_I ($I = H,L$) states to the state mixing ($c^2_{2I}(I = H,L)$) as well as on parameters which depend on relative rates of ionizations (α_I and γ_I; $I = H,L$) is derived.[12,23] The state mixings depend on the energy spacings between levels with same J' quantum numbers for the Rydberg state (1) and the $2H$ and $2L$ states, respectively, ($\Delta E_{J'}(1,2H)$ and $\Delta E_{J'}(1,2L)$) as well as the corresponding interaction strengths (W_L and W_H). The energy spacings can easily be derived from energy levels (Table I). To a first approximation $W_L = W_H = W$, $\alpha_L = \alpha_H = \alpha$ and $\gamma_L = \gamma_H = \gamma$ is assumed. α measures the rate of the X^+ formation for excitation from the ion-pair states to the HX^+ formation from the Rydberg state, whereas γ represents the rate of X^+ formation via the Rydberg state to that of its formation from the ion-pair states.

The intensity ratios shown in Fig. 4 were fitted to derive the contributions due to the E vs. V_L and E vs. V_H state mixings as well as the α and γ values in the following way.

Careful investigation of the ion intensity ratio for $H^{35}Cl$, $E(1)$ (Fig. 4(a)) revealed that the values for $J' = 0$ and 1, where mixing with $V_L(V(14))$ is dominant, are equal within experimental error. This suggests that the mixings, c^2_1 and c^2_{2L} are equal, i.e., $c^2_1 = c^2_{2L} = 0.5$. This corresponds to a value of $W(E(1), V_L) = \Delta E_{J'}/2$[15] which gives $W \approx 123$ cm^{-1} (see Table I). This allows to estimate the fractional contributions to the mixing as a function of J'. A fit shown in Fig. 4(a), for the parameters listed in Table II, was obtained. This shows that the drop in the intensity ratio for $J' > 1$ is mostly due to the decreasing mixing of $E(1)$ and $V(14)$ as J' increases whereas the contribution due to the $E(1)$ and $V(15)$

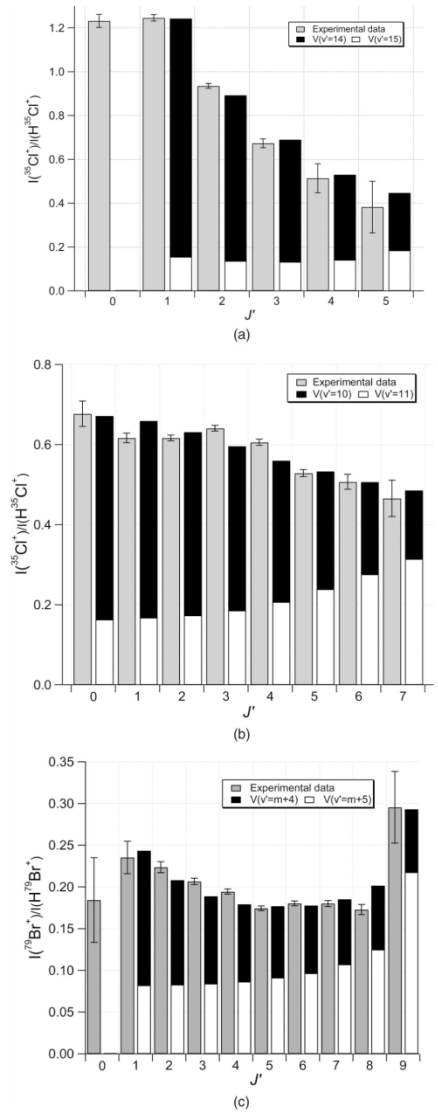

FIG. 4. (a) and (b) $H^{35}Cl$: Relative ion signal intensities, $I(^{35}Cl^+)/I(H^{35}Cl^+)$ vs. J' derived from Q rotational lines of REMPI spectra due to two-photon resonance excitations to the Rydberg states $E^1\Sigma^+$ ($v' = 1$) (a) and $E^1\Sigma^+$ ($v' = 0$) (b). (c) $H^{79}Br$: Relative ion signal intensities, $I(^{79}Br^+)/I(H^{79}Br^+)$ vs. J' derived from Q rotational lines of REMPI spectra due to two-photon resonance excitations to the Rydberg state $E^1\Sigma^+$ ($v' = 0$). Gray columns are experimental values. The black and white columns are calculated values for the contributions due to the interactions of the $E(v')$ states with the lower energy V states (V_L) and the higher energy V states (V_H), respectively.

TABLE II. Parameters used in analysis if relative ion signal intensities $I(^iX^+)/I(H^iX^+)$ ($^iX = {}^{35}Cl$, ^{79}Br) as a function of J' for $(2 + n)$ REMPI of $E^1\Sigma^+(v')$ Rydberg states (see definitions in text).

	$E(v' = 1)$ HCl	$E(v' = 0)$ HCl	$E(v' = 0)$ HBr
W_L (cm^{-1})	123	152	57
W_H (cm^{-1})	123	152	100
α	1.1	0.9	0.2
γ	~0	~0	0.4

mixing is almost unchanged with J'. The value for γ of about zero suggests that dissociation of $E(1)$ is negligible.

The monotonically decreasing intensity ratio as a function of J' observed for $E(0)$, HCl, did not allow an unique solution of all the variables to be derived. Deperturbation analysis of HCl spectral data by Liyanage *et al.*[20] revealed interaction strength of about 187 cm^{-1} for the interaction between $E(0)$ and $V(10)$. An improved fit for the ion intensity ratio vs. J' was obtained by lowering the interaction strength, but accurate value for W could not be determined. Figure 4(b) shows fit of the intensity ratio for $E(0)$ vs J' for the parameters listed in Table II. Clear decrease in the contribution due to the $E(0)$ and $V(10)$ mixing and increase in the contribution due to the $E(0)$ and $V(11)$ mixing is seen as J' increases. This shows a resemblance with results given by Liyanage *et al.*[20,26] derived from deperturbation analysis for $E(0)$, $V(10)$, and $V(11)$, where percentage mixing of the $V(10)$ and $V(11)$ states with $E(0)$ are found to decrease and increase with J', respectively. The results presented by Liyanage *et al.*[26] on the other hand show a decreasing diabatic character of the $E(0)$ state with J' considering also mixing with the Rydberg states $g^3\Sigma_0^-$ and $g^3\Sigma_1^-$ whereas our intensity ratios, which only represent Rydberg to ion-pair state mixing, show close to constant mixing of $E(0)$ as J' increases.[23] A value for γ of about zero suggests that dissociation of $E(0)$ is minor, analogous to that found for $E(1)$.

Analysis of the intensity ratio data for HBr, $E(0)$ revealed decrease in the contribution due to the $E(0)$ and $V(m + 4)$ mixing and increase in the contribution due to the $E(0)$ and $V(m + 5)$ mixing as J' increases as shown in Fig. 4(c). These results were obtained for the parameters listed in Table II. The nonzero value for γ differs from that derived for HCl and suggests that photodissociation via $E(0)$ excitation is of important. This is further supported by line-width analysis (see below).

Line shifts and deperturbations

In cases of weak near-resonance level-to-level interactions, localized line shifts, hence energy level shifts, from regular patterns, can be used to evaluate deperturbed energy levels and interaction strengths. In cases of stronger off-resonance interactions, such as between E and V states, where gradually changing state mixing, is observed, more sophisticated treatment of state interactions needs to be performed. As an attempt to evaluate deperturbed energy levels and spectroscopic constants, as well as interaction strengths, for $E(1)$ for HCl and $E(0)$ for HBr, we performed simplified

TABLE III. Spectroscopic parameters derived from direct analysis of observed spectral lines (Obs.) and from deperturbation analysis (Dep.) (see text), (a) for $E^1\Sigma^+(v' = 1)$, $V^1\Sigma^+(v' = 14, 15)$ ($H^{35}Cl$) by using interaction strengths $W_L = 124\ cm^{-1}$ and $W_H = 126\ cm^{-1}$. Observed values are from this work (above) and from Ref. 3 (below). (b) For $E^1\Sigma^+(v' = 0)$, $V^1\Sigma^+(v' = 10, 11)$ ($H^{35}Cl$) by using interaction strengths $W_L = 191\ cm^{-1}$ and $W_H = 194\ cm^{-1}$. Observed values are from this work and from Ref. 3 (below). (c) For $E^1\Sigma^+(v' = 0)$, $V^1\Sigma^+(v' = m + 4, m + 5)$ ($H^{79}Br$) by using interaction strengths $W_L = 57\ cm^{-1}$ and $W_H = 97\ cm^{-1}$. Observed values are from this work (top) and from Refs. 8 (middle) and 2 (bottom).

(a) For $E^1\Sigma^+(v' = 1)$, $V^1\Sigma^+(v' = 14, 15)$ ($H^{35}Cl$)

	$E(v' = 1)$		$V(v' = 14)$		$V(v' = 15)$	
	Obs.	Dep.	Obs.	Dep.	Obs.	Dep.
ν^0	85 919.7	85 843	85 674	85 773	86 405	86 374
	85 919.8		85 671.7		86 404.6	
B'	6.18	10.1	…	4.2	3.99	4.1
	6.028		6.126		4.01	
$D' \times 10^3$	−69.9	0.12	…	−10	−6.66	12
	−79.55		4.529		−3.648	

(b) For $E^1\Sigma^+(v' = 0)$, $V^1\Sigma^+(v' = 10, 11)$ ($H^{35}Cl$)

	$E(v' = 0)$		$V(v' = 10)$		$V(v' = 11)$	
	Obs.	Dep.	Obs.	Dep.	Obs.	Dep.
ν^0	83 780.4	83 696	83 434.5	83 609	84 207.66	84 125
	83 780.0		83 434.0		84 208.0	
B'	6.40	9.2	5.27	1.6	4.41	3.9
	6.6257		5.05		4.348	
$D' \times 10^3$	0.29	0.39	19.45	−76	−7.58	16
	3.1134		−24.1		−6.872	

(c) For $E^1\Sigma^+(v' = 0)$, $V^1\Sigma^+(v' = m + 4, m + 5)$ ($H^{79}Br$)

	$E(v' = 0)$		$V(v' = m + 4)$		$V(v' = m + 5)$	
	Obs.	Dep.	Obs.	Dep.	Obs.	Dep.
ν^0	77 940.8	77 927	77 830	77 865	78 389	78 369
	77 939.5		…		…	
	77 940		77 832		78 389.5	
B'	7.78	8.6	4	3.2	3.8	3.5
	7.721		…		…	
	7.6		3.9		3.79	
$D' \times 10^3$	0.8	0.16	0.4	−6	−10.7	−9
	0.3		…		…	
	−1.7		−2.1		−1.4	

deperturbation calculations. To a first approximation, we assumed that the perturbation effects on an $E(v')$ state is only due to homogeneous ($\Delta\Omega = 0$) interactions with the V states closest in energy (V_L and V_H). The diagonal matrix elements (unperturbed energy levels) are expressed in terms of the spectroscopic parameters (ν^0_X, B'_X, D'_X; $X = E, V_L, V_H$).[23] The off-diagonal matrix elements are the interaction strengths W_L and W_H. The perturbed energy levels were derived from observed spectral lines and known energy levels for the ground state. The spectroscopic parameters for the E and V states were searched for in the deperturbation procedure. An emphasis was placed on the derivation of the rotational constants B'_E and corresponding energy levels for unperturbed E states. In order to evaluate the B'_E's the number of unknown parameters needed to be lowered. This was done, based on the following criteria:

(i) $0 < D'_E < 0.001$ was assumed. The unperturbed $E(v')$ states belong to a series of Rydberg states, which converges to the ground ionic states $X^2\Pi$. We, therefore, assume that the Rydberg states resemble the ionic states as well as the ground neutral states in terms of centrifugal distortions. The D_e values for $H^{35}Cl^+$ and $H^{81}Br^+$ are $5.47 \times 10^{-4}\ cm^{-1}$ and $3.48 \times 10^{-4}\ cm^{-1}$, respectively.[24,25] The corresponding values for the neutral ground states are $5.3194 \times 10^{-4}\ cm^{-1}$ ($H^{35}Cl$) and $3.457 \times 10^{-4}\ cm^{-1}$ ($H^{81}Br$), respectively.[24,25] Assuming the D's for the $E(v')$ states to be of the same order of magnitude, it is realistic to assume $0 < D'_E < 0.001$.

(ii) $W_L \leq W_H$ was assumed for W_L and W_H close to the W values derived from the intensity ratio analysis, mentioned earlier. In the diabatic approximation, the state interaction strength (W) is proportional to the vibrational wavefunction overlap[11,20] for the Rydberg vs. the ion-pair states. For a fixed $E(v')$ state, this corresponds to an increasing value of W as a function of v' for the ion-pair state, hence $W_L \leq W_H$.

As a test of this method, we calculated B' of $E(0)$ ($B'_{E(0)}$) for HCl as a function of W_L and W_H.[23] A value of $B'_{E(0)} = 8.6\ cm^{-1}$ was obtained by using equal interaction strengths

of 187 cm^{-1}, corresponding to the W_L derived by Liyanage *et al.*[20] in a more detailed deperturbation analysis. This is close to their value of $B'_{E(0)} = 8.37$ cm^{-1}. These B'_E values are significantly larger than those derived from the perturbed energy levels ($B'_{E(0)} = 6.6257$ cm^{-1})[3] but smaller than B_e values for the ground ionic state (9.9566 cm^{-1}) and the ground neutral state (10.59341 cm^{-1})[24] as well as B'_v values of unperturbed Rydberg states of HCl, which are typically $B'_v = 9$–10.5 cm^{-1}.[3] Considering the criteria (i) and (ii), on the other hand, values of $B'_{E(0)} = 9.2 \pm 0.3$ cm^{-1} and $D'_{E(0)} = 3.9 \times 10^{-4}$ cm^{-1} were obtained for $W_L = 191$ cm^{-1} and $W_H = 194$ cm^{-1} (see Table III).

Analogous analysis of the data for $E(1)$(HCl) and $E(1)$(HBr) gave $B'_{E(1)} = 10.1 \pm 0.2$ cm^{-1} for $W_L = 124$ cm^{-1} and $W_H = 126$ cm^{-1} (HCl) and $B'_{E(0)} = 8.6 \pm 0.2$ cm^{-1} for $W_L = 57$ cm^{-1} and $W_H = 97$ cm^{-1} (HBr) (see Table III). The latter value is an increase from the value of 7.721 cm^{-1} for the perturbed state.[8] It can be compared to the B_e values of 8.072 cm^{-1} and 8.46488 cm^{-1} for the ground ionic and neutral states of HBr, respectively,[24] as well as values of B'_v for unperturbed Rydberg states ($B'_v \approx 7.6$–8.7 cm^{-1}).[2,8,10]

Further conclusions, which can be drawn from the deperturbation analysis (see Table III and Fig. 3), are as follows: (a) Term values (band origins), ν^0, for all the E states and the higher energy V states (V_H) decrease from the observed ν^0-values whereas an increase is observed for the V_L's. Therefore, the energy spacing between the vibrational states, V_L and V_H, which has been found to be unusually large,[9,14] is found to decrease. The energy spacing between the HCl, $E(0)$ and $E(1)$ states increases slightly to about 2147 cm^{-1}. (b) Rotational constants (B'), hence rotational energy level spacing ($\Delta E_{J',J'-1}$), for all the V_I ($I = L,H$) states lower (or stay unchanged) compared to values observed for the perturbed states, in agreement with expectations.[14] (c) The second order rotational constants, D', increase on an absolute scale for all V_H states and lower for all the V_L 's as a result of deperturbation. For HCl the D' values in fact switch sign from negative to positive values for V_H and from positive to negative values for V_L, which corresponds to a change in $\Delta E_{J',J'-1}$ vs J' plots from showing positive to negative curvatures for V_H and vice versa for V_L (see Fig. 3). These observations are clear indications of further perturbations due to interactions of the V states with other Rydberg states, not taken account of in the deperturbation calculations.

Line-widths

Rotational line-widths of the $E(v')(v' = 0,1)$ and $V(v')$ ($v' = 10,11,14$, and 15) states REMPI spectra for H^iCl are all close to our detection limit of about 0.3–0.4 cm^{-1} which suggests that predissociation is not of major importance for these states[18,27] (see Figs. 1(a) and 1(b)). This agrees with the derivation of $\gamma \approx 0$ values, hence negligible dissociation, for the E states according to the intensity ratio analysis mentioned before. The lifetime (τ), being inversely proportional to the line-width as[18,27,28]

$$\tau(\text{ps}) = 5.3/\,\Gamma(\text{cm}^{-1}) \qquad (1)$$

gives the lower limit value for τ of about 13 ps.

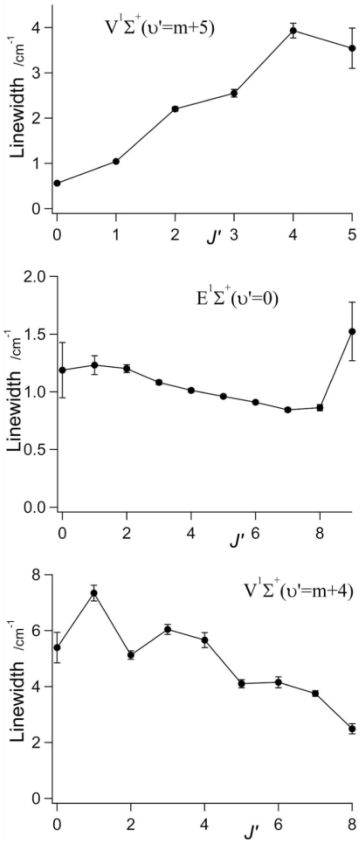

FIG. 5. HBr: Rotational line-widths vs J' derived from Q lines of $H^{79}Br$ REMPI spectra for $V^1\Sigma^+(v' = m + 5)$ (top), $E^1\Sigma^+(v' = 0)$ (middle) and $V^1\Sigma^+(v' = m + 4)$ (bottom).

Line-widths of the $E(0)$ and $V(m + i)$ ($i = 4$ and 5) state spectra for H^iBr, on the other hand, are larger, suggesting that predissociaton processes are significant in agreement with the conclusion derived from the intensity ratio analysis which gave $\gamma \neq 0$. Furthermore, the line-widths vary significantly depending on the rotational levels as seen in Figs. 1(c) and 6. Those for the Q lines of the $V(m + 5)$ spectrum increase with J' whereas those for the $V(m + 4)$ spectrum decrease with J' (Figs. 5(a) and 5(c)). The line-widths for the Q lines of the $E(0)$ spectrum (Fig. 5(b)), generally are smaller and show close correspondence to the intensity ratios as a function of J' (Fig. 4(c)) previously explained to reflect interactions with $V(m + 4)$ as well as $V(m + 5)$. Because of the inverse relationship between τ and Γ (Eq. (1)), the lifetimes of the $E(0)$ state rotational levels generally are longer than those for the $V(m + 4)$ and $V(m + 5)$ state levels

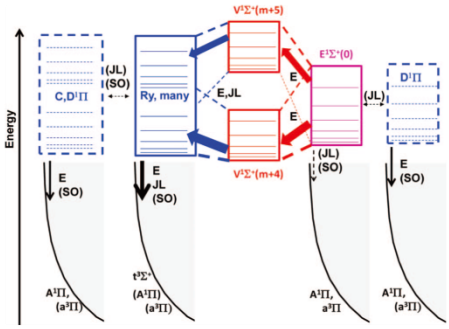

FIG. 6. Semischematic figure, showing the HBr energetics, state interactions and energy transfers of relevance to the data presented (see text). Electrostatic, rotational and spin-orbit couplings are marked *E*, *JL* and *SO*, respectively. Red boxes represent the ion-pair states. Blue and purple boxes are Rydberg states and black curves are repulsive states. The blue box with solid lines represents a manifold of many Rydberg states, which couple with the ion-pair states. The blue boxes with broken lines are gateway states with respect to predissociation of other states. Relative importance of couplings and transfers are indicated by different boldness of arrows and broken lines as well as by use of brackets or not. The colored arrows indicate the major paths towards predissociation for the *V* and *E* states.

and the lifetimes of the rotational levels for the $V(m+5)$ and $V(m+4)$ decrease and increase with J', respectively. The alteration in lifetimes, hence line-widths, with J' and the dependence on electronic states reflects different rates of predissociation. This observation suggests that the predissociation of the $E(0)$ state is primarily determined by that of the $V(m+5)$ and $V(m+4)$ states following the state interactions described earlier. Large average internuclear distance of the *V* state makes crossing to repulsive states, hence direct predissociation, highly improbable.[18] The Rydberg states, on the other hand, are either in close vicinity of, or crossed by, repulsive states to make predissociation processes more probable. Possible interactions involved in indirect predissociations of the $E(0)$, $V(m+4)$, and $V(m+5)$ states are presented semischematically in Fig. 6.[28,29] These involve strong electrostatic interactions (*E*) between the $E(0)$ and the *V* states, electrostatic (*E*) and rotational (*JL*) couplings of the *V* states with a manifold of a large number of Rydberg states, such as $g^3\Sigma_0^-$, $g^3\Sigma_1^-$, $e^3\Sigma_0^+$, $e^3\Sigma_1^+$, $j^3\Delta$, $F^1\Delta$[28,29] as well as predissociations of the Rydberg states or gateway-Rydberg states due to state couplings of different nature (*E*, *JL*, *SO*) and strengths. Generally, the *E*-interactions are the strongest, whereas the *JL*- and *SO*-interactions are weak-to-intermediate (Hunds cases (a)-(b)).[28] Furthermore, the Franck-Condon-overlap of the Rydberg states with the $t^3\Sigma^+$ states exceeds that of the overlap with the $A^1\Pi$ and $a^3\Pi$ states.[29] The major direct predissociation channels, therefore, are believed to be those involving *E*-interactions between Rydberg states, such as the $e^3\Sigma_0^+$and $e^3\Sigma_1^+$ states, and the repulsive $t^3\Sigma^+$ states. *C* and $D\,^1\Pi_1$ state spectra for HBr (as well as for HCl) all show diffuse structures,[2,3] which suggests that these states could act as gateway states by strong *E*-interactions with the $A^1\Pi$ state following weaker *JL* (and *SO*) couplings with other Rydberg states. All in all, this shows that quantum interference effects, involving several states, play important role in the overall interaction process and that the major paths of indirect predissociations of the $E(0)$, $V(m+4)$ and $V(m+5)$ states are likely to be as indicated by the arrows shown in Fig. 6.

CONCLUSIONS

$(2+n)$, 2D REMPI spectra of $H^iCl(i=35,37)$ and $H^iBr(i=79,81)$ for resonance transitions to $E^1\Sigma^+(v')$ Rydberg states and $V^1\Sigma^+$ (v') states, close in energy, have been recorded and analysed in terms of state interactions, energetics, and photofragmentations. Spectra show large perturbation effects due to J' dependent Rydberg-to-ion-pair state interactions as line shifts and intensity alterations for HCl and HBr as well as line broadenings for HBr. The data are analysed in terms of off-resonance interactions between the $E^1\Sigma^+(v')$ states and two $V^1\Sigma^+$ (v') states, closest in energy, one higher (V_H) and one lower (V_L) in energy. Variation in ion signal intensity ratios $(I(^iX^+)/I(H^iX^+))$ as a function of J' are shown to be due to altering contributions of the two Rydberg-to-ion-pair state mixing depending on energy differences between quantum levels for the same J' quantum numbers. In cases when different observations depend on the same dynamical properties (state interactions and/or photofragmentations) analysis results are found to be supportive in nature. Thus, simulation calculations of ion signal intensity ratios and deperturbation analyses of line positions as a function of J' reveal interaction strengths as well as deperturbed spectroscopic parameters for the $E^1\Sigma^+(v'=1)$ state of HCl and the $E^1\Sigma^+(v'=0)$ state of HBr. Analysis of both intensity ratios and line-widths are indicative of predissociation processes being negligible for the HCl, $E^1\Sigma^+(v'=0,1)$ states but of significant importance for the HBr, $E^1\Sigma^+(v'=0)$ state. An overall interaction and dynamical scheme, to describe the observations for HBr is proposed, where the ion-pair states play central role in the dissociation of the *E* states via off-resonance interactions followed by predissociation of Rydberg states.

ACKNOWLEDGMENTS

The financial support of the University Research Fund, University of Iceland, the Icelandic Science Foundation as well as the Norwegian Research Council is gratefully acknowledged.

[1]S. G. Tilford, M. L. Ginter, and A. M. Bass, J. Mol. Spectrosc. **34**, 327 (1970); S. G. Tilford, M. L. Ginter, and J. T. Vanderslice, *ibid.* **33**, 505 (1970); S. G. Tilford and M. L. Ginter, *ibid.* **40**, 568 (1971); J. B. Nee, M. Suto, and L. C. Lee, J. Chem. Phys. **85**, 4919 (1986); **85**, 719 (1986).
[2]D. S. Ginter, M. L. Ginter, and S. G. Tilford, J. Mol. Spectrosc. **90**, 152 (1981).
[3]D. S. Green, G. A. Bickel, and S. C. Wallace, J. Mol. Spectrosc. **150**, 303 (1991).
[4]D. S. Green, G. A. Bickel, and S. C. Wallace, J. Mol. Spectrosc. **150**, 354 (1991); D. S. Green and S. C. Wallace, J. Chem. Phys. **96**, 5857 (1992); Á. Kvaran and H. Wang, J. Mol. Spectrosc. **228**, 143 (2004).
[5]D. S. Green, G. A. Bickel, and S. C. Wallace, J. Mol. Spectrosc. **150**, 388 (1991).
[6]E. d. Beer, B. G. Koenders, M. P. Koopmans, and C. A. d. Lange, J. Chem. Soc. Faraday Trans. **86**, 2035 (1990); E. d. Beer, W. J. Buma, and C. A. d. Lange, J. Chem. Phys. **99**, 3252 (1993); T. A. Spiglanin, D. W. Chandler,

and D. H. Parker, Chem. Phys. Lett. **137**, 414 (1987); Á. Kvaran, H. Wang, and Á. Logadóttir, *Recent Research Development in Physical Chemistry* (Transworld Research Network, 1998), vol. 2, p. 233; Á. Kvaran, H. Wang, and B. G. Waage, Can. J. Phys. **79**, 197 (2001); H. Wang and Á. Kvaran, J. Mol. Struct. **563-564**, 235 (2001); Á. Kvaran and H. Wang, Mol. Phys. **100**, 3513 (2002); S. A. Wright and J. D. McDonald, J. Chem. Phys. **101**, 238 (1994); S. T. Pratt and M. L. Ginter, J. Chem. Phys. **102**, 1882 (1995); K. Matthiasson, H. S. Wang, and A. Kvaran, J. Mol. Spectrosc. **255**, 1 (2009).
[7]Y. Xie, P. T. A. Reilly, S. Chilukuri, and R. J. Gordon, J. Chem. Phys. **95**, 854 (1991).
[8]R. Callaghan and R. J. Gordon, J. Chem. Phys. **93**, 4624 (1990).
[9]Á. Kvaran, H. Wang, and Á. Logadóttir, J. Chem. Phys. **112**, 10811 (2000).
[10]J. Long, H. Wang, and A. Kvaran, J. Mol. Spectrosc. **282**, 20 (2012).
[11]H. Lefebvre-Brion, H. P. Liebermann, and G. J. Vazquez, J. Chem. Phys. **134**, 204104 (2011).
[12]K. Matthiasson, J. Long, H. Wang, and A. Kvaran, J. Chem. Phys. **134**, 164302 (2011).
[13]D. S. Ginter and M. L. Ginter, J. Mol. Spectrosc. **90**, 177 (1981).
[14]Á. Kvaran, Á. Logadóttir, and H. Wang, J. Chem. Phys. **109**, 5856 (1998).
[15]Á. Kvaran, K. Matthíasson, H. Wang, A. Bodi, and E. Jonsson, J. Chem. Phys. **129**, 164313 (2008).
[16]S. Kauczok, C. Maul, A. I. Chichinin, and K. H. Gericke, J. Chem. Phys. **133**, 024301 (2010).
[17]A. Kvaran, K. Matthiasson, and H. Wang, J. Chem. Phys. **131**, 044324 (2009).
[18]J. Long, H. R. Hrodmarsson, H. Wang, and A. Kvaran, J. Chem. Phys. **136**, 214315 (2012).
[19]M. Bettendorff, S. D. Peyerimhoff, and R. J. Buenker, Chem. Phys. **66**, 261 (1982); D. M. Hirst and M. F. Guest, Mol. Phys. **41**, 1483 (1980); C. Maul, A. I. Chichinin, and K.-H. Gericke, J. At., Mol., Opt. Phys. **2011**, 410108 (2011).
[20]R. Liyanage, R. J. Gordon, and R. W. Field, J. Chem. Phys. **109**, 8374 (1998).
[21]A. I. Chichinin, C. Maul, and K. H. Gericke, J. Chem. Phys. **124**, 224324 (2006); A. I. Chichinin, P. S. Shternin, N. Godecke, S. Kauczok, C. Maul, O. S. Vasyutinskii, and K. H. Gericke, *ibid.* **125**, 034310 (2006); C. Romanescu and H. P. Loock, Phys. Chem. Chem. Phys. **8**, 2940 (2006); J. Chem. Phys. **127**, 124304 (2007); C. Romanescu, S. Manzhos, D. Boldovsky, J. Clarke, and H. Loock, *ibid.* **120**, 767 (2004).
[22]A. Kvaran, K. Sveinbjornsson, J. Long, and H. Wang, Chem. Phys. Lett. **516**, 12 (2011); A. Kvaran, H. Wang, K. Matthiasson, and A. Bodi, J. Phys. Chem. A **114**, 9991 (2010).
[23]See supplementary material at http://dx.doi.org/10.1063/1.4776260 for intensity ratio analysis, typical experimental parameters, Hamiltonian matrix elements, contour plots showing B'_E as a function W_L and W_H, $I(^{35}Cl^+)/I(H^{35}Cl^+)$ vs. J' for $H^{35}Cl$, $E(0)$, fractional state mixing of $E(0)$, $V(10)$, and $V(11)$ for $H^{35}Cl$.
[24]NIST (National Institute of Standards and Technology) Chemistry WebBook, online at http://webbook.nist.gov/chemistry/form-ser.html.en-us.en.
[25]K. P. Huber and G. Herzberg, *Constants of Diatomic Molecules* (Van Nostrand-Reinhold, New York, 1979).
[26]See supplementary material in Ref. 20.
[27]K. Matthiasson, H. Wang, and A. Kvaran, Chem. Phys. Lett. **458**, 58 (2008).
[28]H. Lefebvre-Brion and R. W. Field, *The Spectra and Dynamics of Diatomic Molecules* (Elsevier Academic, 2004).
[29]M. H. Alexander, X. N. Li, R. Liyanage, and R. J. Gordon, Chem. Phys. **231**, 331 (1998).

Paper II

Jingming Long, Helgi Rafn Hróðmarsson, Huasheng Wang, Ágúst Kvaran, Photofragmentations, State Interactions and Energetics of Rydberg and Ion-pair states Two Dimensional Resonance Enhanced Multiphoton Ionization of HBr via singlet-, triplet-, $\Omega = 0$ and 2 states. J. Chem. Phys., 2012. **136**: p. 214315.

Photofragmentations, state interactions, and energetics of Rydberg and ion-pair states: Two-dimensional resonance enhanced multiphoton ionization of HBr via singlet-, triplet-, $\Omega = 0$ and 2 states

Jingming Long, Helgi Rafn Hróðmarsson, Huasheng Wang, and Ágúst Kvaran[a)]
Science Institute, University of Iceland, Dunhagi 3, 107 Reykjavík, Iceland

(Received 15 March 2012; accepted 16 May 2012; published online 7 June 2012)

Mass spectra were recorded for one-colour resonance enhanced multiphoton ionization (REMPI) of H^iBr ($i = 79, 81$) for the two-photon resonance excitation region 79 040–80 300 cm^{-1} to obtain two-dimensional REMPI data. The data were analysed in terms of rotational line positions, intensities, and line-widths. Quantitative analysis of the data relevant to near-resonance interactions between the $F^1\Delta_2(v' = 1)$ and $V^1\Sigma^+(v' = m + 7)$ states gives interaction strengths, fractional state mixing, and parameters relevant to dissociation of the F state. Qualitative analysis further reveals the nature of state interactions between ion-pair states and the $E^1\Sigma^+$ $(v' = 1)$ and $H^1\Sigma^+(v' = 0)$ Rydberg states in terms of relative strengths and J' dependences. Large variety in line-widths, depending on electronic states and J' quantum numbers, is indicative of number of different predissociation channels. The relationship between line-widths, line-shifts, and signal intensities reveals dissociation mechanisms involving ion-pair to Rydberg state interactions prior to direct or indirect predissociations of Rydberg states. Quantum interference effects are found to be important. Moreover, observed bromine atom (2 + 1) REMPI signals support the importance of Rydberg state predissociation channels. A band system, not previously observed in REMPI, was observed and assigned to the $k^3\Pi_0(v' = 0) \leftarrow\leftarrow X$ transition with band origin 80 038 cm^{-1} and rotational parameter $B_{v'} = 7.238$ cm^{-1}.
 [http://dx.doi.org/10.1063/1.4723810]

INTRODUCTION

Photofragmentation (photodissociation and photoionization) studies of small volatile molecules is a vast research field associated with a number of intriguing and contemporary fields such as atmospheric chemistry,[1] astrochemistry,[2] and photochemical synthesis.[3] Although the literature in the field of molecular photodissociation is abundant, it is limited in terms of excitation energy ranges studied and energy- and time-resolution used in experiments. Most work deals with processes following excitations to low energy repulsive valence states. Photodissociation processes of neutrals in the less explored high energy regions largely occur via excitations to Rydberg states[4–6] followed by state interactions and curve crossings to repulsive and/or ion-pair states.[5,7]

The hydrogen halides are ideal molecules to study molecular photodissociation processes via Rydberg state excitations on a quantum energy level basis. The UV, VUV, and multiphoton excitation spectroscopy of these compounds show clearly resolved rotational structures due to excitations to Rydberg and ion-pair states.[8–11] The spectral structures are found to be rich in intensity anomalies due to state interactions and predissociation processes.[9,12–14] Since the pioneering work of Green *et al.* on HCl in 1991 (Ref. 9) and Callaghan and Gordon on HBr in 1990 (Ref. 10) a large emphasis has been on spectroscopic studies of these compounds as well as on HI to determine its high energy state properties.[11–13,15,16] More recently an increased emphasis has been on studies of state interactions and photofragmentation (photodissociation and photoionization) processes in HCl. Resonance enhanced multiphoton ionization (REMPI) techniques have proven to be powerful tools in this respect. Photofragment imaging techniques coupled with REMPI (Refs. 17 and 18) have shone light on a number of photodissociation and photoionization processes in HCl and HBr. Detailed studies of spectroscopic anomalies, such as line shifts and signal intensity irregularities, in one-colour REMPI spectra have revealed state interaction strengths as well as importance of photodissociation processes in HCl.[19–22] Theoretical *ab initio* calculations to determine excited state potential energy surfaces for HCl (Ref. 23) have proven to be very helpful for interpreting experimental data.

Most recent work, relevant to state interactions and photofragmentation processes in the hydrogen halides, in our group, has been on a number of Rydberg states and the $V^1\Sigma^+$ ion-pair state for HCl (Refs. 19–22) by the one-colour REMPI technique. Our observations can be grouped into categories depending on the strengths of Rydberg to ion-pair state interactions as follows:

a) Very weak near-resonance state interactions, distinguishable by negligible rotational line shifts but significant alterations in signal line intensities,[20] observed for triplet Rydberg states and $\Delta\Omega > 0$ state interactions.
b) Weak near-resonance state interactions, distinguishable by localized line shifts, (hence energy level shifts), as well as alterations in signal line intensities,[19,22] observed for singlet states and $\Delta\Omega > 0$ state interactions.

[a)]Author to whom correspondence should be addressed. Electronic mail: agust@hi.is. Telephone: +354-525-4672/+354-525-4800. Fax: +354-552-8911.

c) Medium to strong off-resonance state interactions, distinguishable by large scale line/energy level shifts, as well as alterations in signal intensities,[22,24] observed for triplet and singlet states and $\Delta\Omega = 0$ state interactions.

Whereas quite an extensive study, relevant to photofragmentations via Rydberg states of the hydrogen halides, relating to HCl has been performed, as mentioned above, limited emphasis has been placed on the heavier compounds HBr and HI. State assignments for HBr and HI resemble those for HCl. Energies for analogous states decrease with increasing molecular masses. Vibrational assignments (v') for the ion-pair states, $V^1\Sigma^+$ are uncertain and marked as $v' = m + i$, where i is integer numbers starting from $i = 1$ for the lowest energy level observed and m is an unknown integer. Based on the resemblance in the energetics of the HX's (X = Cl, Br, I) there is a reason to believe that the major photofragmentation processes in one-colour $(2 + n)$ REMPI of the hydrogen halides is similar to that summarized, pictorially, for HCl in Ref. 20. Thus the major photofragmentation processes following two-photon excitations to rovibrational (v', J') quantum levels of Rydberg (HX^{**}(Ry)) and ion-pair states (HX^{**}(V)) will typically be

(i) $HX^{**}(Ry) + h\nu \rightarrow HX^+ + e^-$;
(ii) $HX^+ + h\nu \rightarrow H^+ + X$;
(iii) $HX^{**}(V) + h\nu \rightarrow HX^+ + e^-$;
(iv) $HX^+ + h\nu \rightarrow H^+ + X$;
(v) $HX^{**}(V) + h\nu \rightarrow H + X^{**}$; $X^{**} + h\nu \rightarrow X^+ + e^-$;
(vi) $HX^{**}(V) + h\nu \rightarrow H^{**} + X$; $H^{**} + h\nu \rightarrow H^+ + e^-$;
(vii) $HX^{**}(V) + h\nu \rightarrow H^+ + X^-$;
(viii) $HX^{**}(Ry) \rightarrow H + X/X^*$; $X/X^* + 3h\nu \rightarrow X^+ + e^-$;
(ix) $HX^{**}(Ry) + h\nu \rightarrow H + X^{**}$; $X^{**} + h\nu \rightarrow X^+ + e^-$.

H^{**} and X^{**} are atomic Rydberg states but X and X* refer to the ground ($^2P_{3/2}$) and the spin-orbit excited ($^2P_{1/2}$) states, respectively. Channels (i) and (v–vi) typically dominate. The number of photons in the excitation processes (i–ix), however, may vary, depending on the photon energies. The initial Rydberg or ion-pair state excitations may either occur by direct two-photon excitations or via J' quantum number dependent state mixing.

In this paper, we present a REMPI work on HBr with main focus on photofragmentation and state interaction processes involving singlet Rydberg and ion-pair states. Quantitative and qualitative multiparameter analysis of line-shifts, signal intensities, and line-widths illuminate state involvements and interactions in photodissociation processes. Furthermore, observations of new spectral features will be presented.

EXPERIMENTAL

Two-dimensional (2D) REMPI data were recorded for a HBr molecular beam, created by jet expansion of a pure sample through a pulse nozzle. Apparatus used is similar to that described in Refs. 16 and 25. Excitation radiation was generated by a pulsed excimer laser-pumped dye laser systems, using a Lambda Physik COMPex205 excimer laser and a Coherent ScanMatePro dye laser. Frequency doubled radiation was focused on the molecular beam inside an ionization chamber between a repeller and an extractor plate. Ions formed by multiphoton excitations were directed into a time-of-flight tube and detected by a micro-channel plate (MCP) detector. Signals were fed into a LeCroy WaveSurfer 44MXs-A, 400 MHz storage oscilloscope and stored as a function of ion time of flights and laser radiation wavenumbers. Average signal levels were evaluated and recorded for a fixed number of laser pulses. The data were corrected for laser power and mass-calibrated to obtain ion yields as a function of mass and excitation wavenumber (2D-REMPI data). REMPI spectra for certain ions as a function of excitation wavenumber (1D-REMPI) were obtained by integrating mass signal intensities for the particular ion. Care was taken to prevent saturation effects as well as power broadening by minimising laser power. Laser calibration was based on observed $(2 + 1)$ bromine atom REMPI peaks. The accuracy of the calibration was typically found to be about ± 2.0 cm^{-1} on a two-photon wavenumber scale. Equipment condition parameters are listed in Table I.

TABLE I. Typical equipment/condition parameters for REMPI experiments.

HBr gas sample	Merck Schuchardt, Germany, Purity: 99.8%
Laser dye	C503
Frequency doubling crystal	BBO-2
Laser repetition rate	10 Hz
Dye laser bandwidth	0.095 cm^{-1}
Laser intensity used	0.1–0.3 mJ/pulse
Nozzle size	500 μm
Sample backing pressure	2.0–2.5 bars
Pressure inside ionization chamber	10^{-6} mbar
Nozzle opening time	150–200 μs
Delay time for laser excitation	450–550 μs
Excitation wavenumber step sizes	0.05–0.1 cm^{-1}
Time of flight step sizes	10 ns

RESULTS AND ANALYSIS

Spectra

2D-REMPI data corresponding to resonance transitions to the $F^1\Delta_2(v' = 1)$, $E^1\Sigma^+(v' = 1)$, $H^1\Sigma^+(v' = 0)$, $V^1\Sigma^+(v' = m + 7)$, and $V^1\Sigma^+(v' = m + 8)$ states of H^iBr ($i = 79$, 81) (see Fig. 1) in the two-photon wavenumber region 79 040–80 300 cm^{-1} were recorded, assigned, and analysed in terms of rotational line-shifts, signal intensities, and line-widths. These are hereafter named $F(1)$, $E(1)$, $H(0)$, $V(m + 7)$, and $V(m + 8)$, respectively. Figure 2 shows 1D-REMPI spectra for the H^+, $^{81}Br^+$, and $H^{81}Br^+$ ions. Within experimental error, no significant difference in rotational line positions are observed for the two isotopes, $i = 79$ and 81. Rotational line positions are listed in Table II. Several new rotational lines, not previously reported,[10] are observed. Most other peak positions agree reasonably well with those given by Callaghan and Gordon.[10] In addition to the above-mentioned resonances, weak peaks due to transitions to a Rydberg state, previously unobserved in REMPI, are observed in the region 80 028–80 040 cm^{-1} (see Fig. 2 and Table II). Furthermore, three Br atomic

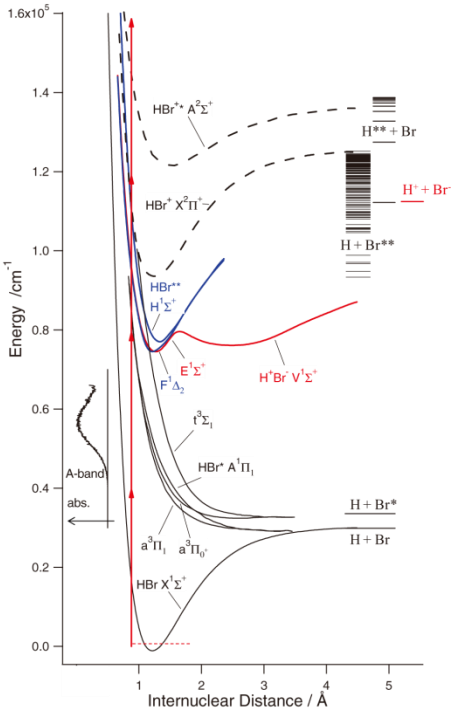

FIG. 1. HBr energetics. Potential energy curves, asymptotic energies (right), photon excitations (red arrows; left) corresponding to two-photon resonance excitation to the $F^1\Delta_2(v'=1)$ state and relative absorption intensity of the *A*-band (Ref. 33) (tilted to the left). Potential curves other than the repulsive states are derived from Fig. 1 in Ref. 18. Repulsive potentials (*A*, *t* and the *a* states) are derived from Fig. 1 in Ref. 34. Threshold energies are derived from atom energy levels.[35]

(2 + 1) REMPI resonances, due to transitions from ground state Br($^2P_{3/2}$) to the excited states $^4S_{3/2}$ (79 178 cm^{-1}), $^2P_{3/2}$ (79 696 cm^{-1}), and $^2P_{1/2}$ (79 868 cm^{-1}), were identified in the spectral region.

Analysis of the spectrum near 80 040 cm^{-1}, based on the assumption that the peaks are *Q* lines, gave rotational constants $B_{v'} = 7.238 \pm 0.070$ cm^{-1} and $D_{v'} = -0.016 \pm 0.005$ cm^{-1} and band origin value of 80 038 ± 2 cm^{-1} for the Rydberg state. Based on comparison with absorption data given by Ginter *et al.*,[26] the state of concern is assigned $k^3\Pi_0$ ($v' = 0$).

Energetics and line-shifts vs. state interactions

Rotational level energies for all five states were derived from the line positions (Table II) and the rotational level energies of the H^{81}Br ground state[27] (see Fig. 3). To a first approximation an unperturbed state will show linear behaviour

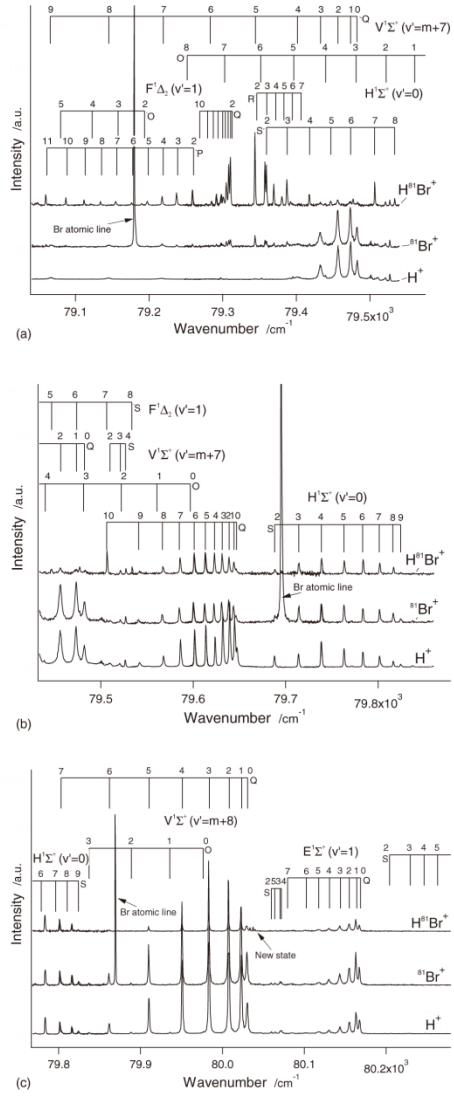

FIG. 2. 1D-REMPI spectra for H$^+$, ^{81}Br$^+$, and H^{81}Br$^+$ and J' assignments for rotational peaks corresponding to two-photon resonance excitations to the $F^1\Delta_2(v'=1)$, $V^1\Sigma^+(v'=m+7)$, $H^1\Sigma^+$ ($v'=0$), $V^1\Sigma^+(v'=m+8)$, and $E^1\Sigma^+$ ($v'=1$) states. New, previously unreported spectrum in REMPI, assigned to two-photon resonance transition to the $k^3\Pi_0(v'=0)$ state is marked in figure (d). Three atomic lines due to (2 + 1) REMPI of Br are also marked (see Table VI).

TABLE II. Rotational lines for H^{i}Br (i = 79, 81), due to two-photon resonance transitions to the $V^1\Sigma^+(v' = m + 7)$, $V^1\Sigma^+(v' = m + 8)$, $E^1\Sigma^+(v' = 1)$, $F^1\Delta_2(v' = 1)$, $H^1\Sigma^+(v' = 0)$ and "New" ($k^3\Pi_0(v' = 0)$) states (see text).

	$V(m+7)$		$V(m+8)$			E(1)				
J'	Q	S	O	Q	S	Q	S			
0	79 481.3		79 975.5	80 029.0		80 166.3				
1	79 472.5		79 934.8	80 021.8		80 162.0				
2	79 455.4	79 508.8	79 887.3	80 006.6	80 058.5	80 153.8	80 203.1			
3	79 431.7	79 520.0	79 836.0	79 982.4	80 069.3	80 142.2	80 228.3			
4	79 399.6	79 525.6[a]		79 949.7	80 070.9	80 129.1	80 245.2			
5	79 343.4[a]			79 909.0	80 063.3	80 116.4	80 261.6			
6	79 282.1[a]			79 860.5	80 045.5	80 101.2[a]	80 278.0[a]			
7	79 218.1[a]			79 801.8[a]		80 083.5[a]	80 296.3[a]			
8	79 144.2[a]						80 314.6[a]			
9	79 064.5[a]									

	$F(1)$					$H(0)$			New
J'	O	P	Q	R	S	O	Q	S	Q
0						79 595.6	79 645.6		80 039.8[a]
1						79 559.5	79 642.9		80 037.5[a]
2	79 191.2	79 258.2	79 309.6	79 343.0	79 358.6	79 520.9	79 637.7	79 686.8	80 033.8[a]
3	79 155.2	79 236.6	79 307.3	79 356.6	79 386.5	79 480.1	79 630.2	79 712.9	80 028.8[a]
4	79 120.1	79 216.9	79 304.1	79 368.6	79 417.0	79 438.6	79 621.8	79 737.3	
5	79 077.1[a]	79 196.6	79 300.2	79 379.7	79 445.8	79 395.5	79 611.8	79 761.7	
6	79 047.0	79 175.5	79 296.7	79 391.2	79 472.7	79 350.5	79 599.8	79 782.0	
7		79 153.9	79 290.4	79 403.1	79 505.2[a]	79 301.6[a]	79 583.7	79 800.0	
8		79 133.2[a]	79 283.9		79 532.4[a]	79 250.6[a]	79 565.4	79 814.8	
9		79 111.0[a]	79 276.1				79 539.7	79 823.2[a]	
10		79 086.2[a]	79 265.7				79 505.2[a]		
11		79 058.9[a]							

[a]New, previously unobserved peaks in REMPI.

for the energy spacing between neighbour energy levels, $\Delta E_{J',J'-1}$ ($= E(J') - E(J'-1)$) as a function of J' with a slope value $2B_{v'}$, where $B_{v'}$ is the v'-dependent rotational constant. Irregular, nonlinear, shape of $\Delta E_{J',J'-1}$ vs J' plots is a clear indication of perturbation effects due to state interactions (see Fig. 4) showing as level-to-level repulsions between levels with same J' numbers.[12,28] The shift of an energy level of a perturbed state (1) ($\Delta E_{J'}(1) = E_{J'}(1) - E^0_{J'}(1)$, where $E^0_{J'}(1)$ is the zero order energy for the unperturbed state) depends on the interaction strength (W_{12}) between that state (1) and the perturbing state (2) and the observed energy level difference, between the two states, for same J' (i.e., $\Delta E_{J'}(1, 2) = E_{J'}(1) - E_{J'}(2)$),

$$\Delta E_{J'}(1) = \frac{1}{2}\left(\Delta E_{J'}(1,2) - \sqrt{(\Delta E_{J'}(1,2))^2 - 4\,|W_{12}|^2}\right). \tag{1a}$$

Equation (1a) is derived from the classical expression given by Herzberg[28] for energies in case of level-to-level interactions,

$$E_{J'}(i) = \frac{1}{2}\left(E^0_{J'}(1) + E^0_{J'}(2)\right) \pm \frac{1}{2}\sqrt{4\,|W_{12}|^2 + (\Delta E^0_{J'}(1,2))^2}; \quad i = 1, 2$$
$$\Delta E^0_{J'}(1,2) = E^0_{J'}(1) - E^0_{J'}(2). \tag{1b}$$

Small, but significant, positive deviation of the $\Delta E_{J',J'-1}$ value from linearity for $J' = 6$ (slight negative deviation for $J' = 7$) in $F(1)$ is an indication of near-resonance interactions between $F(1)$ and $V(m + 7)$ (Ref. 13) (see Fig. 3(a)). Strictly, interaction between the $F^1\Delta_2$ and $V^1\Sigma^+(0^+)$ states violates the selection rule $\Delta\Omega = 0, \pm 1$. Most probably, however, the F-state is a mixed state analogous to HCl, where the F-state wave function is believed to be a linear combination of $\Omega = 1$, 2, and 3 components, and F to V perturbations observed therefore due to heterogeneous ($\Delta\Omega = 1$).[19,29] The larger irregularities in energy levels, observed for the $V(m + 7)$ state, however, (Fig. 4(a)) indicates further involvement of larger homogeneous ($\Delta\Omega = 0$) state interactions with $\Omega = 0$ states, of which interaction with the $E(1)$ state, slightly higher in energy, will dominate. Involvement of the closer in energy $H(0)$ state, however, will also be affective. A positive deviation in $\Delta E_{J',J'-1}$ values vs. J' observed for $E(1)$ (see Fig. 4(a)) acts in accordance with a large negative deviation observed for $V(m + 7)$ near $J' = 4$–6. The $E(1)$ state does, however, "experience" still stronger interactions from the "closer in energy" $V(m + 8)$ and $V(m + 9)$ states which all together will affect the observed irregularities in $\Delta E_{J',J'+1}$ vs. J' for $E(1)$. Whereas almost a linear behaviour of $\Delta E_{J',J'-1}$ vs. J' is observed for $H(0)$ (Fig. 4(b)), in the low J' region, large negative deviation is observed for high J' ($J' > 6$). The major perturbation effects on $H(0)$ will be due to interactions

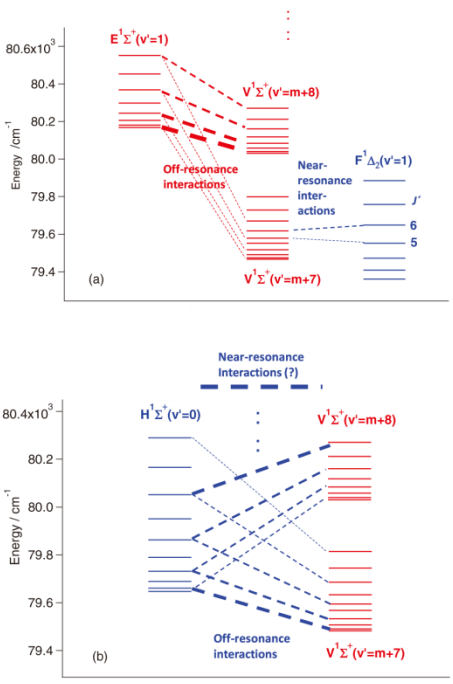

FIG. 3. Rotational energy levels, derived from observed REMPI rotational peaks for the $F^1\Delta_2(v' = 1)$(a), $V^1\Sigma^+(v' = m+7)$((a) and (b)), $H^1\Sigma^+$ $(v' = 0)$(b), $V^1\Sigma^+(v' = m + 8)$((a) and (b)) and $E\,^1\Sigma^+$ $(v' = 1)$(a) states. Observed level-to-level near-resonance interactions between $F(1)$ and $V(m + 7)$ and off-resonance interactions between the $V(m + 7)$ and $V(m + 8)$ ion-pair states and the $E(1)$ and $H(0)$ Rydberg states are indicated by broken lines. Strength and alterations in state mixings are indicated, roughly, by varying thickness of broken lines.

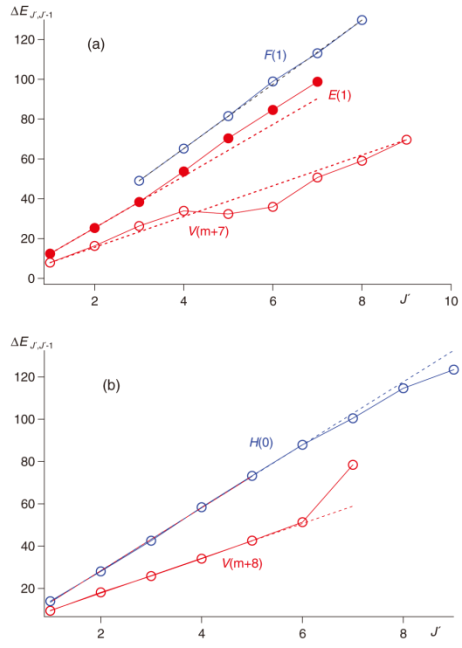

FIG. 4. H^iBr: Spacings between rotational levels $(\Delta E_{J',J'-1})$ as a function of J' for $F^1\Delta_2(v' = 1)$(a), $E^1\Sigma^+(v' = 1)$(a), $V^1\Sigma^+(v' = m + 7)$(a), $H^1\Sigma^+(v' = 0)$(b), and $V^1\Sigma^+(v' = m + 8)$(b). Dots connected by solid lines are derived from Q rotational lines. Broken lines are line fits for, $J' = 3$–5 and 8 values for $F(1)$, $J' = 1$–3 values for $E(1)$, $J' = 1$–6 values for $H(0)$, and $J' = 1$–5 values for $V(m + 8)$. The broken line for $V(m + 7)$ joins the dots for $J' = 1$ and 9 to guide the eye.

with the V state. These observations, therefore, suggest that overall effects due to level-to-level interactions with the $V(m + 7)$ and $V(m + 8)$ states "cancel", such that a decreasing level repulsions with J' by $V(m + 7)$ matches an increasing repulsions with J' by $V(m + 8)$ (Fig. 3(b)), resulting in an effective lowering in the slope, hence the rotational constant. The growing negative deviation for high J', on the other hand, is due to increasing near-resonance-interactions with $V(m + 8)$ also observed as positive deviation in the $\Delta E_{J',J'-1}$ vs. J' plot for $V(m + 8)$.

Assuming only level-to-level interaction with $V(m + 7)$ to be responsible for the energy deviations observed in $F(1)$ (Fig. 4(a)), the interaction strength for $J' = 6$ could be evaluated from Eq. (1) as $W_{12} = 4.4 \pm 0.4$ cm^{-1}. Furthermore, by assuming the heterogeneous interaction to change with J' as

$$W_{12} = W'_{12}(J'(J' + 1))^{1/2}. \tag{2}$$

$W'_{12} = 0.68 \pm 0.07$ cm^{-1} was derived and W_{12} values for J' = 2–7 evaluated (Table III). The fractional contributions to the state mixing, c_1^2 and c_2^2, for the states 1(F(1)) and 2(V($m + 7$)) respectively can now easily be derived from

$$c_1^2 = \frac{1}{2} + \frac{\sqrt{(\Delta E_{J'}(1,2))^2 - 4\,|W_{12}|^2}}{2\,|\Delta E_{J'}(1,2)|}; \quad c_2^2 = 1 - c_1^2 \tag{3}$$

(see Table III).

Signal intensities vs. state interactions

Rotational lines were fitted by Lorentzian functions to obtain integrated intensities as well as line-widths. $^iBr^+$ signal intensities relative to H^iBr^+ signal intensities $(I(^iBr^+)/I(H^iBr^+))$ as a function of J', for the Rydberg state spectra (see Fig. 5) show certain resemblance to analogous plots of $I(^iCl^+)/I(H^iCl^+)$ for H^iCl (Refs. 19–22) where an increase in the ratio has been shown to indicate an accession of state mixing and stronger interaction with the $V^1\Sigma^+$ ion-pair state. Thus the plot of the Q line intensity ratios for the $F(1)$ state shows a weak but significant increase for $J' = 6$ (Fig. 5(a)) corresponding to the near-resonance

TABLE III. Parameters derived from line-shift and intensity-ratio ($I(^iBr^+)/I(H^iBr^+)$) analysis of the $F(1) \leftarrow\leftarrow X$ system (see Figs. 4(a), 6(a), and 6(b))

J'	$\Delta E = E(F(1) - E(V(m+7)))$	W_{12}	${c_1}^2$	${c_2}^2$
2	−145.9	1.67	1.00	0.000
3	−124.4	2.36	1.00	0.000
4	−95.5	3.046	1.00	0.000
5	−43.2	3.73	0.993	0.007
6	14.6	4.41	0.898	0.102
7	72.3	5.09	0.995	0.005
W'_{12}	0.68 ± 0.07 cm^{-1}			
γ (β_1/α_2)	0.11			
α (α_2/α_1)	1.3			
$\alpha\gamma$ (β_1/α_1)	0.14			

interaction with $V(m+7)$ (see Fig. 3(a)). This near-resonance effect also displays itself as alterations in absolute ion signals. Thus the P line series for H^iBr^+ displays minimum for $J' \sim 6$ (see Fig. 2(a)) and the $J' = 6$ peak for H^+ in the Q line series exhibits enlargement. The intensity ratios ($I(^iBr^+)/I(H^iBr^+)$) for the $E(1)$ state gradually decrease with J' (Fig. 5(c)), indicating less off-resonance interactions with $V(m+8)$ as the spacing between the levels ($\Delta E_J(E(1),V(m+8))$) increases with equal J' (Fig. 3(a)). There is, however, a slight indication of an enhanced ratio near $J' = 6$ (Fig. 5(c)). The intensity ratios for $H(0)$ show clear effect of "double" state interactions, showing decreasing values with J' for low J' (for $J' > 0$) but increasing values with J' for high J', with minimum at $J' \sim 5$ (Fig. 5(d)). This is due to a decreasing interaction with $V(m+7)$ but increasing interaction with $V(m+8)$ as a function of J' and the $\Delta E_J(H(0),V)$'s increase and decrease for $V(m+7)$ and $V(m+8)$ respectively (Fig. 3(b)).

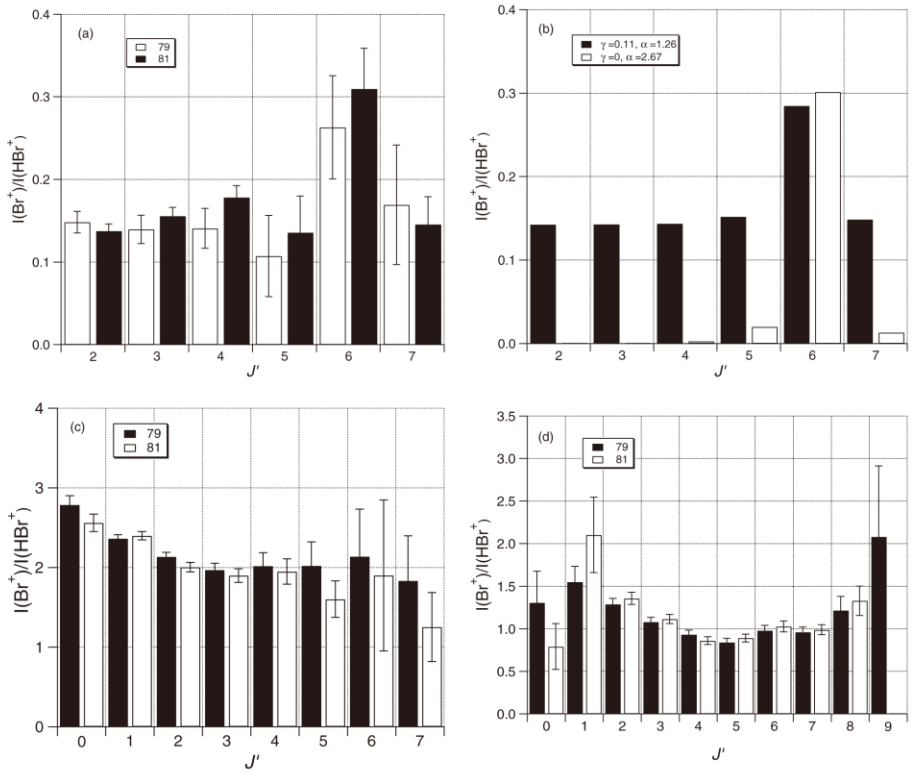

FIG. 5. Relative ion signal intensities, $I(^iBr^+)/I(H^iBr^+)$ (i = 79, 81) vs. J' derived from Q rotational lines of REMPI spectra due to two-photon resonance transitions to the Rydberg states $F(1)$ (a), $E(1)$(c), and $H(0)$(d). (b) shows simulation for (a), assuming J' level-to-level interactions between the $F(1)$ and $V(m+7)$ states (black columns) for $W'_{12} = 0.68$ cm^{-1}, $\alpha = 1.26$, and $\gamma = 0.11$ as well as calculated ratios for same W'_{12}, $\alpha = 2.67$, and $\gamma = 0$ (white columns) (see text).

By analogy with the observations for HCl, as mentioned before, in case of level-to-level interactions between two states (1) (Rydberg state) and (2) (ion-pair state), $I(^i\mathrm{Br}^+)/I(\mathrm{H}^i\mathrm{Br}^+)$ can be expressed as

$$\frac{I(^i\mathrm{Br}^+)}{I(\mathrm{H}^i\mathrm{Br}^+)} = \frac{\alpha\left[\gamma + c_2^2(1-\gamma)\right]}{\left(1-c_2^2\right)}, \tag{4}$$

where

$$I(^i\mathrm{Br}^+) = \alpha_2 c_2^2 + \beta_1 c_1^2; \quad I(\mathrm{H}^i\mathrm{Br}^+) = \alpha_1 c_1^2 + \beta_2 c_2^2$$
$$\alpha = \alpha_2/\alpha_1; \quad \gamma = \beta_1/\alpha_2; \quad \alpha\gamma = \beta_1/\alpha_1 .$$

α_i and β_i (i = 1, 2) are ionization rate coefficients for the excited molecular states (1) and (2). By least square fitting the expression on the right side of Eq. (3) to the experimental intensity ratios, as a function of J', derived from the $F(1)$ state spectra (Fig. 5(a)) using the W_{12} values obtained from the line shift analysis mentioned above and the energy level differences ($\Delta E_{J'}(1, 2)$; Table III), $\alpha = 1.26$, $\gamma = 0.11$, and $\alpha\gamma = 0.14$ values were obtained (see Fig. 5(b)). γ, hence $\alpha\gamma$, are measures of $^i\mathrm{Br}^+$ ion formations via dissociation of the Rydberg state, relative to that of the formations of $^i\mathrm{Br}^+$ via exciations of the ion-pair state and relative to that of the formations of $\mathrm{H}^i\mathrm{Br}^+$ via excitation of the Rydberg state respectively. Whereas no γ and $\alpha\gamma$ values have been reported for HBr before, γ derived for HCl are found to be in the range γ = 0–0.03 (Refs. 20 and 22) depending on Rydberg states. The significance of the nonzero and relatively high γ value of 0.11, derived here, can be deduced from the dramatic effect of replacing it with $\gamma = 0$ in the calculations (see Fig. 5(b)). This suggests that predissociation of the $F(1)$ state to form H + Br/Br* is important.

Line-widths and fragmentations vs. state interactions

Rotational line-widths vary a lot depending on the resonance excited states and rotational levels as seen in Fig. 2, indicating a large variation in lifetimes of states. Figure 6 shows rotational line-widths (Γ) as a function of J'. Lower limit lifetimes (τ) derived from[6,30]

$$\tau(\mathrm{ps}) = 5.3/\,\Gamma(\mathrm{cm}^{-1}) \tag{5}$$

are listed in Table IV. The line-widths for the Q lines of the $H(0)$ spectrum (Fig. 6(f)) show close correspondence to the intensity ratios as a function of J' (Fig. 5(d)) previously explained to reflect interactions with both $V(m + 7)$ and $V(m + 8)$. For $F(1)$, line-widths as a function of J', derived from the line series P, Q, R, and S all show small but significant maxima, hence lifetime minima, near $J' = 5$ (see Figs. 6(a)–6(c)). The $V(m + 7)$ state, showing very broad peaks, also exhibits maximum bandwidth (minimum lifetime) for $J' \sim 5$–6 and much shorter lifetimes than $F(1)$ (Fig. 6(d)). Due to very weak intensity and breadth of the $V(m + 7)$, Q line, $J' = 5$ peak line-width could not be determined. Line-widths for the $E(1)$ state are in range between those for $F(1)$ and $V(m + 7)$, also reaching maximum for $J' = 5$ (Fig. 6(e)). This further indicates close interactions between the states involved in agreement with previous interpretations of line shifts and intensity ratios. There are, however, considerable, important correlation differences between the various observation parameters for $F(1)$ and $E(1)$. The maximum line-shifts and $I(^i\mathrm{Br}^+)/I(\mathrm{H}^i\mathrm{Br}^+)$ intensity ratios, for $F(1)$, are observed for $J' = 6$ whereas the maximum bandwidths (minimum lifetime) are found for $J' = 5$. Furthermore, line-widths of the Q lines for $E(1)$ (Fig. 6(e)) show significantly different behaviour with J' compared to that of the intensity ratios (Fig. 5(c)). The explanation lies in the fundamental differences in the observation parameters. Line-widths, hence lifetimes, are primarily determined by the rates of crossing from the bound excited states to continua (i.e., predissociation), whereas the line-shifts and intensity irregularities are primarily indicative of bound-to-bound state interactions. However, predissociation can occur via interacting gateway states, thus making the lifetimes state interaction dependent. Figures 3(a) and 3(b) summarize the major level-to-level state interactions of concern. The large average internuclear distance of the V state makes crossing to repulsive states, for which the repulsive walls are at much shorter internuclear distances (see Fig. 1), highly improbable. The Rydberg states, on the other hand, are either in close vicinity of or crossed by repulsive states to make predissociation processes more probable. Therefore, we believe that the short lifetimes observed, are mainly due to predissociation of Rydberg states, either directly or via Rydberg gateway states analogous to that assumed to hold for HCl.[20,22,31] Hence, the particularly short lifetimes, observed for the $V(m + 7)$ state are due to predissociation processes following crossings from $V(m + 7)$ to Rydberg states such as the $E(1)$, $F(1)$, and $H(0)$ states. This is demonstrated schematically in Fig. 7 for the $V(m + 7)$, $E(1)$, and $F(1)$ states. Based on a coupling scheme given by Alexander *et al.*[31] a summary of state couplings due to spin-orbit-(SO) and rotational-(JL and JS) interactions between relevant states are shown in Table V. SO couplings, generally, are the strongest interactions with coupling strengths independent of rotational energies, whereas weaker rotational interactions will increase with rotational energies. It should be noted, however, that in both cases the bound-to-bound state mixing (c_i^2) will depend on the spacing between the rotational levels with same rotational quantum numbers ($\Delta E_{J'}$) (Eq. (3)) making the effective interaction in both

TABLE IV. (Lower limit) lifetimes (ps) of rotational states (J') derived from REMPI spectra line-widths (see text). The values were derived from Q lines of $\mathrm{H}^i\mathrm{Br}^+$ (i = 79, 81) signals for $E(1)$, $F(1)$, and $H(0)$ but from Q lines of H^+ signals for $V(m + 7)$.

J'	$V(m+7)$	$E(0)$	$F(1)$	$H(0)$
0	1.69 ± 0.34	2.29 ± 0.07		1.96 ± 0.38
1	1.64 ± 0.28	2.50 ± 0.04		3.86 ± 0.38
2	1.41 ± 0.07	1.86 ± 0.04	3.96 ± 0.05	3.65 ± 0.15
3	1.16 ± 0.12	1.39 ± 0.04	4.01 ± 0.07	3.78 ± 0.13
4	0.65 ± 0.06	1.24 ± 0.07	3.10 ± 0.08	4.38 ± 0.15
5		1.08 ± 0.11	2.37 ± 0.16	4.52 ± 0.16
6	0.48 ± 0.13	1.36 ± 0.34	3.23 ± 0.22	4.10 ± 0.17
7	0.59 ± 0.03	1.46 ± 0.63	3.84 ± 0.27	3.63 ± 0.15
8	0.86 ± 0.05		4.05 ± 0.74	2.99 ± 0.31
9	1.03 ± 0.07		3.44 ± 2.23	3.21 ± 1.46

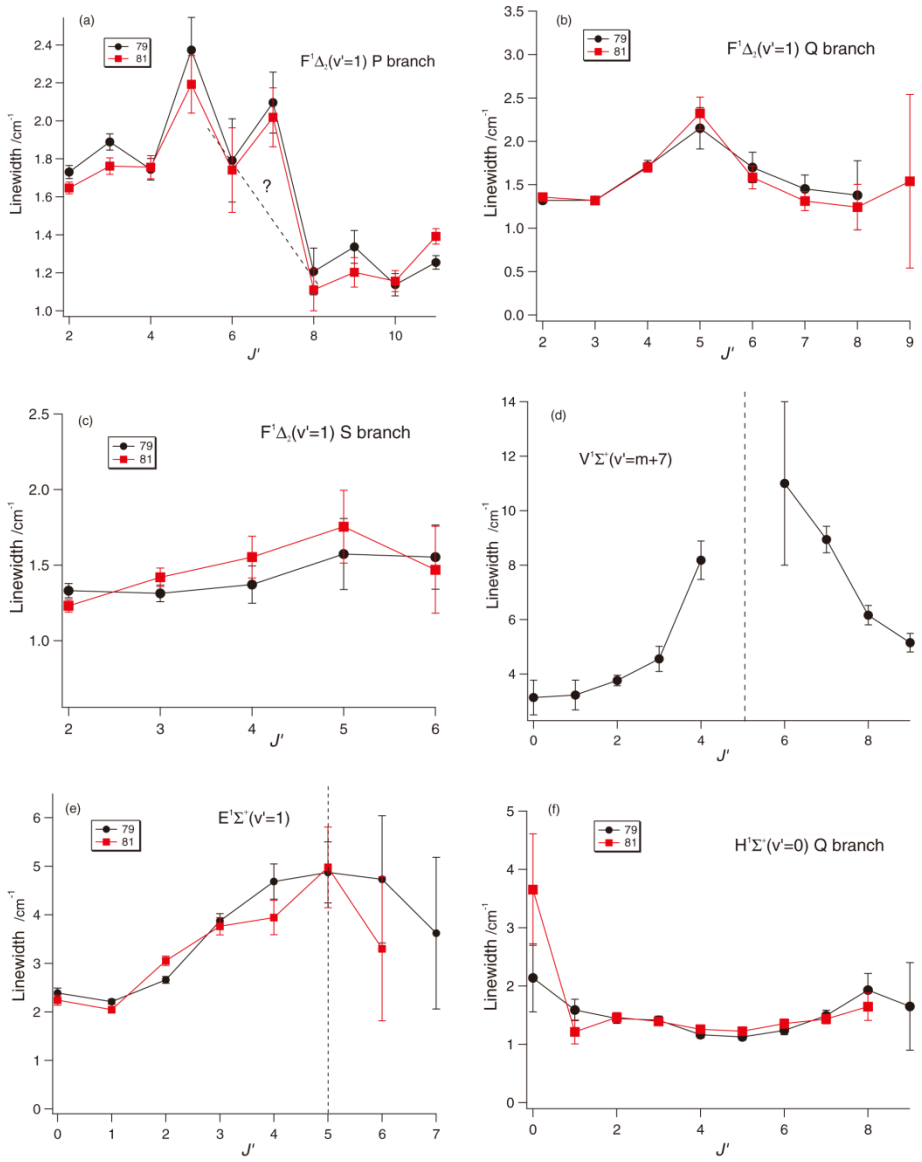

FIG. 6. Rotational line-widths vs. J' derived from REMPI spectra for (a) $F(1)$, P lines, H^iBr^+ (i = 79, 81), (b) $F(1)$, Q lines, H^iBr^+, (c) $F(1)$, S lines, H^iBr^+, (d) $V(m + 7)$, Q lines, H^+, (e) $E(1)$, Q lines, H^iBr^+, (f) $H(0)$, Q lines, H^iBr^+. The line-width derived for $F(1)$, P line, $J' = 7$ (a) is overestimated due to overlap of peaks $P(J' = 7)$ and $O(J' = 4)$ (see Fig. 2(a)). Due to very weak intensity and breadth of the $V(m + 7)$, Q line, $J' = 5$ peak line-width could not be determined (d).

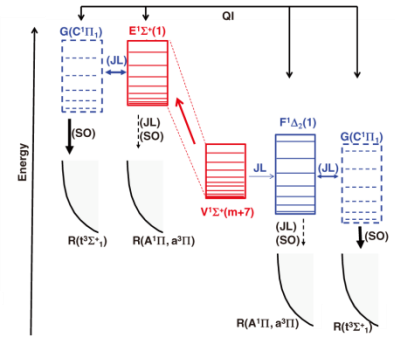

FIG. 7. Semischematic figure, showing the H^{i}Br energetics, state interactions, and transfers of relevance. Rotational and spin-orbit couplings are marked *JL* and *SO*, respectively. States marked *G* and *R* are gateway and repulsive states, respectively. States and couplings inside brackets are example cases believed to be of importance. Relative importance of couplings and transfers are indicated by different boldness of arrows. Quantum interference effects between states are indicated by arrows marked *QI*.

cases rotational energy dependent. Furthermore, interaction strengths will depend on Franck-Condon-overlaps, favouring interactions between Rydberg states and repulsive states close to curve-crossings. Involvements of the repulsive states $t^3\Sigma$ (see Fig. 1) are therefore expected to be important in predissociation processes. Considering all these factors, the $E(1)$ and $F(1)$ states (hence the mixed $V(m+7)$ state) could be largely affected by *SO* couplings of the $C^1\Pi_1$-gateway state with the repulsive $t^3\Sigma^+{}_1$ state following rotational (*JL*) couplings with the *C*-state. Direct predissociation of the $E(1)$ and $F(1)$ states by the *A* and the *a* states will also be involved but to a less extent (see Fig. 7). Furthermore the *C* to *F* state mixing will be important in enhancing the rotational/heterogeneous ($\Delta\Omega = 1$) coupling between the $V(m+7)$ and the $F(1)$ state. The bound-bound rotational couplings (*JL*) will have the greatest effect on the rotational

TABLE V. State couplings based on correlation diagrams from Ref. 31. Spin-orbit couplings are marked *SO*. Rotational couplings, *L* uncoupled and *S*-uncoupled, are marked *JL* and *JS*, respectively.

State interactions		Bound states					
		E, H, V	*F*	*C,D* $^1\Pi_1$	$b^3\Pi_0$	$b^3\Pi_2$	$g^3\Sigma_0^-$
Continuum states	$A^1\Pi_1$	*JL*	*JL*				
	$a^3\Pi_2$		*SO*				
	$a^3\Pi_1$			*SO*	*JS*	*JS*	*JL*
	$a^3\Pi_0^-$(e)	*SO*					*SO*
	$t^3\Sigma_1^+$			*SO*		*JL*	
	$t^3\Sigma_0^+$(f)				*SO*		
Bound states	*C,D* $^1\Pi_1$		*JL*				
	$b^3\Pi_0$	*SO*					
	$b^3\Pi_2$		*SO*				
	$g^3\Sigma_0^-$	*SO*					

energy dependence of the line-width/lifetime. The close correlation observed between the $E(1)$ and $F(1)$ states, in terms of the J'-dependent line-widths, showing as maxima for the same J' ($J' \sim 5$) strongly suggests that quantum interference (*QI*; Fig. 7) effects apply, involving the Rydberg states $E(1)$, $F(1)$, and $C^1\Pi$. The slight increases observed in the intensity ratios ($I(^i\mathrm{Br}^+)/I(\mathrm{H}^i\mathrm{Br}^+)$) both for the $E(1)$ and $F(1)$ states at $J' = 6$ (Figs. 5(a) and 6(c)) further demonstrate this.

Considering interaction schemes such as the one presented in Fig. 7, an approximation expression, relating lifetimes of the $V(m+7)$, $E(1)$, $F(1)$, and $H(1)$ states, can be derived. The basic idea is that the lifetime of $V(m+7)$ is determined by the lifetimes of the Rydberg states, which $V(m+7)$ couples with. Assuming the rate of dissociation of $V(m+7)$, due to a coupling with a Rydberg state, to be proportional to the rate of dissociation of that Rydberg state and the state mixing the following approximation expression, relating rate coefficients ($1/\tau_i$), can be written,

$$\frac{1}{\tau_{V7}} = f_{E1}\frac{1}{\tau_{E1}} + f_{F1}\frac{1}{\tau_{F1}} + f_{H0}\frac{1}{\tau_{H0}} + f_{\mathrm{other}}\frac{1}{\tau_{\mathrm{other}}}, \qquad (6)$$

where τ_i ($i = V7$, $E1$, $F1$, $H0$, other) are the lifetimes of the $V(m+7)$, $E(1)$, $F(1)$, $H(0)$, and other states, respectively. The f_i's are proportionally coefficients, depending on coupling rates. Since the rate of dissociation of $V(m+7)$, via coupling with a particular Rydberg state, cannot exceed the rate of dissociation of that Rydberg state the corresponding f_i-factor cannot be larger than one, hence $0 \le f_i \le 1$. Consistent variations in the bandwidths with J', observed for all measurements in ranges larger than our detection limit of about 0.3 cm^{-1}, make us believe that the lifetime values for the $V(m+7)$, $E(1)$, $F(1)$, and $H(0)$ states (Table IV) are reasonable estimates for the absolute values within uncertainty limits. There is a reason to expect that the states $E(1)$, $F(1)$, and $H(0)$ contribute the most to the observed dissociation rate of $V(m+7)$ and that contributions from other states are less or minor in the case of the shortest lifetimes. For $J' = 4$, 6, and 7 the rate of dissociation for $V(m+7)$ ($1/\tau_{V7}$) derived from the lifetimes in Table IV is in fact found to be close to or only slightly higher than the sum of the dissociation rates of the $E(1)$, $F(1)$, and $H(0)$ ($1/\tau_{E1} + 1/\tau_{F1} + 1/\tau_{H0}$), within uncertainty limits. This suggests that the corresponding f_i factors are close to unity. Analogous comparison could not be made for $J' = 5$, since its bandwidth for $V(m+7)$ could not be determined (see figure caption 6(d)). Assuming $fi = 1$ ($i = E1$, $F1$, $H0$) and $f_{\mathrm{other}} = 0$ the lifetime for $J' = 5$ is estimated to be about 0.64 ps, hence the line-width about 8.3 cm^{-1}.

Bromine atomic lines

Generally it is believed that Br atomic lines observed in REMPI of HBr are primarily due to REMPI of Br atoms following one-photon photodissociation via the repulsive state $A^1\Pi$.[18] Considering the number of evidences for photofragmentations via Rydberg states, mentioned above, these must also be, partly or largely, due to REMPI of Br atoms formed by predissociations of Rydberg states following two-photon excitations. Thus it will resemble

TABLE VI. (2 + 1) REMPI bromine atomic lines and closest H^{i}Br rotational lines.

Bromine atomic lines			H^{i}Br rotational peaks		
Two-photon transitions	ν (cm^{-1}), our values	Relative intensity	Rotational transition	ν (cm^{-1}), our values	$\Delta\nu$ (cm^{-1})
$^4S_{3/2} \leftarrow\leftarrow {}^2P_{3/2}$	79 178.70	573	$F(1; J' = 6) \leftarrow\leftarrow X(0, J'' = 7); P$	79 175.5	3.2
$^2P_{3/2} \leftarrow\leftarrow {}^2P_{3/2}$	79 693.67	1000	$H(0; J' = 2) \leftarrow\leftarrow X(0, J'' = 0); S$	79 686.8	6.8
$^2P_{1/2} \leftarrow\leftarrow {}^2P_{3/2}$	79 867.67	319	$V(m + 8; J' = 6) \leftarrow\leftarrow X(0, J'' = 6); Q$	79 860.5	7.2

analogous findings for other Br-containing compounds.[32] The three strong bromine atomic lines observed in the spectral region discussed here (see above) are all observed in an excitation region corresponding to the low energy tail of the weak *A*-band spectrum where one-photon absorption cross section is very low, of the order 10^{-21} cm^2 molecule^{-1} at room temperature (to be compared with the cross section of about 2.5 $\times$ 10^{-18} cm^2 molecule^{-1} for the maximum of the *A*-band[33]) (see Fig. 1). The two-photon excitation wavenumbers for these lines happen to be very close to HBr molecular resonances (see Fig. 2), the closest of which are listed in Table VI along with details concerning the observed atomic lines. These two-photon absorptions will involve small but nonzero molecular excitations corresponding to the tails of the closest molecular bands. Based on the analysis above all these molecular resonances correspond to excitations to predissociating states which will form bromine atoms. The atom resonance signals will depend on uncertain transition probability parameters, for the molecule and the bromine atom, as well as the density of bromine atoms formed. The relatively largest signal due to the $^2P_{3/2} \leftarrow\leftarrow {}^2P_{3/2}$ atom resonance could be mainly associated with favourable selection rules ($\Delta L = \Delta S = \Delta J = 0$) whereas the significantly larger signal for the $^4S_{3/2} \leftarrow\leftarrow {}^2P_{3/2}$ ($\Delta L = \Delta S = 1$, $\Delta J = 0$) resonance compared to that for the $^2P_{1/2} \leftarrow\leftarrow {}^2P_{3/2}$ ($\Delta L = \Delta S = 0$, $\Delta J = 1$) resonance could be associated with the smaller difference in molecular vs. atom resonances in the former case (Table VI).

CONCLUSIONS

The analyses presented in this paper shine important light on mechanisms of photodissociation processes for H^{i}Br involving Rydberg and ion-pair state interactions. One colour REMPI spectra for atom- and molecular ions of H^{i}Br ($i = 79$, 81) in the two-photon excitation region 79 040–80 300 cm^{-1} have been analysed in terms of rotational line positions, intensities and line-widths. The analyses reveal state interactions of varying strength between Rydberg and ion-pair states. Quantitative analysis of the data relevant to near-resonance interactions between the $F^1\Delta_2(v' = 1)$ and $V^1\Sigma^+(v' = m + 7)$ states give interaction strengths (W_{12}) and fractional state mixing (c_1^2 and c_2^2) as a function of rotational quantum numbers and parameters characteristic for the degree of state mixing (α) and dissociation (γ) of the $F(1)$ state (Table III). Qualitative analysis further reveals the nature of state interactions between the ion-pair states $V(m + k)$ ($k = 7,8$) and the $E^1\Sigma^+(v' = 1)$ and $H^1\Sigma^+(v' = 0)$ Rydberg states in terms of relative strengths and J' dependences. A great variety in line-widths, hence lifetimes (Table IV), depending on electronic states and J' quantum numbers, is indicative of a number of different predissociation channels. Correlations between those observations and line-shifts and signal intensities reveal dissociation mechanisms involving ion-pair to Rydberg state interactions prior to direct or indirect (via Rydberg gateway states) predissociations of Rydberg states. Major channels are summarized in Fig. 7. The interaction between the $V(m + 7)$ and $F(1)$ states is made possible via heterogeneous coupling(s) of the $F(1)$ state, of which mixing with the $C^1\Pi_1$ state is believed to be important. The $C^1\Pi_1$ state is likely to be a gateway state prior to predissociating by the $r^3\Sigma$ repulsive state, both for the $F(1)$ and the $E(1)$ states. Furthermore, quantum interference effects between states clearly play an important role. Thus lifetimes, of the $E(1)$ state, hence the $V(m + 7)$ state, as well as interactions between these states as a function of J' are found to depend on the interaction between the $V(m + 7)$ and $F(1)$ states. Observed bromine atom (2 + 1) REMPI signals support the importance of Rydberg states predissociation channels. A band system, not previously reported in REMPI, is assigned to the Q branch of the $k^3\Pi_0(v' = 0) \leftarrow\leftarrow X^1\Sigma^+$ transition and analysed to give the band origin 80 038 $\pm$ 2 cm^{-1} and the rotational parameters $B_{v'} = 7.238 \pm 0.070$ cm^{-1} and $D_{v'} = -0.016 \pm 0.005$ cm^{-1} for the k state.

ACKNOWLEDGMENTS

The financial support of the University Research Fund, University of Iceland, the Icelandic Science Foundation as well as the Norwegian Research Council is gratefully acknowledged.

[1] J. H. Seinfeld and S. N. Pandis, *Atmospheric Chemistry and Physics: From Air Pollution to Climate Change* (Wiley, 2006); M. J. Simpson, R. P. Tuckett, K. F. Dunn, C. A. Hunniford, and C. J. Latimer, J. Chem. Phys. **130**, 194302 (2009).
[2] J. I. Lunine, *Astrobiology* (Pearson/Addison-Wesley, 2005); A. M. Shaw, *Astrochemistry: From Astronomy to Astrobiology* (Wiley, 2006).
[3] N. Hoffmann, Chem. Rev. **108**, 1052 (2008).
[4] C. Sandorfy, *The Role of Rydberg states in Spectroscopy and Photochemistry: Low and High Rydberg States* (Kluwer Academic, New York, 2002).
[5] H. Lefebvre-Brion, in *The Role of Rydberg states in Spectroscopy and Photochemistry: Low and High Rydberg States*, edited by C. Sándorfy (Kluwer Academic, New York, 2002), Vol. 20, p. 267.
[6] H. Lefebvre-Brion and R. W. Field, *The Spectra and Dynamics of Diatomic Molecules* (Elsevier, 2004).
[7] A. J. Yencha, D. K. Kela, R. J. Donovan, A. Hopkirk, and Á. Kvaran, Chem. Phys. Lett. **165**, 283 (1990); Á. Kvaran, A. J. Yencha, D. K. Kela, R. J. Donovan, and A. Hopkirk, *ibid.* **179**, 263 (1991); D. Kaur, A. J. Yencha, R. J. Donovan, Á. Kvaran, and A. Hopkirk, Org. Mass Spectrom. **28**, 327 (1993); A. J. Yencha, D. Kaur, R. J. Donovan, Á. Kvaran, A. Hopkirk, H. Lefebvre-Brion, and F. Keller, J. Chem. Phys. **99**, 4986 (1993); K. P. Lawley, A. C. Flexen, R. R. J. Maier, A. Manck, T. Ridley, and R. J. Donovan, Phys. Chem. Chem. Phys. **4**, 1412 (2002); T. Ridley, J. T. Hennessy, R. J.

Donovan, K. P. Lawley, S. Wang, P. Brint, and E. Lane, J. Phys. Chem. A **112**, 7170 (2008).
[8]A. E. Douglas and F. R. Greening, Can. J. Phys. **57**, 1650 (1979).
[9]D. S. Green, G. A. Bickel, and S. C. Wallace, J. Mol. Spectrosc. **150**, 303 (1991); **150**, 354 (1991); **150**, 388 (1991).
[10]R. Callaghan and R. J. Gordon, J. Chem. Phys. **93**, 4624 (1990).
[11]D. Ascenzi, S. Langford, M. Ashfold, and A. Orr-Ewing, Phys. Chem. Chem. Phys. **3**, 29 (2001).
[12]Á. Kvaran, Á. Logadóttir, and H. Wang, J. Chem. Phys. **109**, 5856 (1998).
[13]Á. Kvaran, H. Wang, and Á. Logadóttir, J. Chem. Phys. **112**, 10811 (2000).
[14]R. Liyanage, R. J. Gordon, and R. W. Field, J. Chem. Phys. **109**, 8374 (1998).
[15]Á. Kvaran, B. G. Waage, and H. Wang, J. Chem. Phys. **113**, 1755 (2000); Á. Kvaran, H. Wang, and B. G. Waage, Can. J. Phys. **79**, 197 (2001); Á. Kvaran and H. Wang, J. Mol. Spectrosc. **228**, 143 (2004); S. M. Hurley, Q. Zhong, and J. A. W. Castleman, J. Chem. Phys. **112**, 4644 (2000).
[16]Á. Kvaran and H. Wang, Mol. Phys. **100**, 3513 (2002).
[17]A. I. Chichinin, C. Maul, and K. H. Gericke, J. Chem. Phys. **124**, 224324 (2006); A. I. Chichinin, P. S. Shternin, N. Godecke, S. Kauczok, C. Maul, O. S. Vasyutinskii, and K. H. Gericke, *ibid.* **125**, 034310 (2006); S. Kauczok, C. Maul, A. I. Chichinin, and K. H. Gericke, *ibid.* **133**, 24301 (2010); C. Romanescu and H. P. Loock, *ibid.* **127**, 124304 (2007); C. Romanescu, S. Manzhos, D. Boldovsky, J. Clarke, and H. Loock, *ibid.* **120**, 767 (2004).
[18]C. Romanescu and H. P. Loock, Phys. Chem. Chem. Phys. **8**, 2940 (2006).
[19]Á. Kvaran, H. Wang, K. Matthíasson, A. Bodi, and E. Jonsson, J. Chem. Phys. **129**, 164313 (2008).
[20]A. Kvaran, K. Matthiasson, and H. S. Wang, J. Chem. Phys. **131**, 044324 (2009).
[21]K. Matthiasson, H. S. Wang, and A. Kvaran, J. Mol. Spectrosc. **255**, 1 (2009).
[22]K. Matthíasson, J. M. Long, H. Wang, and Á. Kvaran, J. Chem. Phys. **134**, 164302 (2011).
[23]M. Bettendorff, S. D. Peyerimhoff, and R. J. Buenker, Chem. Phys. **66**, 261 (1982); H. Lefebvre-Brion, H. P. Liebermann, and G. J. Vazquez, J. Chem. Phys. **134** (2011); D. M. Hirst and M. F. Guest, Molecular Physics **41**, 1483 (1980).
[24]J. Long, H. Wang, and A. Kvaran (unpublished).
[25]Á. Kvaran, Ó. F. Sigurbjörnsson, and H. Wang, J. Mol. Struct. **790**, 27 (2006).
[26]D. S. Ginter, M. L. Ginter, and S. G. Tilford, J. Mol. Spectrosc. **90**, 152 (1981).
[27]*NIST Chemistry WebBook* (NIST (National Institute of Standards and Technology) Chemistry WebBook); K. P. Huber and G. Herzberg, *Constants of Diatomic Molecules* (Van Nostrand Reinhold, New York, 1979); online at http://webbook.nist.gov/chemistry/form-ser.html.en-us.en.
[28]G. Herzberg, *Molecular Spectra and Molecular Structure; I. Spectra of Diatomic Molecules*, 2nd ed. (Van Nostrand Reinhold, New York, 1950).
[29]Y. Xie, P. T. A. Reilly, S. Chilukuri, and R. J. Gordon, J. Chem. Phys. **95**, 854 (1991).
[30]A. Kvaran, K. Matthiasson, and H. S. Wang, Chem. Phys. Lett. **458**, 58 (2008).
[31]M. H. Alexander, X. N. Li, R. Liyanage, and R. J. Gordon, Chem. Phys.**231**, 331 (1998).
[32]A. Kvaran, H. S. Wang, K. Matthiasson, and A. Bodi, J. Phys. Chem. A **114**, 9991 (2010); A. Kvaran, K. Sveinbjornsson, J. M. Long, and H. S. Wang, Chem. Phys. Lett. **516**, 12 (2011).
[33]C. E. Brion, A. Dyck, and G. Cooper, J. Electron Spectrosc. Relat. Phenom. **144**, 127 (2005).
[34]A. G. Smolin, O. S. Vasyutinskii, G. G. Balint-Kurti, and A. Brown, J. Phys. Chem. A **110**, 5371 (2006).
[35]J. M. W. Chase, *NIST-JANAF Thermochemical Tables*, 4th ed. (1998), p. 1; online at http://www.nist.gov/pml/data/asd.cfm.

Paper III

Jingming Long, Huasheng Wang, Ágúst Kvaran, *Rydberg and Ion-pair states of HBr: New REMPI observations and analysis.* Journal of Molecular Spectroscopy, 2012. **282** p. 20–26.

Journal of Molecular Spectroscopy 282 (2012) 20–26

Contents lists available at SciVerse ScienceDirect

Journal of Molecular Spectroscopy

journal homepage: www.elsevier.com/locate/jms

Rydberg and ion-pair states of HBr: New REMPI observations and analysis

Jingming Long, Huasheng Wang, Ágúst Kvaran *

Science Institute, University of Iceland, Dunhagi 3, 107 Reykjavík, Iceland

ARTICLE INFO

Article history:
Received 13 July 2012
In revised form 12 October 2012
Available online 24 October 2012

Keywords:
Rydberg states
Ion-pair states
REMPI
State interactions
Photoionization
Photofragmentation

ABSTRACT

Two-dimensional REMPI data, obtained by recording ion mass spectra for HBr as a function of two-photon wavenumber, revealed previously unobserved $(2+n)$ REMPI spectra for $H^{79}Br$ and $H^{81}Br$. Spectra were assigned and analyzed to derive band origins and rotational parameters of Rydberg and ion-pair states. Perturbation effects, showing as line-shifts and/or signal intensity alterations, were found to be helpful in spectra assignments.

1. Introduction

Vacuum ultraviolet absorption spectra of the hydrogen halides were first reported and studied in 1938 by Price [1]. Since then a wealth of spectroscopic data has been derived from high resolution absorption spectroscopy [2–12], fluorescence studies [12,13], as well as from resonance enhanced multiphoton ionization (REMPI) [14–29]. Largest emphasis has been on studies of HCl [4–6,12,14–20,22,25–27,30] (DCl [4,5]), but studies of HBr [2,3,9,13,21,22,26–29] (DBr [9]) and HI [7,8,11,22–24,26] (DI [7,8,10]) have been significantly less. These studies have revealed and led to characterization of large number of Rydberg states as well as number of vibrational states of the $V^1\Sigma^+$ ion-pair state. Theoretical *ab initio* calculations, to determine excited state potential energy surfaces for HCl [31–33], have proven to be very helpful for interpreting experimental data. Analogous calculations for HBr [34] and HI are more limited.

Whereas most of the studies of the Rydberg and ion-pair states have been dealing with the energetics of the states, an increasing attention has been brought to state interactions, energy transfers and photodissociation processes recently, again with largest emphasis on HCl [35–44]. The hydrogen halide spectra are rich in intensity anomalies and line-shifts due to perturbation effects, which makes them ideal for studying state mixing and photo-fragmentation processes. Interactions between ion-pair vibrational states and Rydberg states, of various strengths, have been seen. These can be grouped into three main categories as,

(a) Very weak near-resonance state interactions, distinguishable by negligible rotational line shifts but significant alterations in signal line intensities [44], observed for triplet Rydberg states and $\Delta\Omega > 0$ state interactions.
(b) Weak near-resonance state interactions, distinguishable by localized line shifts (hence energy level shifts), as well as alterations in signal line intensities [43,45], observed for singlet states and $\Delta\Omega > 0$ state interactions.
(c) Medium to strong off-resonance state interactions, distinguishable by large scale line- and energy-level shifts, as well as alterations in signal intensities [45], observed for $\Delta\Omega = 0$ state interactions.

These characteristics can also be useful in spectra assignments [45,46]. Thus, observations due to near-resonance interactions between states with same J' quantum numbers can be useful to assign rotational transitions to peaks [45,46] and interaction strengths can be decisive about electronic state terms involved [47].

A summary of Rydberg states observed in classical absorption spectra for HBr was given by Ginter et al. in 1981 [9]. A pioneering work by Callaghan and Gordon in 1990 [21] summarizes large number of Rydberg and ion-pair states which have been observed for HBr in REMPI. In 1998 we published a paper with some additional observations for $\Omega = 0$ states of HBr seen in REMPI [26]. Recently we have performed detailed photofragmentation and state interaction studies based on perturbation observations in REMPI seen for resonance excitations to selected Rydberg and ion-pair states of HBr [47]. We will now present two-dimensional REMPI data within the two-photon excitation region 74000–86000 cm^{-1} and interpretations relevant to new spectroscopic identifications.

* Corresponding author. Fax: +354 552 8911.
E-mail address: agust@hi.is (Á. Kvaran).

0022-2852/$ - see front matter © 2012 Elsevier Inc. All rights reserved.
http://dx.doi.org/10.1016/j.jms.2012.10.008

Perturbation effects, showing as line-shifts and/or signal intensity alterations, are found to be very useful in the spectra assignments.

2. Experimental

Two dimensional (2D) REMPI data were recorded for a HBr molecular beam, created by jet expansion of a pure sample through a pulse nozzle. Apparatus used is similar to that described elsewhere [48–50]. Excitation radiation was generated by pulsed excimer laser-pumped dye laser systems, using a Lambda Physik COMPex 205 excimer laser and a Coherent ScanMatePro dye laser. Frequency doubled radiation was focused on the molecular beam inside an ionization chamber between a repeller and extractor plates. Ions formed by multiphoton excitations were directed into a time-of-flight tube and detected by a micro-channel plates (MCPs) detector. Signals were fed into a LeCroy WaveSurfer 44MXs-A, 400 MHz storage oscilloscope and stored as a function of ion time-of-flights and laser radiation wavenumbers. Average signal levels were evaluated and recorded for a fixed number of laser pulses. The data were corrected for laser power and mass calibrated to obtain ion yields as a function of mass and excitation wavenumber (2D-REMPI data). REMPI spectra for certain ions as a function of excitation wavenumber (1D-REMPI) were obtained by integrating mass signal intensities for the particular ions. Care was taken to prevent saturation effects as well as power broadening by minimizing laser power. Laser calibration was based on observed (2 + 1) bromine atom REMPI peaks. The accuracy of the calibration was typically found to be about ±2.0 cm^{-1} on a two-photon wavenumber scale. Equipment condition parameters are listed in Table 1.

Table 1
Typical equipment/condition parameters for REMPI experiments.

HBr gas sample	Merck Schuchardt, Germany, Purity: 99.8%
Laser dyes	C480, C503, R540
Frequency doubling crystal	Sirah BBO-2
Laser repetition rate	10 Hz
Dye laser bandwidth	0.095 cm^{-1}
Laser intensity used	0.1–0.3 mJ/pulse
Nozzle size	500 μm
Sample backing pressure	2.0–2.5 bar
Pressure inside ionization chamber	10^{-6} mbar
Nozzle opening time	150–200 μs
Delay time for laser excitation	450–550 μs
Excitation wavenumber step sizes	0.05–0.1 cm^{-1}
Time of flight step sizes	10 ns

3. Results and analysis

Most HBr molecular spectra, previously detected in REMPI studies [21,26], in the two-photon resonance excitation region 74 000–86 000 cm^{-1} were identified and assigned. In addition, several "new spectra" were observed and assigned. These are grouped into three categories (see Table 2 and Fig. 1):

(i) Spectra due to two-photon resonance transitions to Rydberg states, not previously detected in REMPI but identified in single-photon absorption studies [9].
(ii) Spectra due to two-photon resonance transitions to Rydberg states, not previously detected.
(iii) Spectra due to two-photon resonance transitions to ion-pair states not previously detected or not analysed previously in terms of rotational energy structures.

Table 2 summarizes the above mentioned findings (i–iii). Fig. 1 shows some relevant 1D-REMPI spectra for parent and fragment ions. Spectra due to transitions to two Rydberg states ($k^3\Pi_1$ and $m^3\Pi_2$), not previously detected in REMPI, but identified in single-photon absorption studies [9], (i) are to be seen in Fig. 1a and b. Spectra due to transitions to two Rydberg states ($W^1\Sigma^+$ ($n = 6$, $v' = 0$) and $u^3\Delta_2(n = 6;\ v' = 0)$) not previously detected, (ii) are to be seen in Fig. 1c and d and spectra due to transitions to the vibrational states of the $V^1\Sigma^+$ ion-pair state, $V(m + 18)$, $V(m + 19)$ and $V(m + 17)$, (iii) are to be seen in Fig. 1c–e respectively. The assignments and analysis of these spectra as well as two more vibrational bands, $V(m - 1)$ and $V(m + 12)$, (iii) will be dealt with in more detail below. In addition to the molecular REMPI spectra observed, several bromine atomic (2 + 1) REMPI resonances were identified. These are believed to be due to excitations of bromine atoms formed by predissociations of Rydberg states and/or following one-photon photodissociation via the repulsive state $A^1\Pi$ [39,47].

3.1. Spectra due to two-photon resonance transitions to Rydberg states, not previously detected in REMPI studies

By comparison with the analysis given by Ginter et al. [9] spectra centred at $v^0 = 80386.0$ cm^{-1} and 80644.0 cm^{-1} (Fig. 1a and b), which have not been seen in REMPI before, are assigned to two-photon resonance transitions to the $k^3\Pi_1$ ($v' = 0$) and $m^3\Pi_2$

Table 2
HBr: Band origin (v^0) and rotational parameters ($B'$and D') for the $k^3\Pi_1$ ($v' = 0$), $m^3\Pi_2$ ($v' = 0$), $W^1\Sigma^+$ ($n = 6$, $v' = 0$), $u^3\Delta_2$ ($v' = 0$), $V^1\Sigma^+$ ($m + 1$), $V^1\Sigma^+$ ($m + 12$), $V^1\Sigma^+$ ($m + 17$), $V^1\Sigma^+$ ($m + 18$) and $V^1\Sigma^+$ ($m + 19$) states.

State	n	v'	v^0		B'/cm^{-1}		$D' \times 10^3$/cm^{-1}		References for others' work
			Our work	Others' work	Our work	Others' work	Our work	Others' work	
$k^3\Pi_1$	5	0	80386.0	80386.0	8.150 ± 0.009	8.13	0.82	0.07	[9]
$m^3\Pi_2$	5	0	80644.0	80647.2	8.038 ± 0.017	8.05	−0.04	0.34	[9]
						8.04		0.23	
$W^1\Sigma^+$	6	0	85464.0	–	6.5 ± 0.1	–	4.4	–	–
$u^3\Delta_2$	6	0	85831.0	–	7.84 ± 0.05	–	0.3	–	–
$V^1\Sigma^+$	–	m − 1	75351.5	–	2.75 ± 0.16	–	−2.5	–	–
$V^1\Sigma^+$	–	m + 12	82416.7	82419.4[a]	4.12 ± 0.06	–	−32	–	[21]
				82417.9[b]			4.0		[21]
				82418					[9]
$V^1\Sigma^+$	–	m+17	85126.9	85027.1[a]	2.61 ± 0.11	–	9.3	–	[21]
				85027.3[b]					[21]
$V^1\Sigma^+$	–	m + 18	85598.4	–	4.02	–	34	–	–
$V^1\Sigma^+$	–	m+19	85918.6	–	3.23 ± 0.16	–	−1.8	–	–

[a] $H^{79}Br$.
[b] $H^{81}Br$.

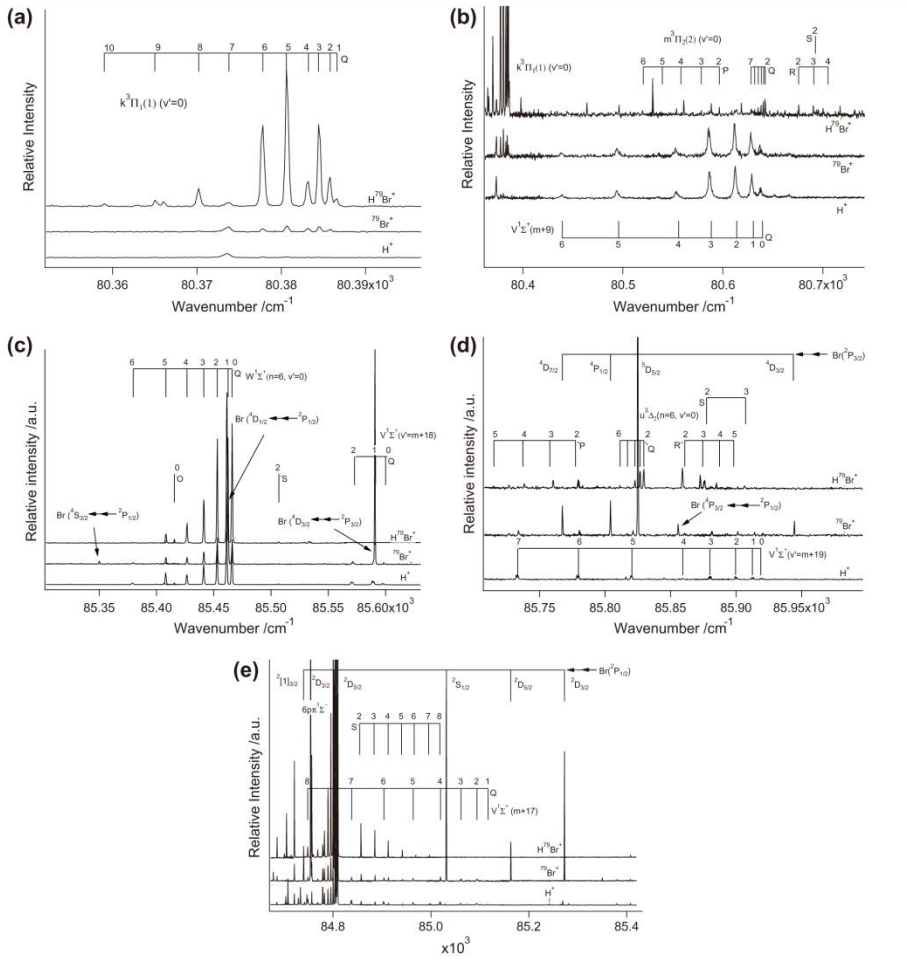

Fig. 1. 1D-REMPI spectra for H^+, $^{79}Br^+$ and $H^{79}Br^+$ and J' assignments of rotational peaks corresponding to two-photon resonance excitations to the $k^3\Pi_1$ ($v' = 0$) (a), $m^3\Pi_2$ ($v' = 0$) (b), $V^1\Sigma^+$ ($m + 9$) (b), $W^1\Sigma^+$ ($n = 6$, $v' = 0$) (c), $V^1\Sigma^+$ ($m + 18$) (c), $u^3\Delta_2$ ($n = 6$, $v' = 0$) (d), $V^1\Sigma^+$ ($m + 19$) (d) $6p\pi^3\Sigma^-$ ($v' = 0$) (e) and $V^1\Sigma^+$ ($m + 17$) (e) states. Bromine atomic (2 + 1) REMPI peaks are also marked.

($v' = 0$) Rydberg states respectively. Spectral analysis reveal rotational constants ($B'$and D') close to those given by Ginter et al. [9] (see Table 2).

Analogous to that observed by Ginter et al. perturbations are seen in the spectrum for $k^3\Pi_1$ ($v' = 0$) for $J' = 4$ and 7. This shows as line shifts, hence energy level shifts, as well as intensity alterations (see Fig. 1a). The intensity alterations show clearly as drops in the parent ion signals ($I(H^iBr^+)$) for $J' = 4$ and 7, but also as enhancements in the fragment ion signals ($I(^iBr^+)$ and I (H^+)), for $J' = 7$ in particular. Thus the intensity ratios $I(^iBr^+)/I(H^iBr^+)$ ($i = 79$, 81) as a function of J' show sharp peaks for $J' = 7$ and slight, but significant, increases for $J' = 4$ (see Fig. 2a). These observations are characteristic for near-resonance, level-to-level interactions between states with same J' values [43–47]. Large enhancement in the intensity ratio for $J' = 7$ is typical for a mixing of a Rydberg state with an ion-pair state, since ionization via an ion-pair state mainly results in fragment ions whereas ionization via pure, unmixed Rydberg states mainly results in parent ions. The Q line series for the ion-pair state $V(m + 9)$, seen in the fragment ion spectra only, shows broad peaks for $J' = 0$–6 on the long wavenumber side of the $k^3\Pi_1$

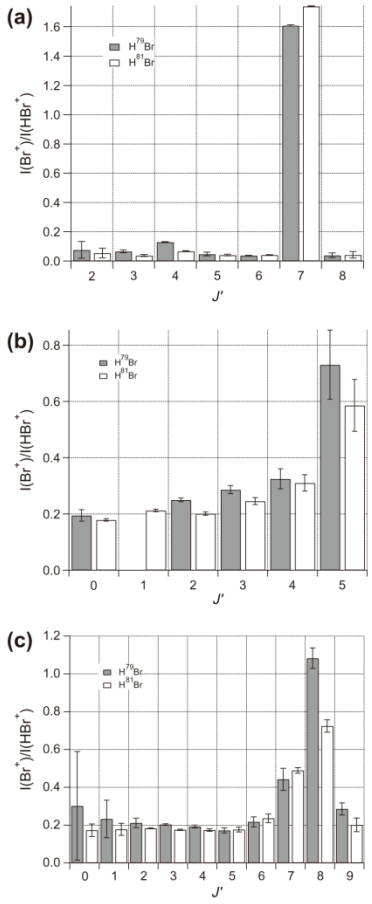

Fig. 2. Relative ion signal intensities, $I(^iBr^+)/I(H^iBr^+)$ (i = 79, 81) vs. J' derived from Q rotational lines of REMPI spectra due to two-photon resonance transitions to the Rydberg states $k^3\Pi_1$ (v' = 0) (a), $W^1\Sigma^+$ (n = 6, v' = 0) (b) and $6p\pi^3\Sigma^-$ (v' = 0) (c).

(v' = 0) spectrum (see Fig. 1b). Although the peak, for $V(m+9)$, J' = 7 is too weak or too broad to be observed, an extrapolation of the Q line series suggests that it should be close to the Q lines for the $k^3\Pi_1$ (v' = 0) system, in which case the near-resonance interaction of concern must be between $k^3\Pi_1$ (v' = 0, J' = 7) and $V(m+9; J'=7)$. Thus an increased fragment ion signal and a decreased parent ion signal for the $k^3\Pi_1$ (v' = 0, J' = 7) resonance excitation is due to enhanced ion-pair state character in the mixed state. The state mixing, most probably is via $k^3\Pi_1$ and $k^3\Pi_0$ state interactions. The perturbation for J' = 4, on the other hand, mainly shows as a decrease in both signals (Fig. 1a) and small change in the intensity ratio, suggesting that it is not due to mixing with an ion-pair state. Most likely, therefore, it is due to mixing with another Rydberg state with lower ionization probability. There are no observed 1D-REMPI signals due to transitions to other Rydberg states, nearby, which could explain this, suggesting that it is a hidden state, i.e. a state not detectable in (2 + n) REMPI. This could be due to low transition probabilities or unfavorable selection rules. A possible candidate for a perturbing state is $i^3\Delta_3$ (v' = 1), which would be about 2100 cm^{-1} higher in energy than the v' = 0 vibrational component [21], as might be expected for an energy spacing between v' = 0 and v' = 1 for a Rydberg state. Coupling between the $i^3\Delta_3$ and the $k^3\Pi_1$ states could occur through the $i^3\Delta_2$ component, which can interact with $i^3\Delta_3$ by rotational coupling [27,43,47].

The weak spectrum observed for $m^3\Pi_2$ (v' = 0) shows P, Q and R lines close to those observed by Ginter et al. [9] as well as the S line J' = 2 ←← J'' = 0 (Table 3; Fig. 1b). In addition to $m^3\Pi_2$ (v' = 0) state peaks seen in that region some unidentified sharp peaks are also seen in the H^iBr^+ spectra in the region 80470–80620 cm^{-1} (Fig. 1b).

Table 3
Rotational lines for H^iBr (i = 79, 81), due to two-photon resonance transitions to the $k^3\Pi_1$ (v' = 0), $m^3\Pi_2$ (v' = 0), $W^1\Sigma^+$ (n = 6, v' = 0), $u^3\Delta_2$ (n = 6, v' = 0), $V^1\Sigma^+$ (m + 1), $V^1\Sigma^+$ (m + 12), $V^1\Sigma^+$ (m + 17), $V^1\Sigma^+$ (m + 18) and $V^1\Sigma^+$ (m + 19) states.

J'	$k^3\Pi_1$	$m^3\Pi_2$			
	Q	P	Q	R	S
0					
1	80385.1				
2	80384.3	80596.5	80642.4	80676.0	80695.6
3	80383.1	80578.4	80640.8	80690.4	
4	80381.7	80558.0	80638.4	80704.8	
5	80379.3	80539.6	80635.4		
6	80376.4	80520.4	80631.7		
7	80372.3		80628.1		
8	80368.8				
9	80363.7				
10	80357.6				
	$W^1\Sigma^+$	$u^3\Delta_2$			
	Q	P	Q	R	S
0	85464.0				
1	85460.4				
2	85451.0	85777.2	85827.4	85856.9	85873.7
3	85439.3	85758.2	85824.5	85870.5	85903.5
4	85424.6	85736.1	85820.6	85882.8	
5	85406.1	85712.5	85814.9		
6	85377.7		85809.2		
7					
8					
9					
10					
	$V^1\Sigma^+$ (m − 1) Q	$V^1\Sigma^+$ (m + 12) Q	$V^1\Sigma^+$ (m + 17) Q	$V^1\Sigma^+$ (m + 18) Q ($H^{79}Br$)	$V^1\Sigma^+$ (m + 19) Q ($H^{79}Br$)
0	75351.5	82416.7		85598.4	85918.6
1	75342.2	82408.7	85114.5	85589.6	85912.1
2	75321.5	82393.1	85092.0	85571.2	85899.2
3	75287.9	82370.2	85059.5		85879.7
4	75241.8	82345.3	85017.5		85855.7
5	75186.3	82318.8	84961.7		85820.5
6	75124.0		84902.0		85779.4
7			84836.2		85732.6
8			84746.4		
9					
10					

3.2. Spectra due to two-photon resonance transitions to Rydberg states, not previously detected

A spectrum, not previously observed, is seen in the two-photon excitation region 85370–85470 cm^{-1} (see Fig. 1c) with a

characteristic shape of a Q branch for a Rydberg state. It shows dominating HBr^+ signals but also significant fragment ion signals (Br^+ and H^+) with a varying intensity ratio $I(^iBr^+)/I(H^iBr^+)$ as a function of J' (see Fig. 2b). This is characteristic for an $\Omega = 0$ state showing strong homogeneous, off resonance, coupling with ion-pair vibrational states [45,47]. Spectral analysis, based on these assumptions, give rotational constant $B' = 6.50\ cm^{-1}$ and band origin $\nu^0 = 85463.0\ cm^{-1}$ (Table 2). This rotational constant is significantly lower than those for Rydberg states, which exhibit small or negligible couplings with ion-pair states, such as $\Omega > 0$ and triplet states and resembles values for the $E^1\Sigma^+$ state [21,26]. Extrapolation of known vibrational energies for the $E^1\Sigma^+$ ($n = 5$), $v' = 0$, 1, 2 and 3 states [21,26] reveals that this state cannot be a vibrationally excited E-state. Quantum defect analysis, on the other hand, gave similar quantum defect values, $\delta = 2.45$ and 2.40, for the $\nu^0 = 85463.0\ cm^{-1}$ and the $E^1\Sigma^+$ ($n = 5$, $v' = 0$) states, respectively in the expression,

$$\nu^0 = IE - R_H/(n-\delta)^2 \quad (1)$$

if $n = 6$ in the former case. IE is the ionization energy ($IE = 94205.52\ cm^{-1}$) and R_H is the Rydberg constant. We assign the $\nu^0 = 85463.0\ cm^{-1}$ state to $W^1\Sigma^+$ ($n = 6$, $v' = 0$). The intensity ratios, $I(^iBr^+)/I(H^iBr^+)$; $i = 79$, 81, gradually increase with J' for $J' = 0$–5 (Fig. 2b). This is typical for an increasing interaction as a function of J' with a higher lying $V(m + (i + 1))$ state and for a decreasing interaction as a function of J' with a lower lying $V(m + i)$ state, in a case where the interaction with the higher V state dominates [45]. That is the case when the higher energy V state ($V(m + (i + 1))$) is closer in energy to the Rydberg state (see Fig. 3). The V states of concern are $V(m + 17)$ and $V(m + 18)$ at $\nu^0 = 85102.0\ cm^{-1}$ and $85598.0\ cm^{-1}$, respectively, as discussed in more detail below. This interaction effect can also be seen from line-shifts, hence energy level shifts. The spacing between neighbor rotational levels ($\Delta E_{J',J'-1} = E(J') - E(J'-1)$) as a function of J', derived from the Q lines in the $W^1\Sigma^+$ ($n = 6$, $v' = 0$) spectrum (Fig. 1c) reveals negative deviation from linearity, which is typical for such off-resonance interactions [45,47].

The Rydberg spectrum shown in Fig. 1d shows only parent ion signals. Its rotational structure resembles number of hydrogen halide spectra for two-photon transitions to $\Omega = 2$ states [15–17,21,27]. Analysis based on that assumption gives $\nu^0 = 85831.0\ cm^{-1}$ and $B' = 7.84\ cm^{-1}$. This B' value is typical for a "pure", unperturbed Rydberg state. Furthermore, no significant perturbation effects are seen from line-shifts. Similar quantum defect parameters, $\delta = 2.35$ and $\delta = 2.38$, are obtained for the $i^3\Delta_2$ ($n = 5$, $v' = 0$) state at $\nu^0 = 78630.7\ cm^{-1}$ and this new state respectively, assuming the latter to be a $n = 6$ state. We assign this spectrum to transitions to the $u^3\Delta_2$ ($n = 6$, $v' = 0$) state.

3.3. Spectra due to two-photon resonance transitions to ion-pair states, not previously detected or analysed

Number of vibrational states of the $V^1\Sigma^+$ ion-pair state have been observed and identified [9,13,21,26]. Since the lowest energy vibrational states have not been observed the absolute vibrational quantum numbers, v', are uncertain. Therefore, it is customary to label the states as $V(v' = m + i)$ where i are positive integers ($i > 0$) and m is an unknown positive integer or zero. REMPI spectra have been observed and assigned to $V(m + i)$ states for $i = 1$–13, 15–17, 19, 22 [21,26]. The $V(m + i)$ ($i = 3$, 4, 6–11, 13, 15, 16, 19, 22) states have been analysed to determine rotational spectroscopic parameters [21,26]. $V(m + i)$ spectra are clearly distinguishable from Rydberg state spectra in (a) – showing larger red degradation of spectra bands to give lower rotational constants ($B' = 3.2$–$4.9\ cm^{-1}$) and in (b) – showing, typically, larger fragment ion signals than parent ion signals, hence intensity ratios $I(^iBr^+)/I(H^iBr^+) > 1$. Furthermore, (c) line-widths of ion-pair bands are often found to be larger than those for Rydberg spectra, close in energy [47]. This is clearly seen in Fig. 1b, which shows the spectrum for $V(m + 9)$ along with the spectra for the Rydberg states $k^3\Pi_1$ ($v' = 0$) and $m^3\Pi_2$ ($v' = 0$). (d) In contradiction with observations for Rydberg state spectra isotope splittings are sometimes seen in the $V(m + i)$ spectra. We now report detection of five $V(m + i)$ states ($i = -1$, 12, 17, 18 and 19), three of which, ($V(m - 1)$, $V(m + 18)$ and $V(m + 19)$), have not been detected before (see Table 2 and Fig. 1c and e). The REMPI spectra for $V(m + 12)$ and $V(m + 17)$ have not been analysed spectroscopically in detail, before. The spectrum for $V(m + 19)$ differs from the one assigned to $i = 19$, earlier [26], which has been reassigned accordingly.

A weak but clear ion-pair state spectrum is identified at $\nu^0 = 75353.0\ cm^{-1}$ (see Table 2). Spectra analysis reveal rotational constant $B' = 2.75\ cm^{-1}$, typical for an ion-pair state. Fragment ion signals ($^iBr^+$ and H^+) are found to be larger than parent ion signals. The wavenumber spacing ($\Delta\nu^0$) between this band origin and the next closest in energy, which has been observed ($V(m + 1)$; $\nu^0 = 76516.0\ cm^{-1}$ [21]) is $1163\ cm^{-1}$, which is about twice that to be expected between neighbor vibrational levels, v' and $v' - 1$. The vibrational energy spacing ($\Delta E_{v',v'-1} = E(v') - E(v'-1)$) in the $V^1\Sigma^+$ state is found to be irregular due to perturbations, ranging between about 400 and 600 cm^{-1} for $i = 1$–8 [26]. This suggests that the new state is $V(m - 1)$. Calculations predict the band origin for $V(v' = 0)$ to be at $\nu^0 = 75548\ cm^{-1}$ [34] suggesting that this band could be due to transitions to $V(v' = 0)$ in which case $m = +1$. A search for a $V(m + 0)$ state spectrum in the excitation range between 75353 cm^{-1} and 76516 cm^{-1} was unsuccessful.

Few weak Q lines of an ion-pair state are seen for the fragment ion signals, slightly above the $W^1\Sigma^+$ ($n = 6$, $v' = 0$) spectrum (see Fig. 1c), as one would expect from the analysis of the W state, mentioned earlier. Small but clear isotope shift of about 1.4 cm^{-1} is detected. Analysis reveal values of $\nu^0 = 85598.0\ cm^{-1}$ and $B' = 4.02\ cm^{-1}$ for this new state (Table 2). Judging from the observation of the $V(m + 17)$ state [21], which band origin is found, here, to be $\nu^0 = 85102.0\ cm^{-1}$ (see below) the energy spacing between this state and the $V(m + 17)$ state is $\Delta\nu^0 = 496\ cm^{-1}$, something to be expected for vibrational energy level spacing. This suggests that the new state is $V(m + 18)$.

Weak but clear ion-pair state spectra (Q lines) for $^iBr^+$ and H^+, with isotope splitting of about 1.1 cm^{-1}, are seen in the neighborhood of the $i^3\Delta_2$ ($n = 6$, $v' = 0$) state spectrum (Fig. 1d). Analysis reveal values of $\nu^0 = 85918.6\ cm^{-1}$ and $B' = 3.23\ cm^{-1}$ for this new state (Table 2). The energy spacing between this state and the $V(m + 18)$ state is about $\Delta\nu^0 = 320\ cm^{-1}$, suggesting that this spectrum is due to a transition to the $V(m + 19)$ state. The ion-pair state reported in Ref. [26] to be $V(m + 19)$ at $86314.7\ cm^{-1}$ therefore must be $V(m + 20)$. Furthermore, the state reported in the same reference as $V(m + 22)$ at $87607.5\ cm^{-1}$ therefore is more likely to be the $V(m + 23)$. The lower energy spacing between $V(m + 18)$ and $V(m + 19)$ of $320\ cm^{-1}$ compared to that between $V(m + 17)$ and $V(m + 18)$ ($496\ cm^{-1}$) is understandable because the strong state interactions between the $W(n = 6, v' = 0)$ state and the lower energy $V(m + 17)$ state and the higher energy $V(m + 18)$ state is repulsive in nature, resulting in an increased energy spacing between $V(m + 17)$ and $V(m + 18)$, hence decreasing spacing between $V(m + 18)$ and $V(m + 19)$.

Weak, broad, Q lines for the $V(m + 12)$ state are observed for the fragment ion signals, only. Analysis give $\nu^0 = 82417.0\ cm^{-1}$ and $B' = 4.12\ cm^{-1}$ (Table 2).

Relatively sharp Q lines, centred at $\nu^0 = 85102.0\ cm^{-1}$, are assigned to the $V(m + 17)$ state (Fig. 1e). Analysis give $B' = 1.31\ cm^{-1}$. This spectrum differs from that reported by Callaghan and Gordon ($\nu^0 \approx 85027\ cm^{-1}$ [21]). Further verification for our assignment is

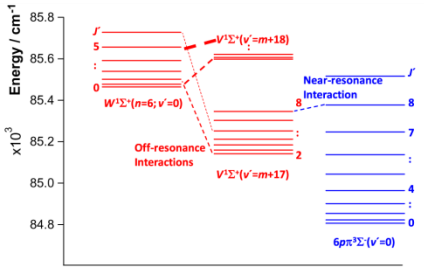

Fig. 3. Rotational energy levels, derived from observed REMPI rotational peaks for the $W^1\Sigma^+$ ($n = 6$, $v' = 0$), $V^1\Sigma^+$ ($m + 18$), $V^1\Sigma^+$ ($m + 17$) and $6p\pi^3\Sigma^-$ ($v' = 0$) states. Observed level-to-level near-resonance interaction between $6p\pi^3\Sigma^-$ ($v' = 0$) and $V^1\Sigma^+$ ($m + 17$) as well as off-resonance interactions between the ion-pair states ($V^1\Sigma^+$ ($m + 18$), $V^1\Sigma^+$ ($m + 17$)) and $W^1\Sigma^+$ ($n = 6$, $v' = 0$) are indicated by broken lines. Alterations in state mixings are indicated by varying thickness of broken lines.

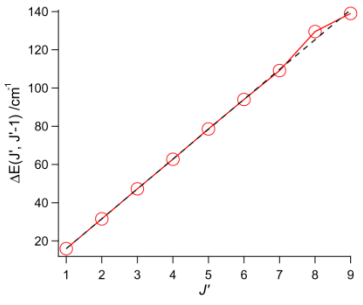

Fig. 4. Spacings between rotational levels ($\Delta E_{J'J'-1}$) as a function of J' for $6p\pi^3\Sigma^-$ ($v' = 0$). Dots connected by solid lines are derived from Q rotational lines. Broken line is linear fit for $J' = 1$–6.

evident from J'-dependent interaction found to occur between this state and the nearby $6p\pi^3\Sigma^-$ Rydberg state. Fig. 4 shows the spacing between neighbor rotational levels ($\Delta E_{J'J'-1} = E(J') - E(J'-1)$) as a function of J' for the $6p\pi^3\Sigma^-$ state. The observed deviations in linearity of $\Delta E_{J'J'-1}$ for $J' = 7$, 8 and 9, with relatively large positive deviation for $J' = 8$ is typical for a near-resonance interaction [27,45,47] between $J' = 8$ levels, in which case the level for the $6p\pi^3\Sigma^-$ state is "pushed upward" due to an interaction from a lower lying $J' = 8$ state to make the energy spacing between levels $J' = 8$ and 7 ($\Delta E_{8,7}$) larger and $\Delta E_{7,6}$ and $\Delta E_{9,8}$ slightly smaller. The interaction of concern is a heterogeneous, $\Delta\Omega = 1$, interaction. This interaction is caused by the $J' = 8$ state of $V(m + 17)$, which Q line (84746.4 cm^{-1}) is found at slightly lower wavenumber than the Q ($J' = 8$) line for the $6p\pi^3\Sigma^-$ state (84777.2 cm^{-1}) (see Table 3 and Figs. 1e and 3). Furthermore, intensity ratios, $I(^iBr^+)/I(H^iBr^+)$, as a function of J' for the $6p\pi^3\Sigma^-$ state (see Fig. 2c), show clear evidence [43–47] for this near-resonance interaction, since the ratio reaches maximum for $J' = 8$.

4. Conclusions

Several new spectra features, observed in two-dimensional ($2 + n$) REMPI of H^iBr, were assigned and analysed. Rotational parameters and band origins were determined. Perturbation effects, seen as line-shifts and/or intensity anomalies, due to interactions between Rydberg states and ion-pair states and/or between two Rydberg states proved to be very helpful in assigning spectra. (i) Firstly, spectra due to resonance transitions to the Rydberg states $k^3\Pi_1$ ($v' = 0$) and $m^3\Pi_2$ ($v' = 0$), not previously observed in REMPI, were identified. Data revealed state interactions between the $k^3\Pi_1$ ($v' = 0$) state and the $V(m + 9)$ ion-pair state as well as between $k^3\Pi_1$ ($v' = 0$) and a hidden Rydberg state. (ii) Secondly, based on quantum defect analysis, two new spectra, not previously observed, were assigned to resonance transitions to the $W^1\Sigma^+$ ($n = 6$, $v' = 0$) and $u^3\Delta_2$ ($n = 6$, $v' = 0$) states. Effects of off-resonance interactions between the $W^1\Sigma^+$ ($n = 6$, $v' = 0$) state and the $V(m + 18)$ and $V(m + 17)$ states, further clarified the $W(n = 6, v' = 0)$ assignment. (iii) Thirdly, five vibrational bands of the ion-pair state $V^1\Sigma^+$, $V(m + i)$ ($i = -1$, 12, 17, 18 and 19), easily distinguishable from Rydberg state spectra, were identified and analysed. The spectra due to the transitions to $V(m - 1)$, $V(m + 18)$ and $V(m + 19)$ have not been detected before and those due to transitions to $V(m + 12)$ and $V(m + 17)$, have not been analysed spectroscopically before. The spectrum for $V(m + 17)$ was reassigned on the basis of observed near-resonance interaction with the $6p\pi^3\Sigma^-$ Rydberg state.

Acknowledgments

The financial support of the University Research Fund, University of Iceland, the Icelandic Science Foundation as well as the Norwegian Research Council is gratefully acknowledged.

References

[1] W.C. Price, Proc. Roy. Soc. Ser. A 167 (1938) 216.
[2] R.F. Barrow, J.G. Stamper, Proc. Roy. Soc. Ser. A. 263 (1961) 277–288.
[3] R.F. Barrow, J.G. Stamper, Proc. Roy. Soc. Ser. A. 263 (1961) 259–276.
[4] S.G. Tilford, M.L. Ginter, J.T. Vanderslice, J. Mol. Spectrosc. 33 (1970) 505–519.
[5] S.G. Tilford, M.L. Ginter, J. Molec, Spectroscopy 40 (1971) 568–579.
[6] D.S. Ginter, M.L. Ginter, J. Mol. Spectrosc. 90 (1981) 177–196.
[7] S.G. Tilford, M.L. Ginter, A.M. Bass, J. Mol. Spectrosc. 34 (1970) 327.
[8] M.L. Ginter, S.G. Tilford, A.M. Bass, J. Mol. Spectrosc. 57 (1975) 271.
[9] D.S. Ginter, M.L. Ginter, S.G. Tilford, J. Mol. Spectrosc. 90 (1981) 152.
[10] D.S. Ginter, M.L. Ginter, S.G. Tilford, A.M. Bass, J. Mol. Spectrosc. 92 (1982) 55.
[11] D.S. Ginter, M.L. Ginter, S.G. Tilford, J. Mol. Spectrosc. 92 (1982) 40.
[12] J.B. Nee, M. Suto, L.C. Lee, J. Chem. Phys. 85 (1986) 719–724.
[13] J.B. Nee, M. Suto, L.C. Lee, J. Chem. Phys. 85 (1986) 4919.
[14] T.A. Spiglanin, D.W. Chandler, D.H. Parker, Chem. Phys. Lett. 137 (5) (1987) 414–420.
[15] D.S. Green, G.A. Bickel, S.C. Wallace, J. Mol. Spectrosc. 150 (2) (1991) 303–353.
[16] D.S. Green, G.A. Bickel, S.C. Wallace, J. Mol. Spectrosc. 150 (2) (1991) 354–387.
[17] D.S. Green, G.A. Bickel, S.C. Wallace, J. Mol. Spectrosc. 150 (2) (1991) 388–469.
[18] D.S. Green, S.C. Wallace, J. Chem. Phys. 96 (8) (1992) 5857–5877.
[19] E.d. Beer, B.G. Koenders, M.P. Koopmans, C.A.d. Lange, J. Chem. Soc. Faraday Trans. 86 (11) (1990) 2035–2041.
[20] Y. Xie, P.T.A. Reilly, S. Chilukuri, R.J. Gordon, J. Chem. Phys. 95 (2) (1991) 854–864.
[21] R. Callaghan, R.J. Gordon, J. Chem. Phys. 93 (1990) 4624–4636.
[22] Á. Kvaran, H. Wang, Á. Logadóttir, Rotational REMPI Spectroscopy: Halogen containing Compounds, in: Recent Res. Devel. in Physical Chem. 1998, Transworld Research, Network, pp. 233–244.
[23] S.A. Wright, J.D. McDonald, J. Chem. Phys. 101 (1) (1994) 238–245.
[24] S.T. Pratt, M.L. Ginter, J. Chem. Phys. 102 (1995) 1882–1888.
[25] E.d. Beer, W.J. Buma, C.A. deLange, J. Chem. Phys. 99 (5) (1993) 3252–3261.
[26] Á. Kvaran, Á. Logadóttir, H. Wang, J. Chem. Phys. 109 (14) (1998) 5856–5867.
[27] Á. Kvaran, H. Wang, Á. Logadóttir, J. Chem. Phys. 112 (24) (2000) 10811–10820.
[28] Á. Kvaran, B.G. Waage, H. Wang, J. Chem. Phys. 113 (5) (2000) 1755–1761.
[29] D. Ascenzi, S. Langford, M. Ashfold, A. Orr-Ewing, Phys. Chem. Chem. Phys. 3 (1) (2001) 29–43.
[30] R. Liyanage, R.J. Gordon, R.W. Field, J. Chem. Phys. 109 (19) (1998) 8374–8387.
[31] M. Bettendorff, S.D. Peyerimhoff, R.J. Buenker, Chem. Phys. 66 (1982) 261–279.
[32] D.M. Hirst, M.F. Guest, Mol. Phys. 41 (6) (1980) 1483–1491.
[33] H. Lefebvre-Brion, H.P. Liebermann, G.J. Vazquez, J. Chem. Phys. 134 (20) (2011) 204104.
[34] S.Z. Zlatkova, Computational investigation of the ionization and photo-ionizationof hydrogen halide acids in water clusters, in: The Department of

Chemistry and Biochemistry, Concordia University Montreal, Quebec, 2006, p. 100.
[35] A.I. Chichinin, C. Maul, K.H. Gericke, J. Chem. Phys. 124 (22) (2006) 224324.
[36] A.I. Chichinin, P.S. Shternin, N. Godecke, S. Kauczok, C. Maul, O.S. Vasyutinskii, K.H. Gericke, J. Chem. Phys. 125 (3) (2006) 034310.
[37] S. Kauczok, C. Maul, A.I. Chichinin, K.H. Gericke, J. Chem. Phys. 133 (2) (2010) 24301.
[38] C. Maul, S. Kauczok, V. Werwein, K.-H. Gericke, The unusual behaviour of the F(1D2) state of HCl: A 3 D Velocity Map Imaging Study, in: The 21st Colloquium on High Resolution Molecular Spectroscopy International Conference, Castellammare di Stabia (Italy), 2009.
[39] C. Romanescu, H.P. Loock, Phys. Chem. Chem. Phys. 8 (25) (2006) 2940–2949.
[40] C. Romanescu, H.P. Loock, J. Chem. Phys. 127 (12) (2007) 124304.
[41] C. Romanescu, S. Manzhos, D. Boldovsky, J. Clarke, H. Loock, J. Chem. Phys. 120 (2) (2004) 767–777.
[42] Kristján Matthíasson, J. Long, Huasheng Wang, A. Kvaran, J. Chem. Phys. 134 (2011) 164302.
[43] A. Kvaran, H.S. Wang, K. Matthiasson, A. Bodi, E. Jonsson, J. Chem. Phys. 129 (16) (2008) 164313.
[44] A. Kvaran, K. Matthiasson, H.S. Wang, J. Chem. Phys. 131 (4) (2009) 044324.
[45] K. Matthiasson, J.M. Long, H.S. Wang, A. Kvaran, J. Chem. Phys. 134 (16) (2011) 164302.
[46] K. Matthiasson, H.S. Wang, A. Kvaran, J. Mol. Spectrosc. 255 (1) (2009) 1–5.
[47] J.M. Long, H.R. Hrodmarsson, W.H. Wang, A. Kvaran, J. Chem. Phys. 136 (2012) 214315.
[48] Á. Kvaran, H. Wang, Mol. Phys. 100 (22) (2002) 3513–3519.
[49] Á. Kvaran, K. Matthíasson, H. Wang, Phys. Chem.: Indian J. 1 (1) (2006) 11–25.
[50] Á. Kvaran, Ó.F. Sigurbjörnsson, H. Wang, J. Mol. Struct. 790 (2006) 27–30.

Paper IV

Ágúst Kvaran, Kári Sveinbjörnsson, Jingming Long, Huasheng Wang, *Two-dimensional REMPI of CF_3Br: Rydberg states and photofragmentation channels.* Chemical Physics Letters, 2011. **516**(1-3): p. 12-16.

Chemical Physics Letters 516 (2011) 12–16

Contents lists available at SciVerse ScienceDirect

Chemical Physics Letters

journal homepage: www.elsevier.com/locate/cplett

Two-dimensional REMPI of CF_3Br: Rydberg states and photofragmentation channels

Ágúst Kvaran *, Kári Sveinbjörnsson, Jingming Long, Huasheng Wang

Science Institute, University of Iceland, Dunhagi 3, 107 Reykjavík, Iceland

ARTICLE INFO

Article history:
Received 12 August 2011
In final form 19 September 2011
Available online 22 September 2011

ABSTRACT

Mass spectra were recorded for $(2 + n)$ REMPI of CF_3Br as a function of resonance excitation energy in the 71 320–84 600 cm^{-1} region to obtain two-dimensional REMPI data. CF_3^+, $^iBr^+$ ($i = 79,81$) and C^+ ions were detected. Laser power dependence experiments were performed for ion signals. CF_3^+ signals due to resonance transitions from the ground state CF_3Br to number of Rydberg states and various vibrational states followed by CF_3^+ and Br^- ion-pair formation via intersystem crossings, were identified. Bromine atom production by predissociation channels via two-photon excitation to the Rydberg states is proposed, based on detecting bromine atom (2 + 1) REMPI.

1. Introduction

CF_3Br and its related counterparts CF_3Cl and CF_3I are all important industrial compounds with wide ranging applications. The freon CF_3Br (Halon 1301) has been used in aircrafts for fuel inerting and as a fire suppressor whereas CF_3Cl (CFC-13) has been used as a refrigerant. The production and use of these two compounds has been banned under the terms of the Montreal Protocol since 2000 [1], due to their significant ozone depletion and global warming properties. More recently CF_3I, which is considered less environmental unfriendly, has been considered as a possible replacement compound for CF_3Br and CF_3Cl. All in all the possible uses or discarding of these compounds rely on their photochemical and photoabsorption properties.

Rather limited detailed information are available on the photoabsorption and photochemistry of CF_3Br as well as of CF_3Cl and CF_3I. Although the vacuum UV spectrum of CF_3Br was reported as early as 1973 [2] only recently reliable absorption cross sections at energies above the lowest lying electronic transitions have appeared [3]. The UV absorption spectroscopy of these compounds is similar. Weak continua due to $n \rightarrow \sigma^*$ C–X (X = Cl, Br, I) transitions (A bands) appear at low energies. More intense structures due to $\sigma \rightarrow \sigma^*$ C–X transitions and transitions from lone pair orbitals with dominant X character (p to sp^3 character) to ns and np Rydberg states appear at higher energies [3,4]. Rydberg states identified, are either believed to belong to series converging to the two spin–orbit components of the ground state ions, $X^2E_{3/2}$ and $X^2E_{1/2}$, or the first excited ionic state $A^2E_{1/2}$ [3,5]. Spectra due to transitions to ns Rydberg states are generally found to be more intense than those due to transitions to np states as one might expect from the basic selection rule $\Delta l = \pm 1$.

In terms of photochemistry studies main emphasise has been on the effect of absorption in the low energy A band corresponding to transitions to several repulsive states followed by dissociation to form $CF_3 + Br(^2P_{3/2})/Br^*(^2P_{1/2})$ [6–8]. The same products are believed to be the main result of photodissociation via higher energy states [4,9]. Fluorescence studies of CF_3Cl and CF_3Br reveal emissions from CF_3^* for excitations above the energy thresholds for $CF_3^* + X$; X = Cl, Br formations [4,10,11] with maximum quantum yields of about 20% and 7% at 112.5 nm (CF_3Cl) and 125.0 nm (CF_3Br), respectively. Judging from negative photoion spectroscopy studies of CF_3X; X = Cl, Br and I insignificant ion-pairs, $CF_3^+ + X^-$ are formed via excitations to the high energy Rydberg state region despite being energetically allowed [9]. This is surprising and contradicts with observations for related compounds such as methyl halides [12,13], hydrogen halides [14–17], halogens [18,19] and interhalogens [20,21] where Rydberg doorway states in ion-pair formations have been evidenced.

Whereas resonance enhanced multiphoton ionization (REMPI) studies have been performed for CF_3Cl [11] and CF_3I [22,23] to our best knowledge no analogous studies have been reported for CF_3Br. 4p and 6p Rydberg states are found to be excited by two-photon resonance excitations of CF_3Cl and CF_3I, respectively. Spectra due to transitions to Rydberg states with total electronic angular momentum quantum numbers $\Omega = 0,1$ and 2 in the series converging to both ion states, $X^2E_{3/2}$ and $X^2E_{1/2}$, have been identified for CF_3I [22]. The fragment ions CF_3^+ and CF^+ and (2 + 1) REMPI of the Cl atoms are detected in REMPI of CF_3Cl, whereas no parent ions have been seen [11]. The CF_3^+ ions are believed to be formed by ionization of CF_3^* after dissociation of the resonance excited Rydberg states and the strong Cl atom resonances are mainly attributed to dissociation channels which form the species $CF_3 + Cl(^2P_{3/2})/Cl^*(^2P_{1/2})$. CF_3^+ and CF_3I^+ ions are detected in REMPI of CF_3I. It has been argued that structure distortions observed in Rydberg states of CF_3I could possibly be due to interactions with ion-pair states [22].

* Corresponding author. Fax: +354 552 8911.
E-mail address: agust@hi.is (Á. Kvaran).

0009-2614/$ - see front matter © 2011 Elsevier B.V. All rights reserved.
doi:10.1016/j.cplett.2011.09.046

The Rydberg and ion-pair state structures of the unfluorinated counterparts CH_3X; X = Cl, Br and I have been studied more extensively than the corresponding fluorinated compounds [24] and limited comparison of spectra structures is available. Considerable differences, however, have been observed in certain Rydberg spectra structures for CF_3I and CH_3I [22].

In this Letter we present (2 + *n*) REMPI studies of CF_3Br. Two-photon resonance excitations to Rydberg states are observed and characterized. Ion-pair formations and predissociation channels are identified.

2. Experimental

Two dimensional (2D) REMPI data for jet cooled CF_3Br gas were recorded. Ions were directed into a time-of-flight (TOF) tube and detected by a micro-channel plate (MCP) detector to record the ion yield as a function of mass and laser radiation wavenumber. The apparatus used is similar to that described elsewhere [25–27]. Tunable excitation radiation in the 562–475 nm wavelength region was generated by Excimer laser-pumped dye laser systems, using a Lambda Physik COMPex 205 Excimer laser and a Coherent ScanMatePro dye laser. The dyes C-540A, C-503, and C-480 were used and frequency doubling obtained with a BBO-2 crystal. The repetition rate was typically 10 Hz. The bandwidth of the dye laser beam was about 0.095 cm^{-1}. Typical laser intensity used was 0.1–0.3 mJ/pulse. The radiation was focused into an ionization chamber between a repeller and an extractor plate. An undiluted, pure CF_3Br gas sample (Pfaltz & Bauer Inc.) was used. It was pumped through a 500 μm pulsed nozzle from a typical total backing pressure of about 2.0–2.5 bar into the ionization chamber. The pressure in the ionization chamber was lower than 10^{-6} mbar during experiments. The nozzle was kept open for about 170 μs and the laser beam was typically fired 500 μs after opening the nozzle. Ions were extracted into a TOF tube and focused onto a MCP detector, of which the signal was fed into a LeCroy WaveSurfer 44MXs-A, 400 MHz storage oscilloscope as a function of flight time. Average signal levels were evaluated and recorded for a fixed number of laser pulses (typically 30 pulses) to obtain the mass spectra. Mass spectra were typically recorded in 0.05 or 0.1 cm^{-1} laser wavenumber steps to obtain 2D REMPI spectra. REMPI spectra for certain ions as a function of excitation wavenumber (1D REMPI) were obtained by integrating mass signal intensities for the particular ion. Care was taken to prevent saturation effects as well as power broadening by minimising laser power. Laser calibration was performed by recording an optogalvanic spectrum, obtained from a built-in Neon cell, simultaneously with the recording of the REMPI spectra. Line positions were also compared with the bromine lines [28]. The accuracy of the calibration was found to be about ±1.0 cm^{-1} on a two-photon wavenumber scale. Intensity drifts during the scan were taken into account, and spectral intensities were corrected for accordingly. Overall spectra are composed of several shorter scans, each of which were normalized. These scans were then normalized to each other using the intensities of bands that are common to neighbouring sections.

3. Results and analysis

2D-REMPI data recorded for the two-photon excitation region 71320–84600 cm^{-1} revealed ion signals for CF_3^+, $^iBr^+$ (i = 79,81) and C^+ only. The CF_3^+ 1D-REMPI showed weak broad features ranging from about 74300 cm^{-1} to 84600 cm^{-1} (see Figure 1). The atom ion signals consisted of $^iBr(^2P_{3/2})/^iBr^*(^2P_{1/2})$ (Figure 2) and $C(^3P_j)/C^*(^1D)$ atom (2 + 1) REMPI's only. The ^iBr atom (2 + 1) REMPI signals observed, were very weak in the lowest wavenumber region (70987–72012 cm^{-1}; $Br^{**}([^3P_2]_c\ 5p) \leftarrow\leftarrow Br^*(4p^5;\ ^2P_{1/2})$ transitions) whereas the ^iBr atom resonance signals above 74300 cm^{-1} were significantly stronger, overall, and very strong signals were observed in the high energy region for the two resonance transitions from $Br^*(4p^5;\ ^2P_{1/2})$ to $Br^{**}([^1D]_c5p;\ ^2F_{5/2})$ (83376.99 cm^{-1}) and $Br^{**}([^1D]_c5p;\ ^2P_{1/2})$ (83814.79 cm^{-1}), respectively (see Figure 2). The C/C* atom REMPI signals all are very weak.

Comparison of the 1D-REMPI spectrum for CF_3^+ and the relative single-photon absorption spectrum derived from Ref. [3] (Figure 1) shows that the strongest features in the REMPI spectrum match the broad absorption peak, near 76550 cm^{-1}, which has been assigned to a transition from the ground state CF_3Br to a 5*p* Rydberg state which belongs to a Rydberg series converging to the ground ionic state (CF_3Br^+, X^2E) [3]. No CF_3^+ signal, on the other hand, was found for excitation in the lower energy region corresponding to excitations to the 5*s* Rydberg states (peak near 70750 cm^{-1}) and the overall CF_3^+ signal in the high energy region gradually decreases with energy between 80000–84600 cm^{-1} where an excitation to a 5*s* Rydberg state, which belongs to a Rydberg series converging to the excited ionic state ($CF_3Br^+\ ^2A_1$), is predicted to occur. We therefore conclude that negligible contribution to the CF_3^+ REMPI spectrum is associated with initial two-photon excitations to 5*s* Rydberg states but that significant contribution to the spectral features can be due to initial transitions to 5*p* Rydberg states. This is what might be expected for a two-photon excitation of a nonbonding electron localized on the halogen atom with dominating *p*-orbital character according to the selection rule $\Delta l = 0$. Assignments of CF_3^+ REMPI spectra features are shown in Figure 1 and listed in Table 1. These were guided by the following.

(i) Rydberg states were assumed to follow the standard expression

$$E([\Omega_c]nl;\omega) = IE([\Omega_c] - R/(n-\delta_l)^2 \quad (1)$$

where $E([\Omega_c]nl;\omega)$ is the energy of the Rydberg state $[\Omega_c]nl;\omega$, IE is the ionization limit to which the series converges ($[\Omega_c]$), R is the Rydberg constant, n is the principal quantum number and δ_l is the relevant quantum defect, depending on l (see Table 2). A search was made for consistent fits of the major spectra peaks to expression [1] for ionization limits of spin–orbit components of the ground ionic state (Table 1) for realistic quantum defect values (see Table 2).

(ii) Assuming that the potential energy surfaces for the Rydberg states closely resembles those for the ground state $CF_3Br(X)$ there is a reason to believe that the strongest spectral features are due to transitions corresponding to unaltered vibrational energy, i.e. that $\Delta v_i = 0$ transitions are the most Franck–Condon-factor favourable for all i. Furthermore frequencies of vibrational modes for Rydberg states are expected to be close to those in the ground state. ν'_i (i = 1,2,3) notations corresponding to a1 symmetry (valid for $CF_3Br(X)$) are assumed.

(iii) By analogy with Rydberg state assignments and observations for the unfluorinated counterpart CH_3Br[12,13] *p* and *d* Rydberg states, both $\omega' = 0$ and $\omega' = 2$ components are expected to be observable with $E(\omega = 2) < E(\omega = 0)$. Whereas ΔE_ω ($=E(\omega = 0) - E(\omega = 2)$) is uncertain its value is expected to decrease with the principal quantum number n [12].

Transitions to four *p* Rydberg states ($[X^2E_{3/2}]5p$, $[X^2E_{3/2}]6p$, $[X^2E_{1/2}]5p$ and $[A^2E_{3/2}]6p$) and one *d* state ($[X^2E_{3/2}]4d$ are identified. Generally the strongest features for each transition are assigned to $\omega = 0$ states, vibrational bands (0,0) whereas spectral features on the long wavenumber side of these, within about 1000 cm^{-1} wave-

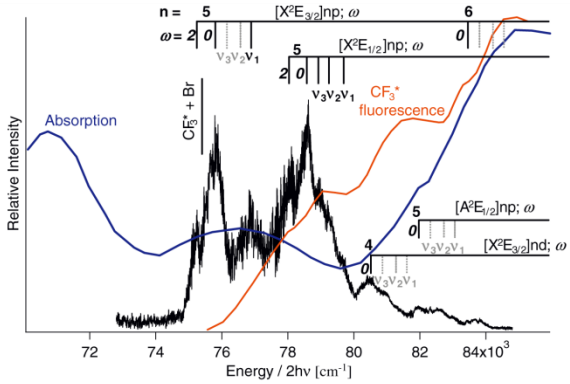

Figure 1. CF_3^+ 1D REMPI spectrum, relative absorption spectrum from Ref. [3] (blue curve) and relative CF_3^* fluorescence spectrum from Ref. [4] (red curve). Assignments of Rydberg states are shown as unbroken sticks. Dotted sticks are estimated vibrational bands based on vibrational frequencies for the ground state. Threshold for $CF_3^+ + Br$ formation is marked.(For interpretation of the references to colour in this figure legend, the reader is referred to the web version of this article.)

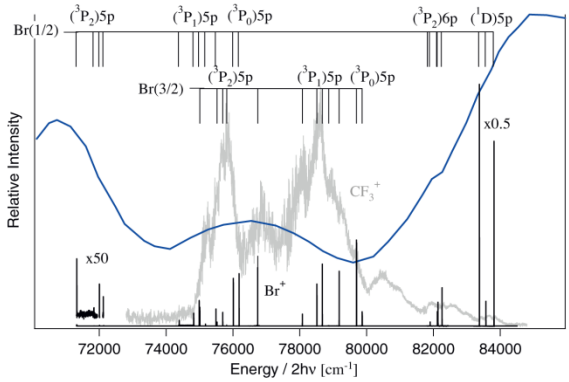

Figure 2. Br^+ 1D REMPI spectra (bold) along with the CF_3^+ 1D REMPI spectrum (Figure 1) (grey) and the absorption spectrum from Ref. [3] (blue curve). Assignments of Br atomic lines are indicated.(For interpretation of the references to colour in this figure legend, the reader is referred to the web version of this article.)

number region, are attributed to transitions to $v_i' = 1$ and $v_j' = 0$ ($j \neq i$). $\omega = 2$ components were identified for the $[X^2E_{3/2}]5p$ and $[X^2E_{1/2}]5p$ states with $\Delta E_\omega = 560$ and 540 cm^{-1}, respectively. Quantum defect values derived from the analysis and *IE*'s used are listed in Table 1.

Whereas the very weak bromine atomic REMPI signals observed between 70987–72012 cm^{-1} are in the region where no significant Rydberg state excitation is found to occur the medium to strong bromine atomic lines between 74300 and 84600 cm^{-1} are observed where the transitions to the *p* and *d* Rydberg states are observed (Figure 2). The strong lines at 83376.99 and 83814.79 cm^{-1} are associated with transitions to the $[X^2E_{3/2}]6p$ state. We therefore believe that the corresponding Br atoms ($Br(^2P_{3/2})$ and $Br^*(^2P_{1/2})$ are formed via predissociation of the excited Rydberg states ($CF_3Br^{**}(Ry)$) followed by (2 + 1) REMPI, as

$$CF_3Br(X) + 2h\nu \rightarrow CF_3Br^{**}(Ry) \quad (2a)$$

$$CF_3Br^{**}(Ry) \rightarrow CF_3 + Br/Br^* \quad (2b)$$

$$CF_3Br^{**}(Ry) \rightarrow CF_3^* + Br/Br^* \quad (2c)$$

$$Br/Br^* + 2h\nu \rightarrow Br^{**}; Br^{**} + h\nu \rightarrow Br^+ + e^- \quad (2d)$$

The predissociation can either occur by channel (2b) for all energy excitations or by channel (2c) for energies larger than 75332 cm^{-1} [4]. According to Suto and Lee [4] the maximum fluorescence quantum yield for CF_3^* is only 7% (for 125.0 nm/80000 cm^{-1} one-photon excitation) suggesting that channel (2b) dominates over (2c). Log–log plots of signal intensities as a function of the laser power showed typical 'levelling off curvature' [13], which makes it hard to determine the number of photons required for the ionization. This is characteristic of saturation effect, as may be expected for a multiple step (2 + 2 + 1) REMPI [13,29].

Table 1
Transition wavenumbers, assignments, quantum defect values (δ_l) and ionization energies (IE) relevant for bands due to transitions from ground state CF_3Br to Rydberg states.

Peaks/shoulders (cm^{-1})	Assignments $[\Omega_c]nl;\omega(v_1,v_2,v_3)$	δ_l	IE/cm^{-1}
75243	$[X^2E_{3/2}]5p$; 2 (0,0,0)		91979.4[a]
75803	$[X^2E_{3/2}]5p$; 0 (0,0,0)	2.40	91979.4[a]
76890	$[X^2E_{3/2}]5p$; 0 1,0,0		
78036	$[X^2E_{1/2}]5p$; 2 (0,0,0)		94366.8[b]
78576	$[X^2E_{1/2}]5p$; 0 (0,0,0)	2.36	94366.8[b]
78922	$[X^2E_{1/2}]5p$; 0 (0,0,1)		
79244	$[X^2E_{1/2}]5p$; 0 (0,1,0)		
79692	$[X^2E_{1/2}]5p$; 0 (1,0,0)		
81967	$[A^2E_{1/2}]5p$; 0 (0,0,0)	2.39	98077.0[c]
83455	$[X^2E_{3/2}]6p$; 0 (0,0,0)	2.38	91979.4[a]
80515	$[X^2E_{3/2}]4d$; 0 (0,0,0)	0.91	91979.4[a]

[a] From Ref. [5].
[b] Based on Ref. [5]: $IE([X^2E_{1/2}]_c) = IE([X^2E_{3/2}]_c) + \Delta E_{S/O}(CF_3Br^+(X))$; $\Delta E_{S/O}$ ($CF_3Br^+(X)$) is the spin–orbit splitting in $CF_3Br^+(X)$ (0.30 eV).
[c] Based on Ref. [5]: $IE([A^2E_{1/2}]_c) = IE([X^2E_{1/2}]_c) + \Delta E_{S/O}$;(Br); $\Delta E_{S/O}$;(Br) is the spin–orbit splitting in Br (0.46 eV).

Table 2
Quantum defect values (δ_l) for Rydberg states of bromine atoms and bromine containing compounds.

	δ_l		
Atom/molecular species	*s*-States	*p*-States	*d*-States
Br	3.14[a]	2.69[a]	1.30[a]
Br_2	2.96[b]		1.29[b]
CH_3Br		2.57[c]	0.97[c]
CF_3Br	2.97[d], 3.10[d]	2.71[d], 2.38[e]	0.91[e]

[a] Average values derived from fitting expression (1) to bromine atom Rydberg state energy values [28] vs. principal quantum numbers n.
[b] Average values derived from reference [30].
[c] Average values derived from reference [12].
[d] Values from reference [3].
[e] Average values from this work; see Table 1.

CF_3^+ ions could either be formed by one-photon ionization of CF_3^* after its minor formation by (2c), or, more likely, by state-transfer from the Rydberg states to an inner wall of an ion-pair state above its dissociation limit to form CF_3^+ and Br^- ion pairs (see Figure 3),

$$CF_3^* + h\nu \rightarrow CF_3^+ + e^- \quad (3a)$$

$$CF_3Br^{**}(Ry) \rightarrow CF_3^+Br^- \rightarrow CF_3^+ + Br^- \quad (3b)$$

(3b) is analogous to many observations reported for related halogen containing compounds [12,21]. Comparison of the CF_3^+ 1D REMPI spectral structure and the relative fluorescence spectrum from reference [4] (see Figure 1) shows no clear correlation between the two. Furthermore, we performed careful power dependence experiments for the CF_3^+ signals as a function of the laser power for several wavenumber excitations in the region 77200–81600 cm^{-1} to derive consistent slope values of about 2 (1.9 ± 0.3) from log–log plots of signal intensities as a function of the laser power suggesting that only two photons are needed to form CF_3^+. All in all we therefore conclude that the major channel for the CF_3^+ formation is (3b).

Energetically C/C^* atoms can not be formed by dissociation of excited CF_3Br states formed by the initial two-photon excitation of concern. The very weak C/C^* atom (2 + 1) REMPI signals, observed, therefore must follow a minimum of initial three-photon excitation.

4. Conclusions

(2 + n) REMPI of CF_3Br reveals weak CF_3^+, medium to strong $^iBr^+$ (i = 79.81) and very weak C^+ ion signals, only, in the two-photon excitation region 71320–84600 cm^{-1}. The CF_3^+ signal shows

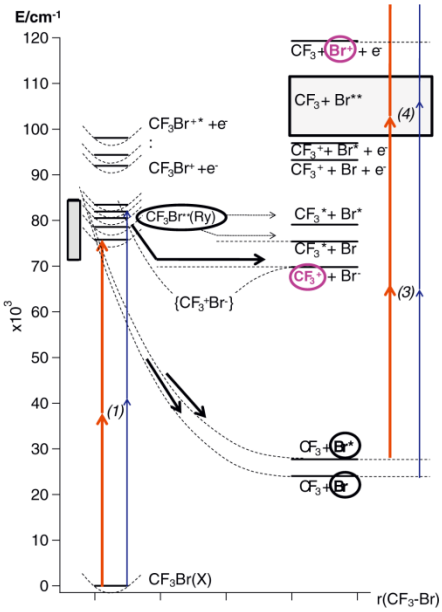

Figure 3. (2 + n) REMPI of CF_3Br: energetics, excitations (red and blue arrows) and photofragmentation processes. The excitation region studied is marked by a shaded area to left. Numbers inside brackets in italic indicate number of photons needed for the particular excitations shown in red and blue. Intermediate species of major importance in the photoexcitation and photofragmentation processes are highlighted with black circles. The major photodissociation processes are indicated by bold arrows. The shaded area on the right marks the range for bromine atomic energy levels excited in (2 + 1) REMPI. Major ion species detected are highlighted in purple. See text for further clarification.(For interpretation of the references to colour in this figure legend, the reader is referred to the web version of this article.)

molecular structures whereas only (2 + 1) atom REMPI signals for $^iBr^+$ and C^+ are observed. The CF_3^+ signals are associated with initial two-photon excitation to *p* and *d* Rydberg states followed by crossing to ion-pair states and formation of CF_3^+ and Br^- ion pairs in agreement with general observations for large number of halogen containing reagents. This is further supported by laser power dependence of CF_3^+ signals. The CF_3^+ spectra peaks observed are assigned to transitions to Rydberg states, ω = 0 and 2 and various vibrational states, v_i' (i = 1–3). The $^iBr^+$ (2 + 1) REMPI observed most probably follows predissociation of the excited Rydberg states of concern. More than two-photon initial excitation is needed prior to C/C^* formation and (2 + 1) C atom REMPI.

Acknowledgements

The financial support of the University Research Fund, University of Iceland, the Icelandic Science Foundation as well as the Norwegian Research Council is gratefully acknowledged.

References

[1] <http://www.unep.ch/ozone/index.shtml>.
[2] J. Doucet, P. Sauvagea, C. Sandorfy, Journal of Chemical Physics 58 (1973) 3708.

[3] S. Eden, P. Limao-Vieira, S.V. Hoffmann, N.J. Mason, Chemical Physics 323 (2006) 313.
[4] M. Suto, L.C. Lee, Journal of Chemical Physics 79 (1983) 1127.
[5] J.T. Clay, E.A. Walters, J.R. Grover, M.V. Willcox, Journal of Chemical Physics 101 (1994) 2069.
[6] T.K. Kim, K.W. Lee, K.S. Lee, E.K. Lee, K.H. Jung, Chemical Physics Letters 446 (2007) 31.
[7] T.K. Kim, M.S. Park, K.W. Lee, K.H. Jung, Journal of Chemical Physics 115 (2001) 10745.
[8] M.A. Thelen, P. Felder, Chemical Physics 204 (1996) 135.
[9] M.J. Simpson, R.P. Tuckett, K.F. Dunn, C.A. Hunniford, C.J. Latimer, Journal of Chemical Physics 130 (2009).
[10] N. Washida, M. Suto, S. Nagase, U. Nagashima, K. Morokuma, Journal of Chemical Physics 78 (1983) 1025.
[11] D. Ardelt, F. Stuhl, Chemical Physics Letters 304 (1999) 323.
[12] T. Ridley, J.T. Hennessy, R.J. Donovan, K.P. Lawley, S. Wang, P. Brint, E. Lane, Journal of Physical Chemistry A 112 (2008) 7170.
[13] A. Kvaran, H. Wang, K. Matthiasson, A. Bodi, Journal of Physical Chemistry A 114 (2010) 9991.
[14] A.J. Yencha, D. Kaur, R.J. Donovan, Á. Kvaran, A. Hopkirk, H. Lefebvre-Brion, F. Keller, Journal of Chemical Physics 99 (1993) 4986.
[15] K. Matthíasson, J. Long, H. Wang, A. Kvaran, Journal of Chemical Physics 134 (2011) 164302.
[16] A. Kvaran, K. Matthiasson, H. Wang, Journal of Chemical Physics 131 (2009) 044324.
[17] Á. Kvaran, K. Matthíasson, H. Wang, A. Bodi, E. Jonsson, Journal of Chemical Physics 129 (2008) 164313.
[18] A.J. Yencha, D.K. Kela, R.J. Donovan, A. Hopkirk, Á. Kvaran, Chemical Physics Letters 165 (1990) 283.
[19] Á. Kvaran, A.J. Yencha, D.K. Kela, R.J. Donovan, A. Hopkirk, Chemical Physics Letters 179 (1991) 263.
[20] D. Kaur, A.J. Yencha, R.J. Donovan, Á. Kvaran, A. Hopkirk, Organic Mass Spectrometry 28 (1993) 327.
[21] K.P. Lawley, A.C. Flexen, R.R.J. Maier, A. Manck, T. Ridley, R.J. Donovan, Physical Chemistry Chemical Physics 4 (2002) 1412.
[22] N.A. Macleod, S. Wang, J. Hennessy, T. Ridley, K.P. Lawley, R.J. Donovan, Journal of the Chemical Society-Faraday Transactions 94 (1998) 2689.
[23] G. VandenHoek, J.W. Thoman Jr., D.W. Chandler, S. Stolte, Chemical Physics Letters 188 (1992) 413.
[24] D.A. Shaw, D.M.P. Holland, I.C. Walker, Journal of Physics B-Atomic Molecular and Optical Physics 39 (2006) 3549.
[25] Á. Kvaran, H. Wang, Molecular Physics 100 (2002) 3513.
[26] Á. Kvaran, K. Matthíasson, H. Wang, Physical Chemistry; An Indian Journal 1 (2006) 11.
[27] Á. Kvaran, Ó.F. Sigurbjörnsson, H. Wang, Journal of Molecular Structure 790 (2006) 27.
[28] NIST Chemistry WebBook, NIST (National Institute of Standards and Technology) Chemistry WebBook.
[29] R.C. Sausa, R.L. Pastel, Resonance Enhanced Multiphoton Ionization (REMPI) and Photoacoustic (PA) Spectroscopic Detection of Nitric Oxide (NO) and Nitrogen Dioxide (NO_2) Near 454 nm, Army Research Laboratory, 1997. p. 1.
[30] T. Ridley, K.P. Lawley, R.J. Donovan, A.J. Yencha, Chemical Physics 148 (1990) 315.

Paper V

Kristján Matthíasson, Jingming Long, Huasheng Wang, Ágúst Kvaran, Two-dimensional resonance enhanced multiphoton ionization of H^iCl; i = 35, 37: State interactions, photofragmentations and energetics of high energy Rydberg states. The Journal of Chemical Physics, 2011. **134**(16): p. 164302.

Two-dimensional resonance enhanced multiphoton ionization of H^{i}Cl; i = 35, 37: State interactions, photofragmentations and energetics of high energy Rydberg states

Kristján Matthíasson, Jingming Long, Huasheng Wang, and Ágúst Kvaran[a)]
Science Institute, University of Iceland, Dunhagi 3, 107 Reykjavík, Iceland

(Received 8 February 2011; accepted 5 March 2011; published online 22 April 2011)

Mass spectra were recorded for $(2 + n)$ resonance enhanced multiphoton ionization (REMPI) of HCl as a function of resonance excitation energy in the 88865-89285 cm^{-1} region to obtain two-dimensional REMPI data. Band spectra due to two-photon resonance transitions to number of Rydberg states ($\Omega' = 0$, 1, and 2) and the ion-pair state $V(^1\Sigma^+(\Omega' = 0))$ for $H^{35}Cl$ and $H^{37}Cl$ were identified, assigned, and analyzed with respect to Rydberg to ion-pair interactions. Perturbations show as line-, hence energy level-, shifts, as well as ion signal intensity variations with rotational quantum numbers, J', which, together, allowed determination of parameters relevant to the nature and strength of the state interactions as well as dissociation and ionization processes. Whereas near-resonance, level-to-level, interactions are found to be dominant in heterogeneous state interactions ($\Delta\Omega \neq 0$) significant off-resonance interactions are observed in homogeneous interactions ($\Delta\Omega = 0$). The alterations in Cl^+ and HCl^+ signal intensities prove to be very useful for spectra assignments. Data relevant to excitations to the $f^3\Sigma(0^+)$ Rydberg states and comparison with $(3 + n)$ REMPI spectra allowed reassignment of corresponding spectra peaks. A band previously assigned to an $\Omega = 0$ Rydberg state was reassigned to an $\Omega = 2$ state ($\nu^0 = 88957.6$ cm^{-1}). © *2011 American Institute of Physics*. [doi:10.1063/1.3580876]

I. INTRODUCTION

Since the original work by Price on the hydrogen halides,[1] a wealth of spectroscopic data on HCl has been derived from absorption spectroscopy,[2–5] fluorescence studies[5] as well as from resonance enhanced multiphoton ionization (REMPI) experiments.[6–20] Relatively intense single- and multiphoton absorption in conjunction with electron excitations as well as rich band structured spectra make the molecule ideal for fundamental studies. A large number of Rydberg states, several low-lying repulsive states as well as the $V(^1\Sigma^+)$ ion-pair state have been identified. A number of spin-forbidden transitions are observed, indicating that spin–orbit coupling is important in excited states of the molecule. Perturbations due to state mixing are widely seen both in absorption[3–5] and REMPI spectra.[7,8,10,12,13,15,16,20] The perturbations appear either as line shifts[4,7,8,10,13,15,16,20] or as intensity and/or bandwidth alterations.[4,7,8,10,12,13,15,16,20] Pronounced ion-pair to Rydberg state mixings are both observed experimentally[3,4,8,10,13,15,16,20,21] and predicted from theory.[21,22] Interactions between the $V(^1\Sigma^+)$ ion-pair state and the $E(^1\Sigma^+)$ state are found to be particularly strong and to exhibit nontrivial rotational, vibrational, and electron spectroscopy due to a production of a mixed (adiabatic) $B^1\Sigma^+$ state with two minima. Perturbations due to Rydberg–Rydberg mixings have also been predicted and identified.[4,12] Both homogeneous ($\Delta\Omega = 0$)[15,16,21,22] and heterogeneous ($\Delta\Omega \neq 0$)[16,20,21] couplings have been reported. Such quantitative data on molecule–photon interactions are of interest in understanding stratospheric photochemistry as well as being relevant to the photochemistry of planetary atmospheres and the interstellar medium.[5]

Photofragment studies of HCl have revealed a large variety of photodissociation and photoionization processes. In a detailed two-photon resonance enhanced multiphoton ionization study, Green *et al.* report HCl^+, Cl^+, and H^+ ion formations for excitations via large number of $\Omega = 0$ Rydberg states as well as via the $V^1\Sigma^+$ ($\Omega = 0$) ion-pair state, whereas excitations via other Rydberg states are mostly found to yield HCl^+ ions.[7] More detailed investigations of excitations via various Rydberg states and the $V^1\Sigma^+$ ion-pair state by use of photofragment imaging and/or mass-resolved REMPI techniques have revealed several ionization channels depending on the nature of the resonance excited state.[23–30] The number of REMPI studies performed by our group for resonance excitations to the $F^1\Delta_2$ Rydberg state[16,27] and several triplet Rydberg states[16,27] as well as the $V^1\Sigma^+$ ion-pair states have revealed near-resonance interactions between the Rydberg and the ion-pair states. This shows as relative ion signal alterations in all cases[27,28,30] and/or as line shifts in all cases except for the weakest interactions.[16,20,29] Data analysis has allowed determination of interaction strength. The resonance interpretation has been confirmed by proton formation studies for REMPI via the $F^1\Delta_2$ ($v' = 1$, $J' = 8$) and $f^3\Delta_2(v' = 0$, $J' = 2$–$6)$ Rydberg states using three-dimensional velocity mapping.[29] All in all REMPI photofragmentation studies of HCl have revealed characteristic ionization channels which have been summarized in terms of excitations via (1)

a)Author to whom correspondence should be addressed. Electronic mail: agust@hi.is. Permanent address: Science Institute, University of Iceland, Dunhagi 3, 107 Reykjavík, Iceland, Tel: +354-525-4672/4800, Fax: +354-552-8911.

excitations via resonance noncoupled (diabatic) Rydberg state excitations, (2) excitations via resonance noncoupled (diabatic) ion-pair excitations, and (3) dissociation channels involving dissociation and/or photodissociation of resonance excited Rydberg states.[28]

In this paper, we use a two-dimensional (2D) REMPI data, obtained by recording ion mass spectra as a function of laser frequency, to study the state interactions and photofragmentation dynamics of HCl following two-photon resonance excitations to the triplet Rydberg states $j^3\Sigma\ (0^+)\ (v' = 0)$, $j^3\Sigma^-_1\ (v' = 0)$, the $V^1\Sigma^+\ (v' = 20, 21)$ ion-pair states as well as to Rydberg states, named *A* and *B* here, which band origins are at $\nu^0 = 88948.4\ \text{cm}^{-1}$ $\nu^0 = 88959.9\ \text{cm}^{-1}$, respectively, according to Green *et al.*[9] Rotational line shifts and quantum level dependent ion signal intensities, due to perturbation effects, are observed for the $H^{35}Cl$ and/or $H^{37}Cl$ isotopomers. By a combined analysis of the line shifts and signal intensities, interaction strengths, fractional state mixings, and parameters relevant to dissociation and ionization processes were evaluated. The perturbation observations as well as comparison of $(2 + n)$ and $(3 + n)$ REMPI data proved to be very helpful for assigning spectra bands. Lines due to transitions to the $j^3\Sigma\ (0^+)\ (v' = 0)$ and the *A* states were reassigned. The $\nu^0 = 88948.4\ \text{cm}^{-1}$ band, previously assigned to an $\Omega = 0$ state was reassigned to an $\Omega = 2$ state.

II. EXPERIMENTAL

Two-dimensional REMPI data for jet cooled HCl gas were recorded. Ions were directed into a time-of-flight tube and detected by a microchannel plate (MCP) detector to record the ion yield as a function of mass and laser radiation wavenumber. The apparatus used is similar to that described elsewhere.[19,30,31] Tunable excitation radiation in the 224.0 –225.0 nm wavelength region was generated by an Excimer laser-pumped dye laser system, using a Lambda Physik COMPex 205 Excimer laser and a Coherent ScanMatePro dye laser. The dye C-440 was used and frequency doubling obtained with a BBO-2 crystal. The repetition rate was typically 10 Hz. The bandwidth of the dye laser beam was about $0.095\ \text{cm}^{-1}$. Typical laser intensity used was 0.1 –0.3 mJ/pulse. The radiation was focused into an ionization chamber between a repeller and an extractor plate. We operated the jet in conditions that limited cooling in order not to lose transitions from high rotational levels. Thus, an undiluted, pure HCl gas sample (Merck-Schuchardt OHG; purity >99.5%) was used. It was pumped through a 500 μm pulsed nozzle from a typical total backing pressure of about 2.0–2.5 bar into the ionization chamber. The pressure in the ionization chamber was lower than 10^{-6} mbar during experiments. The nozzle was kept open for about 200 μs and the laser beam was typically fired 500 μs after opening the nozzle. Ions were extracted into a time-of-flight tube and focused onto a MCP detector, of which the signal was fed into a LeCroy 9310 A, 400 MHz storage oscilloscope and/or a LeCroy WaveSurfer 44MXs-A, 400 MHz storage oscilloscope as a function of flight time. Average signal levels were evaluated and recorded for a fixed number of laser pulses (typically 100 pulses) to obtain the mass spectra. Mass spectra were typically recorded in 0.05 or $0.1\ \text{cm}^{-1}$ laser wavenumber steps to obtain 2D REMPI spectra. REMPI spectra for certain ions as a function of excitation wavenumber (1D REMPI) were obtained by integrating mass signal intensities for the particular ion. Care was taken to prevent saturation effects as well as power broadening by minimizing laser power. Laser calibration was performed by recording an optogalvanic spectrum, obtained from a built-in Neon cell, simultaneously with the recording of the REMPI spectra. Line positions were also compared with the strongest hydrogen chloride rotational lines reported by Green *et al.*[9] The accuracy of the calibration was found to be about $\pm 1.0\ \text{cm}^{-1}$ on a two-photon wavenumber scale. Intensity drifts during the scan were taken into account, and spectral intensities were corrected accordingly. Experimental conditions for the three-photon excitation are described in Ref. 20.

III. RESULTS AND ANALYSIS

A. REMPI spectra and relative ion signals for the $j^3\Sigma^-_1 \leftarrow\leftarrow X^1\Sigma^+$ (0, 0) transitions

Figure 1 shows 2D-REMPI contour (below) and corresponding 1D-REMPI spectra (above) for the narrow spectral region of 88990–89080 cm^{-1}. The figure shows *Q* lines

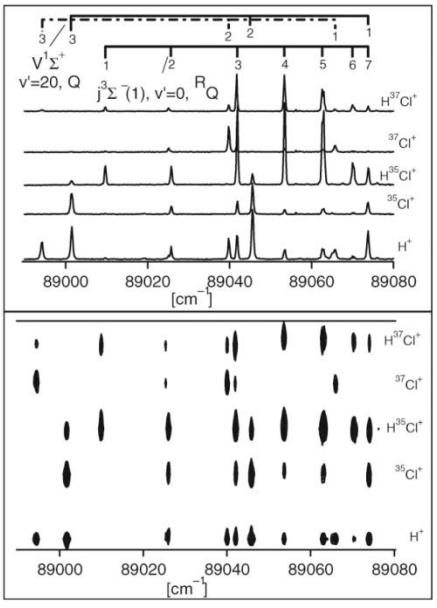

FIG. 1. 2D-$(2 + n)$ REMPI spectra (below) and corresponding 1D REMPI spectra (above) for H^+, $^{35}Cl^+$, $H^{35}Cl^+$, $^{37}Cl^+$, and $H^{37}Cl^+$ derived from HCl with isotope ratios in natural abundance for the two-photon excitation region of 88990– 89080 cm^{-1}. Assignments for the *Q* line series of the $j^3\Sigma_1 \leftarrow\leftarrow X^1\Sigma^+$ (0, 0) ($H^{35}Cl$ and $H^{37}Cl$: solid lines) and $V^1\Sigma^+ \leftarrow\leftarrow X^1\Sigma^+$ (20, 0) ($H^{35}Cl$: solid lines; $H^{37}Cl$: broken lines) spectra are shown. $J = J'$—numbers are indicated in the figure.

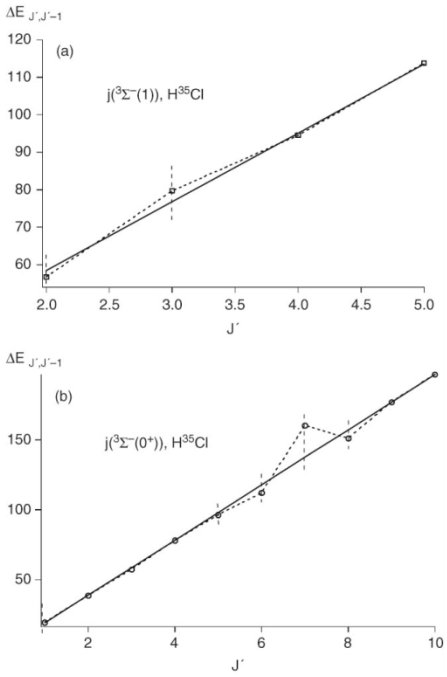

FIG. 2. $H^{35}Cl$: Spacings between rotational levels ($\Delta E_{J',J'-1}$) as a function of J' for the $j^3\Sigma^-(1)$ (a) and $j^3\Sigma^-(0^+)$ (b) Rydberg states for $H^{35}Cl$ derived from Q rotational lines.

due to the transitions $j^3\Sigma^-_1 \leftarrow\leftarrow X^1\Sigma^+$ (0, 0) and $V^1\Sigma^+ \leftarrow\leftarrow X^1\Sigma^+$ (20, 0), for the $H^{35}Cl$ and $H^{37}Cl$ isotopomers and their ion fragments.

Small but significant shift of peaks due to transitions to $J' = 2$ and 3 levels is observed. This shows as deviation in energy level spacings ($\Delta E_{J',J'-1} = E(J')-E(J'-1)$) from linearity for the corresponding rotational energy levels ($E(J')$) derived from measured peak positions and known rotational energy levels for the ground electronic state [see Fig. 2(a)]. This is a characteristic for a near-resonance level-to-level rotational interaction between the Rydberg state (1) and the $V(^1\Sigma^+)$ ion-pair state (2).[16,20] The smallest spacing between rotational energy levels of the two states for the same J' quantum numbers ($\Delta E_{J'} = E_1(J')-E_2(J')$) is found to be for $J' = 2$ and 3 for the $V(v' = 20)$ state (see Table I). First order unshifted energy levels, both for the $j^3\Sigma^-_1$ (1) and the $V(^1S^+)$ (2) states, ${E_1}^0(J')$ and ${E_2}^0(J')$, respectively, were derived from the linear fits for $\Delta E_{J',J'-1}$ versus J' [see Fig. 2(a)] and the energy level values for unshifted levels. From these and energies of perturbed levels ($E(J')$) interaction strengths (W_{12}) could be derived as a function of J' from

$$W_{12}(J') = \left[\frac{1}{4}\left\{\left(2\left(\left\langle\frac{1}{2}\left(E_1^0(J')+E_2^0(J')\right)\right\rangle - E_1(J')\right)\right)^2 - \left(E_1^0(J')-E_2^0(J')\right)^2\right\}\right]^{1/2}. \quad (1)$$

The interaction strength parameter, W'_{12} was derived from the expression $W_{12}(J') = W'_{12}\,(J'(J'+1))^{1/2}$ which holds for a heterogeneous interaction ($\Delta\Omega \neq 0$) (see Table II). The fractional contributions to the state mixing [c_1^2 for the Rydberg state (1) and c_2^2 for the ion-pair state (2)] are now easily derived from W_{12} and the energy difference $\Delta E_{J'} = E_1(J') - E_2(J')$ as

$$c_1^2 = \frac{1}{2} + \frac{\sqrt{(\Delta E_{J'})^2 - 4\,(W_{12})^2}}{2\,|\Delta E_{J'}|}; \quad c_2^2 = 1 - c_1^2. \quad (2)$$

Significant enhancement of the relative Cl^+ signals ($I(^{35}Cl^+)/I(H^{35}Cl^+)$) and $I(^{37}Cl^+)/I(H^{37}Cl^+)$) is observed for $j^3\Sigma^-_1 \leftarrow\leftarrow X^1\Sigma^+$, (0, 0), Q lines, $J' = 2$ [see Figs. 3(a) and 3(b)] also characteristic for the near-resonance interaction.[16,20,27] The $H^{37}Cl$ isotopomer shows considerably larger intensity ratio than the $H^{35}Cl$ isotopomer. An expression for $I(Cl^+)/I(HCl^+)$ as a function of the mixing fraction, c_2^2, based on ionization processes following resonance excitation, has been derived,[28]

$$\frac{I(Cl^+)}{I(HCl^+)} = \frac{\alpha\left[\gamma + c_2^2(1-\gamma)\right]}{\left(1-c_2^2\right)}, \quad (3)$$

$$I(Cl^+) = \alpha_2 c_2^2 + \beta_1 c_1^2; \quad I(HCl^+) = \alpha_1 c_1^2 + \beta_2 c_2^2$$

TABLE I. $\Delta E_{J'}$ relevant to near-resonance interactions for $j^3\Sigma^-_1 \leftrightarrow V^1\Sigma^+, v' = 20$, $j^3\Sigma^-(0^+) \leftrightarrow V^1\Sigma^+, v' = 20$, 21, State $A \leftrightarrow V^1\Sigma^+, v' = 20$, and State $B \leftrightarrow V^1\Sigma^+, v' = 20$.

	$\Delta E_{J'} = E(j^3\Sigma^-_1; v'=0) - E(V^1\Sigma^+; v'=20)$		$\Delta E_{J'} = E(j^3\Sigma^-(0^+); v'=0) - E(V^1\Sigma^+; v'=20/21)$		$\Delta E_{J'} = E(\text{State } A) - E(V^1\Sigma^+; v'=20)$	$\Delta E_{J'} = E(\text{State } B) - E(V^1\Sigma^+; v'=20)$
J'	$H^{35}Cl$	$H^{37}Cl$	$H^{35}Cl$ ($v'=20/21$)	$H^{37}Cl$ ($v'=20/21$)	$H^{35}Cl$	$H^{35}Cl$
0			196.4/−304.3	214.8/–316.1		
1	− 62.2	− 55.7	208.9/−311.6	215,4/–305.7		
2	− 20.6	− 14.7	232.4/−284.2	238.2/–280.6	− 96.6	− 92.7
3	40.2	47.9	271.6/−245.1	278.9/–241.7	− 62.0	− 59.3
4	108.2	115.1	322.5/−193.8	328.9/–190.4	− 22.0	− 13.8
5	187.3	192.1	384.2/−129.6	394.0/–130.7	26.0	45.4
6	279.0		457.4/–71	462.6/–65	88.0	117.2

TABLE II. Parameter values, relevant to state mixing, derived from peak shifts and intensity ratios ($I(^iCl^+)/I(H^iCl^+)$) as a function of J'. See definitions of parameters in the text.

	$j^3\Sigma^-_1; v'=0$		$j^3\Sigma^-(0^+); v'=0$		State B
Isotopomers	$H^{35}Cl$	$H^{37}Cl$	$H^{35}Cl$	$H^{37}Cl$	$H^{35}Cl$
J' closest resonances (J'_{res})	2	2	7(6)	6(7)	4
$\lvert\Delta E(J'_{res})\rvert(cm^{-1})$	20.6	14.7	? (71)[a,b]	65(?)[a,b]	13.8
$W_{12}(cm^{-1})$	6.5	5.8	25	25	2.7
$W'_{12}(cm^{-1})$	2.7	2.4	...	...	0.6
$c_1^2(c_2^2)$	0.89(0.11)	0.81(0.19)	0.88(0.12)	0.82(0.18)	0.96(0.04)
γ	0.004	0.003	(0.031)[c]	0.013	0.002
α	3.5	4.2	(2.1)[c]	4.0	3.1

[a] Values for $J'=7$ could not be determined since rotational peaks due to transitions to $V(v'=21, J'=7)$ were not observed.
[b] Values for $J'=6$ were derived from observations of weak and broad rotational lines in the Q series due to transitions to $V(v'=21, J'=6)$ at 89317.4 cm^{-1} and 89311.1 cm^{-1} for $H^{35}Cl$ and $H^{37}Cl$, respectively.
[c] Parameters are uncertain due to overlap of spectra peaks for transitions to $J'=6$ and 8. The γ value is an upper limit value. The α value is a lower limit value.

where $\alpha(=\alpha_2/\alpha_1)$ measures the relative rate of the two major/characteristic ionization channels, i.e., for the Cl^+ formation for excitation from the diabatic ion-pair state (α_2) to the HCl^+ formation from the diabatic Rydberg state (α_1). Here, $\gamma(=\beta_1/\alpha_2)$ represents the rate of Cl^+ formation via the diabatic Rydberg state (β_1; referred to as the "dissociative channel" in Ref. 28) to that of its formation from the diabatic ion-pair state (α_2), which is one of the major/characteristic ionization channels. Hence, γ is a relative measure of the importance of the "dissociative channel." Expression (3) allows the relative ion signals as a function of J' to be fitted to derive α and γ [Figs. 3(a) and 3(b) and Table II]. The larger Cl^+

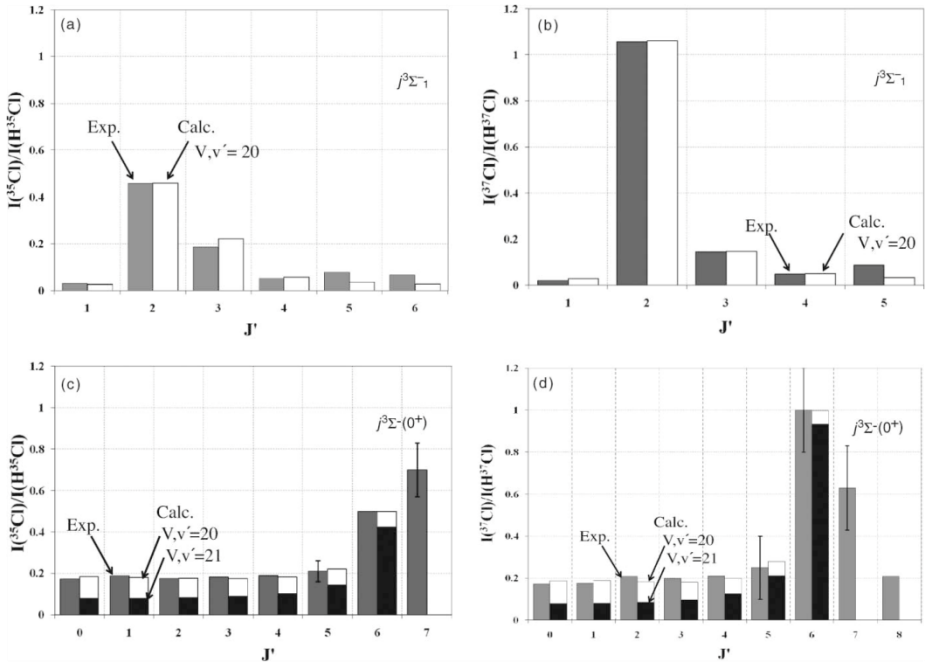

FIG. 3. Relative ion signal intensities, $I(^iCl^+)/I(H^iCl^+)$ ($i=35$ and 37) vs J' derived from Q rotational lines of REMPI spectra due to resonance transitions to Rydberg states (gray columns) and simulations, assuming J' level-to-level interactions between the Rydberg states and the $V^1\Sigma^+$ ($v'=20$, 21) states (white and black columns): (a) $H^{35}Cl$, $j^3\Sigma^-_1 \leftrightarrow V^1\Sigma^+$ ($v'=20$) interactions, (b) $H^{37}Cl$, $j^3\Sigma^-_1 \leftrightarrow V^1\Sigma^+$ ($v'=20$) interactions, (c) $H^{35}Cl$, $j^3\Sigma^-(0^+) \leftrightarrow V^1\Sigma^+$ [$v'=20$ (white columns) and $v'=21$ (black columns)] interactions, and (d) $H^{37}Cl$, $j^3\Sigma^-(0^+) \leftrightarrow V^1\Sigma^+$ [$v'=20$ (white columns) and $v'=21$ (black columns)] interactions.

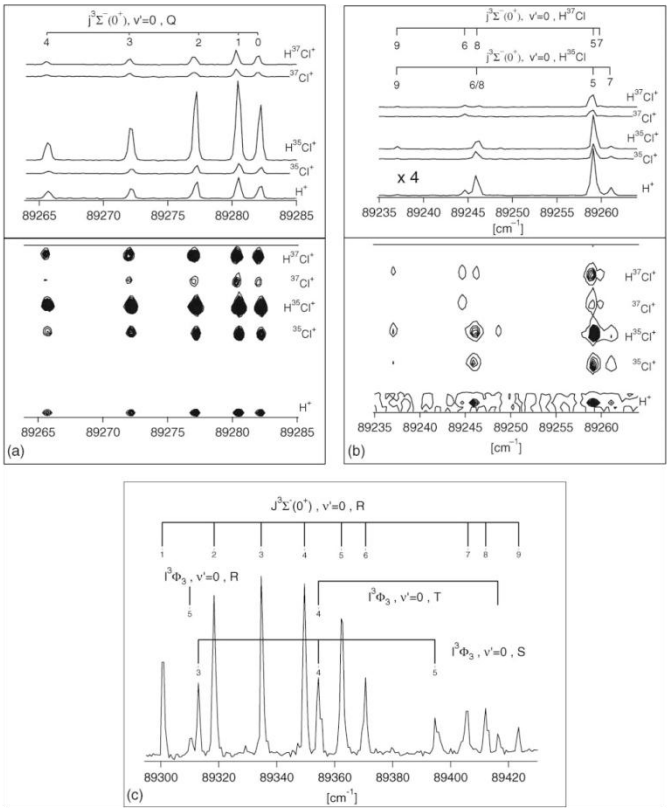

FIG. 4. (a) and (b) 2D-(2 + *n*) REMPI spectra (below) and corresponding 1D REMPI spectra (above) for H^+, $^{35}Cl^+$, $H^{35}Cl^+$, $^{37}Cl^+$, and $H^{37}Cl^+$ derived from HCl with isotope ratios in natural abundance for the two-photon excitation regions of 89264–89285 cm^{-1} (a) and 89235–89265 cm^{-1} (b). Assignments for the *Q* line series of the $j^3\Sigma^-(0^+) \leftarrow\leftarrow X^1\Sigma^+$ (0, 0) ($H^{35}Cl$ and $H^{37}Cl$) spectra are shown. The intensities of the 1D REMPI spectra in the 89235 –89265 cm^{-1} spectral region (b) have been multiplied by factor 4 with respect to the corresponding intensities in 89264–89285 cm^{-1} spectral region (a). (c) 1D-(3 + n) REMPI spectrum for total ionization of HCl for the three-photon excitation region of 89295–89430 cm^{-1}. Assignments for the $j^3\Sigma^-(0^+) \leftarrow\leftarrow X^1\Sigma^+$ (0, 0) and $I^3\Phi_3 \leftarrow\leftarrow X^1\Sigma^+$ (0, 0) transitions ($H^{35}Cl$ and $H^{37}Cl$) are shown. $J = J'$—numbers are indicated in the figures.

fragmentation observed for $H^{37}Cl$ compared to that for $H^{35}Cl$ can be understood by comparison of the derived parameters listed in Table II. Whereas the interaction strengths are comparable, for the two isotopomers the ion-pair mixing fraction (c_2^2) is significantly larger for $H^{37}Cl$ ($c_2^2 = 0.19$) than for $H^{35}Cl$ ($c_2^2 = 0.11$). This is primarily due to the smaller energy gap ($\Delta E_{J'} = 14.7\ cm^{-1}$) between the mixing rotational states for $H^{37}Cl$ compared to that for $H^{35}Cl$ ($\Delta E_{J'} = 20.6\ cm^{-1}$). The gamma values ($\gamma$) obtained, both for the $H^{35}Cl$ ($\gamma = 0.004$) and the $H^{37}Cl$ ($\gamma = 0.003$) isotopomers are small values and comparable to those obtained before for the triplet states $j^3\Delta_1$ and $g^3\Sigma^+$[28,30] indicating a small, but non-negligible contribution of the dissociation channels to the Cl^+ signal. Judging from a coupling scheme given by Alexander *et al.*[32] this could be formed after a direct predissociation of the $j^3\Sigma^-_1$ state by spin–orbit coupling with the repulsive $r^3\Sigma^+_1$ state and/or after predissociation of nearby Rydberg states ($^1\Pi$, $^3\Pi_2$) which could act as gateways via S/O coupling with the $j^3\Sigma^-_1$ states.

B. REMPI spectra and relative ion signals for the $j^3\Sigma^-(0^+) \leftarrow\leftarrow X^1\Sigma^+$ (0, 0) transitions

Figures 4(a) and 4(b) show 2D and 1D (2 + *n*) REMPI spectra for the narrow excitation region of 89235–89285 cm^{-1}. The figures show the *Q* lines due to the $j^3\Sigma^-(0^+) \leftarrow\leftarrow X^1\Sigma^+$ (0, 0) resonance transitions for $H^{35}Cl$ and $H^{37}Cl$. Total 1D (3 + *n*) REMPI spectrum is shown in Fig. 4(c) for the spectral region 89300–89430 cm^{-1}. It shows *R* lines for

TABLE III. Rotational lines for the $j^3\Sigma^-(0^+) \leftarrow\leftarrow X^1\Sigma^+$ (0, 0) transitions (HCl). The line positions are common to $H^{35}Cl$ and $H^{37}Cl$ except for the Q lines, $J' = 6$ and 7, in which case the values for $H^{37}Cl$ are inside brackets.

	$j^3\Sigma^-(0^+) \leftarrow\leftarrow X^1\Sigma^+$ (0, 0)		
J'	O	Q	S
0	89219.6	89282.0	
1	89176.2	89280.5	
2	89131.4	89277.3	89340.1
3		89272.1	89377.3
4		89266.8	89412.8
5		89259.0	89446.7
6		89246.3	89475.9
		(89244.7)	
7		89261.1	
		(89259.9)	
8		89246.3	
9		89237.1	

the same electronic transitions as well as peaks due to transitions to the $l^3\Phi_3$ state.[20] Clear gap between the $J' = 6$ and $J' = 7$ rotational lines is observed for the R lines. This gap corresponds to the smallest spacing between observed rotational energy levels for the $j^3\Sigma^-(0^+)$ ($v' = 0$) and rotational energy levels for the $V^1\Sigma^+$ ($v' = 21$) states for equal J' values (see Table I) suggesting a near-resonance interaction between the two states.[16,20,27] Comparison of peak positions in $(3 + n)$ and $(2 + n)$ REMPI spectra and relative intensities of ion peaks, allowed assignment of the Q line rotational peaks both for $H^{35}Cl$ and $H^{37}Cl$ in the $(2 + n)$ REMPI spectrum. Irregular arrangement of peaks, with respect to J' numbering, is seen for $J' = 5$–9 [see Fig. 4(b)] and enhanced intensity ratios ($I(^lCl^+)/I(H^lCl^+)$) are observed for transitions to $J' = 6$ and 7 [Figs. 3(c) and 3(d)]. See also Table III. Peak assignments differ from earlier assignments.[9,20]

Analogous and relatively large deviation in energy level spacings ($\Delta E_{J',J'-1}$) from linearity is clearly seen both for $H^{35}Cl$ and $H^{37}Cl$ [see Fig. 2(b)]. This allowed the interaction strengths (W_{12}) to be evaluated for $J' = 5$–8 analogous to that described before. A relatively large interaction strength value of about 25 ± 3 cm^{-1} was obtained both for $H^{35}Cl$ and $H^{37}Cl$ independent of J' as to be expected for homogeneous interactions (Table II). Despite difference in line assignments this value is comparable to that reported earlier in Ref. 20 ($W_{12} = 20 \pm 4$ cm^{-1}). The large homogeneous interaction strength results in off-resonance interactions between J' states showing as significant mixing contribution for the ion-pair state (c^2_2) over a wide range of J' states, both for $V(v' = 20)$ and $V(v' = 21)$. This results in significant contributions to the ion ratios from off-resonance interactions according to Eq. (3). Mixing contributions from vibrational states further away in energy ($v' < 20$ and $v' > 21$), on the other hand, are negligible, assuming the interaction strength (W_{12}) to be comparable.

Assuming, to a first approximation, that the ion intensity ratio is a sum of contributions due to interactions from the $V(v' = 20)$ and $V(v' = 21)$ states for common α and γ parameters $I(^{37}Cl^+)/I(H^{37}Cl^+)$ can be expressed as

$$\frac{I(Cl^+)}{I(HCl^+)} = \alpha \left\{ \frac{[\gamma + c^2_{2,20}(1-\gamma)]}{(1-c^2_{2,20})} + \frac{[\gamma + c^2_{2,21}(1-\gamma)]}{(1-c^2_{2,21})} \right\}, \quad (4)$$

where $c^2_{2,20}$ and $c^2_{2,21}$ are the fractional mixing contributions for $V(v' = 20)$ and $V(v' = 21)$, respectively. Figure 3(d) shows least square fit of the data for $I(^{37}Cl^+)/I(H^{37}Cl^+)$ versus J' as well as the $V(v' = 20)$ and $V(v' = 21)$ contributions for the α and γ parameters listed in Table II. The calculations are limited to $J' < 7$ since rotational lines for higher J', hence energy levels, for $V(v' = 21)$ could not be observed. Due to uncertainty in the ion-ratio value for $J' = 6$ because of overlap of Q line peaks for $J' = 6$ and 8 analogous least square analyses could not be performed for $H^{35}Cl$ [Fig. 3(c)]. The characteristic large and J'-independent ion intensity ratios for $J' < 5$, observed both for $H^{35}Cl$ and $H^{37}Cl$ result in a relatively large γ factor, an order of magnitude bigger than those determined for other triplet states, $\Omega' > 0$ mentioned before. This suggests that the "dissociation channels" are of greater importance. As mentioned before the small contributions to the dissociation channels for the other triplet states has been interpreted as being due to predissociation via gateway states.[28] Based on the coupling schemes given by Alexander *et al.*[32] such channels for the $j^3\Sigma^-$ states are limited. The "enhanced" importance of "dissociation channels" therefore could be due to an opening of a dissociation channel via photoexcitation to an inner wall of a bound excited Rydberg state above the dissociation limit.[28]

C. REMPI spectra and relative ion signals for the $A \leftarrow\leftarrow X^1\Sigma^+$ (0, 0) and $B \leftarrow\leftarrow X^1\Sigma^+$ (0, 0) transitions

Figure 5 shows 1D-REMPI spectra for the narrow spectral region of 88865–88985 cm^{-1}. The figure shows the Q lines due to the transitions $A \leftarrow\leftarrow X\ ^1\Sigma^+$ (0, 0) and $B \leftarrow\leftarrow X\ ^1\Sigma^+$ (0, 0) both for the $H^{35}Cl^+$ and $H^{37}Cl^+$ ions and corresponding ion fragments. Also it shows rotational lines due to the transitions $j^3\Sigma^-_1 \leftarrow\leftarrow X^1\Sigma^+$ (0, 0), $\Omega \leq 2 \leftarrow\leftarrow X^1\Sigma^+$ (0, 0), and $V^1\Sigma^+ \leftarrow\leftarrow X^1\Sigma^+$ (20, 0).

Slight but significant enhancement in spacing between rotational levels $J' = 5$ and 4 is observed for the B state and clear increase in the relative $^{35}Cl^+$ signal intensity is detected for the $B \leftarrow\leftarrow X\ ^1\Sigma^+$ (0, 0), $J' = 4$ transition (see Fig. 6). This corresponds to the smallest spacing between observed rotational energy levels of the B and the $V^1\Sigma^+$ ($v' = 20$) states for equal J' values for $J' = 4$ (see Table I) due to a near-resonance interaction between the two states.[16,20,27] Analysis of the line shifts allowed evaluation of $W_{12} = 2.7$ cm^{-1} ($W'_{12} = 0.6$ cm^{-1}) for $J' = 4$ for $H^{35}Cl$. Good consistency in calculated and experimental values for the ion ratios $I(^{35}Cl^+)/I(H^{35}Cl^+)$ was obtained for $\gamma = 0.002$ and $\alpha = 3.1$ (Fig. 6 and Table II). The B state has been assigned as an $\Omega = 2$ state.[9] The low γ value of 0.002 resembles those observed earlier for triplet states (see above and Ref. 28) which indicates that the B state is a $^3\Delta_2$ state.

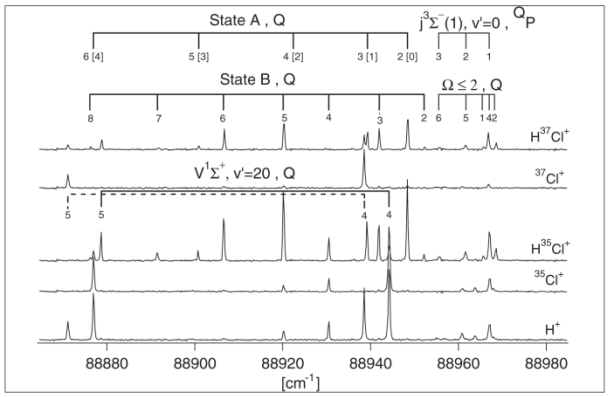

FIG. 5. 1D-$(2 + n)$ REMPI spectra for H^+, $^{35}Cl^+$, $H^{35}Cl^+$, $^{37}Cl^+$, and $H^{37}Cl^+$ derived from HCl with isotope ratios in natural abundance for the two-photon excitation region of 88865–88985 cm^{-1}. Assignments for $A \leftarrow\leftarrow X\,^1\Sigma^+$ (0, 0), $B \leftarrow\leftarrow X\,^1\Sigma^+$ (0, 0), $j^3\Sigma^-_1 \leftarrow\leftarrow X^1\Sigma^+$ (0, 0), and $\Omega' \leq 2 \leftarrow\leftarrow X^1\Sigma^+$ (0, 0) spectra ($H^{35}Cl$ and $H^{37}Cl$) are shown. Assignments for $V^1\Sigma^+ \leftarrow\leftarrow X^1\Sigma^+$ (20, 0) are shown for $H^{35}Cl$ as solid lines and for $H^{37}Cl$ as broken lines. Assignments from Ref. 9 for $A \leftarrow\leftarrow X\,^1\Sigma^+$ (0, 0) are in brackets. $J = J'$—numbers are indicated in the figure.

The spectral peaks due to the $A \leftarrow\leftarrow X\,^1\Sigma^+$ (0, 0) transition are marked according to the assignment given by Green *et al.*[9] with numbers inside brackets in Fig. 5. These have been reassigned based on our analysis of the 2D REMPI data, as shown in the figure, for reasons which will now be discussed.

Both the *A* and the *B* spectra show characteristic drops in peak intensities for the parent ions ($H^{35}Cl^+$ and $H^{37}Cl^+$) as J' increases. The intensities for the *B*-spectra, reach minima for the resonance perturbed levels $J' = 4$. As a matter of fact that peak is hardly observable for $H^{37}Cl^+$. Similarly, the *A*-spectra show either no peaks or very weak peaks[9] corresponding to the $J' = 2$ assignment given by Green *et al.* both for $H^{35}Cl$ and $H^{37}Cl$. This is characteristic for near-resonance interactions with the ion-pair state $V(^1\Sigma^+)^{20}$, which in this case must be for $v' = 20$. Both for the *B* and the *A* states the closes rotational levels, in energy, which belong to the $V(v' = 20)$ state are those for $J' = 4$ (see Fig. 5). The spacing, $\Delta E_{J'=4}$, for the *A* state ($H^{35}Cl$) is about 22.0 cm^{-1} (see Table I for the *B* state). It can, therefore, be concluded that the peaks assigned as $J' = 2$ for the *A* spectrum are in fact due to transitions to $J' = 4$ levels. This puts the first peaks in the line series as $J' = 2$, suggesting that the *A* state is an $\Omega = 2$ state. Other peaks in the *A* spectrum are reassigned accordingly in Fig. 5. Furthermore, there are no significant Cl^+ masses detected for any of the rotational transitions in the $A \leftarrow\leftarrow X\,^1\Sigma^+$ (0, 0) system which would be expected if the *A* state was an $\Omega = 0$ state.[27] Whereas the previous assignment gives a low rotational constant , B', of 5.7941 cm^{-1} for the *A* state, which certainly might be expected if it was an $\Omega' = 0$ state,[15,16] our reassignment gives $B' = 9.08$ cm^{-1}, which is typical for a Rydberg state with weak or negligible Rydberg-valence state mixing. Further analysis of the *A* state spectrum, based on the new assignment gives $D' = 0.0185$ cm^{-1} and $\nu^0 = 88957.6$ cm^{-1}. For comparison, $B' = 8.954$ cm^{-1} and $D' = -0.0042539$ cm^{-1} for the *B* state, which has been assigned as an $\Omega' = 2$ state.[9]

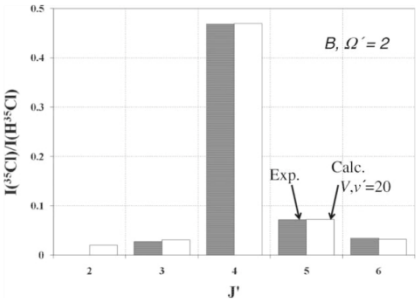

FIG. 6. Relative ion signal intensities, $I(^{35}Cl^+)/I(H^{35}Cl^+)$ vs J' derived from *Q* rotational lines of REMPI spectra due to resonance transitions to the $\Omega' = 2$ (88959.9 cm^{-1}) (*B*) state (gray columns) and simulations, assuming J' level-to-level interactions between the Rydberg state and the $V^1\Sigma^+$ ($v' = 20$) state (white columns).

IV. CONCLUSIONS

Two-dimensional $(2 + n)$ REMPI data for HCl, obtained by recording ion mass spectra as a function of the laser frequency, were recorded for the two-photon resonance excitation region 88865– 89285 cm^{-1}. Spectra for $H^{35}Cl$ and $H^{37}Cl$, due to resonance transitions to the ion-pair states $V^1\Sigma^+$ ($v' = 20$, 21) and four Rydberg states, $j^3\Sigma^-(0^+)(v' = 0)$, $j^3\Sigma^-_1(v' = 0)$ and states centered at = 88957.6 cm^{-1} (*A*) and 88959.9 cm^{-1} (*B*) for $H^{35}Cl$ were studied. A combined analysis of rotational line shifts and ion signal intensities was performed, developed, and used to derive information relevant to state interactions strengths, photofragmentation

channels, rotational energy characterization, and/or state assignments.

Interaction strengths, W_{12}, and fractional state mixing (c_1^2/c_2^2) due to Rydberg to ion-pair ($V^1\Sigma^+$ ($v' = 20$, 21)) state interactions were evaluated for the Rydberg states $j^3\Sigma^-(0^+)(v' = 0)$, $j^3\Sigma^-{}_1(v' = 0)$ for H^iCl; $i = 35$, 37 and for the B state ($H^{35}Cl$) from rotational line shift analysis. Enhancements in relative Cl^+ ion intensities, $I(^iCl^+)/I(H^iCl^+)$, are observed in all cases for J' levels corresponding to near-resonance interactions. Data for intensity ratios as a function of J' were compared to model expressions which take account of the major ion formation channels following excitations to the Rydberg states, state interactions as well as dissociation channels. The observations for the $j^3\Sigma^-{}_1(v' = 0)$ and the B states could be interpreted as being due to level-to-level interactions between the Rydberg states and the $V(v' = 20)$ states, whereas interactions both with $V(v' = 20$ and 21) needed to be taken account of to explain the observation for the $j^3\Sigma^-(0^+)(v' = 0)$ states. Fit analysis gave parameters which measure the importance of dissociation (predissociation and/or photodissociation) channels in the ionization processes. The weight of dissociation channels are found to be significantly larger for the $\Omega' = 0$ states ($j^3\Sigma^-(0^+)$) than for the $\Omega' = 1$, 2 states which have been studied.

Relative ion signals as a function of J' proved to be useful guide to assigning rotational peak spectra and allowed reassignments of the spectra due to the transitions to the $j^3\Sigma^-(0^+)(v' = 0)$ and the A ($v^0 = 88957.6\ cm^{-1}$) state. The A state was characterized as an $\Omega' = 2$ state with rotational parameters $B' = 9.08\ cm^{-1}$ and $D' = 0.0185\ cm^{-1}$.

ACKNOWLEDGMENTS

The financial support of the University Research Fund, University of Iceland, the Icelandic Science Foundation as well as the Norwegian Research Council is gratefully acknowledged.

[1] W. C. Price, Proc. R. Soc. London, Ser. A **167**, 216 (1938).
[2] S. G. Tilford, M. L. Ginter, and J. T. Vanderslice, J. Mol. Spectrosc. **33**, 505 (1970).
[3] S. G. Tilford and M. L. Ginter, J. Mol. Spectrosc. **40**, 568 (1971).
[4] D. S. Ginter and M. L. Ginter, J. Mol. Spectrosc. **90**, 177 (1981).
[5] J. B. Nee, M. Suto, and L. C. Lee, J. Chem. Phys. **85**, 719 (1986).
[6] T. A. Spiglanin, D. W. Chandler, and D. H. Parker, Chem. Phys. Lett. **137**(5), 414 (1987).
[7] D. S. Green, G. A. Bickel, and S. C. Wallace, J. Mol. Spectrosc. **150**(2), 303 (1991).
[8] D. S. Green, G. A. Bickel, and S. C. Wallace, J. Mol. Spectrosc. **150**(2), 354 (1991).
[9] D. S. Green, G. A. Bickel, and S. C. Wallace, J. Mol. Spectrosc. **150**(2), 388 (1991).
[10] D. S. Green and S. C. Wallace, J. Chem. Phys. **96**(8), 5857 (1992).
[11] E. d. Beer, B. G. Koenders, M. P. Koopmans, and C. A. d. Lange, J. Chem. Soc. Faraday Trans. **86**(11), 2035 (1990).
[12] Y. Xie, P. T. A. Reilly, S. Chilukuri, and R. J. Gordon, J. Chem. Phys. **95**(2), 854 (1991).
[13] Á. Kvaran, H. Wang, and Á. Logadóttir, Recent Res. Dev. Physical Chem. **2**, 233 (1998).
[14] E. d. Beer, W. J. Buma, and C. A. d. Lange, J. Chem. Phys. **99**(5), 3252 (1993).
[15] Á. Kvaran, Á. Logadóttir, and H. Wang, J. Chem. Phys. **109**(14), 5856 (1998).
[16] Á. Kvaran, H. Wang, and Á. Logadóttir, J. Chem. Phys. **112**(24), 10811 (2000).
[17] Á. Kvaran, H. Wang, and B. G. Waage, Can. J. Phys. **79**, 197 (2001).
[18] H. Wang and Á. Kvaran, J. Mol. Struct. **563–564**, 235 (2001).
[19] Á. Kvaran and H. Wang, Mol. Phys. **100**(22), 3513 (2002).
[20] Á. Kvaran and H. Wang, J. Mol. Spectrosc. **228**(1), 143 (2004).
[21] R. Liyanage, R. J. Gordon, and R. W. Field, J. Chem. Phys. **109**(19), 8374 (1998).
[22] M. Bettendorff, S. D. Peyerimhoff, and R. J. Buenker, Chem. Phys. **66**, 261 (1982).
[23] C. Romanescu and H. P. Loock, J. Chem. Phys. **127**(12), 124304 (2007).
[24] C. Romanescu, S. Manzhos, D. Boldovsky, J. Clarke, and H. Loock, J. Chem. Phys. **120**(2), 767 (2004).
[25] A. I. Chichinin, C. Maul, and K. H. Gericke, J. Chem. Phys. **124**(22), 224324 (2006).
[26] A. I. Chichinin, P. S. Shternin, N. Godecke, S. Kauczok, C. Maul, O. S. Vasyutinskii, and K. H. Gericke, J. Chem. Phys. **125**(3), 034310 (2006).
[27] Á. Kvaran, K. Matthíasson, H. Wang, A. Bodi, and E. Jonsson, J. Chem. Phys. **129**(17), 164313 (2008).
[28] A. Kvaran, K. Matthiasson, and H. Wang, J. Chem. Phys. **131**(4), 044324 (2009).
[29] S. Kauczok, C. Maul, A. I. Chichinin, and K.-H. Gericke, J. Chem. Phys. **133**, 024301 (2010).
[30] K. Matthiasson, H. Wang, and A. Kvaran, J. Mol. Spectros. **255**(1), 1 (2009).
[31] Á. Kvaran, K. Matthíasson, and H. Wang, Physical Chemistry; An Indian Journal **1**(1), 11 (2006).
[32] M. H. Alexander, X. N. Li, R. Liyanage, and R. J. Gordon, Chem. Phys. **231**(2–3), 331 (1998).

References

[1] S.G. Tilford, M.L. Ginter, J. Mol. Spectrosc. 40 (1971) 568.

[2] D.S. Ginter, M.L. Ginter, S.G. Tilford, J. Mol. Spectrosc. 90 (1981) 152.

[3] D.S. Ginter, M.L. Ginter, J. Mol. Spectrosc. 90 (1981) 177.

[4] D.S. Ginter, M.L. Ginter, S.G. Tilford, J. Mol. Spectrosc. 92 (1982) 40.

[5] D.S. Ginter, M.L. Ginter, S.G. Tilford, A.M. Bass, J. Mol. Spectrosc. 92 (1982) 55.

[6] J.B. Nee, M. Suto, L.C. Lee, J. Chem. Phys. 85 (1986) 719.

[7] S. Kauczok, C. Maul, A.I. Chichinin, K.H. Gericke, J. Chem. Phys. 133 (2010) 024301.

[8] D.S. Green, G.A. Bickel, S.C. Wallace, J. Mol. Spectrosc. 150 (1991) 303.

[9] R. Liyanage, P.T.A. Reilly, Y.-a. Yang, R.J. Gordon, Chem. Phys. Lett. 216 (1993) 544

[10] A.J. Yencha, T. Ridley, R. Maier, R.V. Flood, K.P. Lawley, R.J. Donovan, A. Hopkirk, J. Phys. Chem. 97 (1993) 4582.

[11] J. Long, H. Wang, Á. Kvaran, J. Mol. Spectrosc. 282 (2012) 20.

[12] Á. Kvaran, H. Wang, B.G. Waage, Can. J. Phys. 79 (2001) 197.

[13] A.E. Belikov, M.M. Ahern, M.A. Smith, Chem. Phys. 234 (1998) 195.

[14] D. Ascenzi, S.R. Langford, M.N.R. Ashfold, A.J. Orr-Ewing, Phys. Chem. Chem. Phys. 3 (2001) 29.

[15] A.J. Orr-Ewing, P.M. Regan, D. Ascenzi, C. Clementi, M.N.R. Ashfold, Chem. Phys. Lett. 315 (1999) 187.

[16] K. Matthíasson, H. Wang, Á. Kvaran, J. Mol. Spectrosc. 255 (2009) 1.

[17] K. Matthíasson, H. Wang, Á. Kvaran, Chem. Phys. Lett. 458 (2008) 58.

[18] Á. Kvaran, K. Sveinbjörnsson, J. Long, H. Wang, Chem. Phys. Lett. 516 (2011) 12.

[19] Á. Kvaran, B.G. Waage, H. Wang, J. Chem. Phys. 113 (2000) 1755.

[20] Á. Kvaran, H. Wang, K. Matthíasson, J. Phys. Chem. A 114 (2010) 9991.

[21] D.S. Green, S.C. Wallace, J. Chem. Phys. 96 (1992) 5857.

[22] D.S. Green, G.A. Bickel, S.C. Wallace, J. Mol. Spectrosc. 150 (1991) 354.

[23] D.S. Green, G.A. Bickel, S.C. Wallace, J. Mol. Spectrosc. 150 (1991) 388.

[24] R. Callaghan, R.J. Gordon, J. Chem. Phys. 93 (1990) 4624.

[25] S. Engin, N. Sisourat, S.p. Carniato, J. Chem. Phys. 137 (2012) 154304.

[26] Y. Li, O. Bludsky, G. Hirsch, R.J. Buenker, J Chem Phys 112 (2000) 260.

[27] M.P.J. van der Loo, G.C. Groenenboom, J. Chem. Phys. 123 (2005) 074310.

[28] C. Escure, T. Leininger, B. Lepetit, J. Chem. Phys. 130 (2009) 244305.

[29] Á. Kvaran, H. Wang, K. Matthiasson, A. Bodi, E. Jónsson, J. Chem. Phys. 129 (2008) 164313.

[30] C. Escure, T. Leininger, B. Lepetit, J. Chem. Phys. 130 (2009) 244306.

[31] E. Jónsson, Master thesis (2008).

[32] J. Pitarch-Ruiz, A.S.d. Merás, J. Sánchez-Maín, J. Phys. Chem. A 112 (2008) 3275.

[33] E.F. van Dishoeck, M.C. van Hemert, A. Dalgarno, J. Chem. Phys. 77 (1982) 3693.

[34] E.F. van Dishoeck, J. Chem. Phys. 86 (1987) 196.

[35] L. Singleton, P. Brint, J. Chem. Soc., Faraday Trans. 93 (1997) 21.

[36] Á. Kvaran, H. Wang, K. Matthiasson, A. Bodi, E. Jonsson, J. Chem. Phys. 129 (2008) 164313.

[37] K. Matthíasson, J. Long, H. Wang, Á. Kvaran, J. Chem. Phys. 134 (2011) 164302.

[38] Á. Kvaran, H. Wang, Á. Logadóttir, J. Chem. Phys. 112 (2000) 10811.

[39] Á. Kvaran, K. Matthiasson, H. Wang, J. Chem. Phys. 131 (2009) 044324.

[40] H. Wang, Á. Kvaran, Acta Phys. -Chim. Sin. 23 (2007) 1543.

[41] J. Long, H. Wang, A. Kvaran, J. Chem. Phys. 138 (2013) 044308.

[42] J. Long, H.R. Hróðmarsson, H. Wang, Á. Kvaran, J. Chem. Phys. 136 (2012) 214315.

[43] Á. Kvaran, H. Wang, J. Mol. Spectrosc. 228 (2004) 143.

[44] A. Kvaran, A. Logadottir, H. Wang, J. Chem. Phys. 109 (1998) 5856.

[45] H. Lefebvre-Brion, R.W. Field, The Spectra and Dynamics of Diatomic Molecules, Elsevier Academic Press, Amsterdam, 2004.

[46] R. Liyanage, R.J. Gordon, R.W. Field, J. Chem. Phys. 109 (1998) 8374.

[47] H. Lefebvre-Brion, R.W. Field, Perturbations in the Spectra of Diatomic Molecules, Academic Press, Inc., London, 1986.

[48] H. Lefebvre-Brion, P.M. Dehmer, W.A. Chupka, J. Chem. Phys. 85 (1986) 45.

[49] N. Bartels, T. Scha¨ fer, J. Hu¨ hnert, R.W. Field, A.M. Wodtke, J. Chem. Phys. 136 (2012) 214201.

[50] E.d. Beer, W.J. Buma, C.A.d. Lange, J.Chem.Phys. 99 (1993) 3252.

[51] N.P.L. Wales, W.J. Buma, C.A.d. Lange, H. Lefebvre-Brion, J. Chem. Phys. 105 (1996) 5702.

[52] C. Romanescu, S. Manzhos, D. Boldovsky, J. Clarke, H.-P. Loock, J. Chem. Phys. 120 (2004) 767.

[53] A.I. Chichinin, C. Maul, K.H. Gericke, J. Chem. Phys. 124 (2006) 224324.

[54] H. Lefebvre-Brion, H.P. Liebermann, G.J. Vázquez, J. Chem. Phys. 134 (2011) 204104.

[55] M. Bettendorff, S.D. Peyerimhoff, R.J. Buenker, Chem. Phys. 66 (1982) 261.

[56] J.J. O'Brien, S.A. Ryan, L.C. O'Brien, J. Mol. Spectrosc. 265 (2011) 110.

[57] A. Kvaran, K. Matthiasson, H.S. Wang, J. Mol. Spectrosc. 255 (2009) 1.

[58] A.I. Chichinin, P.S. Shternin, N. Gö decke, S. Kauczok, C. Maul, O.S. Vasyutinskii, K.H. Gericke, J. Chem. Phys. 125 (2006) 034310.

[59] Y.F. Zhu, E.R. Grant, H. Lefebvre-Brion, J. Chem. Phys. 99 (1993) 2287.

[60] Y. Xie, P.T.A. Reilly, S. Chilukuri, R.J. Gordon, J. Chem. Phys. 95 (1991) 854.

[61] H. Frohloch, P.M. Guyon, J. Chem. Phys. 94 (1991) 1102.

[62] H. Lefebvre-Brion, F. Keller, J. Chem. Phys. 90 (1989) 7176.

[63] T.P. Rakitzis, P.C. Samartzis, R.L. Toomes, L. Tsigaridas, M. Coriou, D. Chestakov, A.T.J.B. Eppink, D.H. Parker, T.N. Kitsopoulos, Chem. Phys. Lett. 364 (2002) 115.

[64] C. Romanescu, H.-P. Loock, J. Chem. Phys. 127 (2007) 124304.

[65] C. Romanescu, H.-P. Loock, Phys. Chem. Chem. Phys. 8 (2006) 2940.

[66] S. Manzhos, C. Romanescu, H.P. Loock, J.G. Underwood, J. Chem. Phys. 121 (2004) 11802.

[67] C. Maul, A.I. Chichinin, K.-H. Gericke, Journal of Atomic, Molecular, and Optical Physics 2011 (2011) 410108.

[68] A.I. Chichinin, K.H. Gericke, S. Kauczok, C. Maul, Int Rev Phys Chem 28 (2009) 607.

[69] S. Kauczok, N. Go¨ decke, A.I. Chichinin, M. Veckenstedt, C. Maul, K.H. Gericke, Rev Sci Instrum 80 (2009) 083301.

[70] C. Maul, S. Kauczok, V. Werwein, K.-H. Gericke, The unusual behaviour of the $F^1\Delta_2$ state of HCl: A 3 D Velocity Map Imaging Study, The 21st Colloquium on High resolution Molecular Spectroscopy International Conference, Castellammare di Stabia (Italy), 2009.

[71] G. Gademann, Y. Huismans, A. Gijsbertsen, J. Jungmann, J. Visschers, M.J.J. Vrakking, Rev Sci Instrum 80 (2009) 103105.

[72] J.H. Jungmann, A. Gijsbertsen, J. Visser, J. Visschers, R.M.A. Heeren, M.J.J. Vrakking, Rev Sci Instrum 81 (2010).

[73] S. Kauczok, C. Maul, A.I. Chichinin, K.H. Gericke, J. Chem. Phys. 132 (2010) 244308.

[74] A.I. Chichinin, T. Einfeld, C. Maul, K.H. Gericke, Rev Sci Instrum 73 (2002) 1856.

[75] A. Kvaran, G. Homar Johannesson, H. Wang, Chem. Phys. 204 (1996) 65.

[76] K. Matthíasson, PhD dissertation (2011).

[77] G.E. Tranter, J.L. Holmes, J.C. Lindon, ***Multiphoton Spectroscopy, Applications, Online Encyclopedia of Spectroscopy and Spectrometry, 2nd Edition. Academic Press, Elsevier Ltd. All rights reserved., 1999, p. 1424.

[78] M.H. Alexander, X. Li, R. Liyanage, R.J. Gordon, Chem. Phys. 231 (1998) 331.

[79] S.M. Hurley, Q. Zhong, J. A. W. Castleman, J. Chem. Phys. 112 (2000) 4644.

[80] K. Matthiasson, J. Long, H. Wang, A. Kvaran, Journal of Chemical Physics 134 (2011) 164302.

[81] Igor , http://www.wavemetrics.com/products/igorpro/igorpro.htm.

[82] P. J. Dagdigian, D.F. Varley, R. Liyanage, R. J.Gordon, R. W.Field, J. Chem. Phys. 105 (1996) 10251.

[83] K. Wang, V. McKay, J. Chem. Phys. 95 (1991) 8718.

[84] J. Long, Á. Kvaran, H. Wang, Acta Phys. Sin. 62 (2013) 163302.

[85] L.C. Lee, J.C. Han, C. Ye, M. Suto, J. Chem. Phys. 92 (1990) 133.

[86] M. Suto, L.C. Lee, J. Chem. Phys. 79 (1983) 1127.

[87] S. Eden, P. Limão-Vieira, S.V. Hoffmann, N.J. Mason, Chem. Phys. 323 (2006) 313.

[88] M. Suto, N. Washid, H. Akimoto, M. Nakamura, J. Chem. Phys. 78 (1983) 1019.

[89] P. Sharma, R.K. Vatsa, D.K. Maity, S.K. Kulshreshtha, Chem. Phys. Lett. 382 (2003) 637.

[90] L. Ji, Y. Tang, R. Zhu, Z. Wei, B. Zhang, Spectrochimica Acta Part A: Molecular and Biomolecular Spectroscopy 67 (2007) 273.

[91] P.-Y. Wei, Y.-P. Chang, W.-B. Lee, Z. Hu, H.-Y. Huang, K.-C. Lin, K.T. Chen, A.H.H. Chang, J. Chem. Phys. 125 (2006) 133319.

[92] J.C. Mössinger, D.E. Shallcross, R. Anthony Cox, Journal of the Chemical Society, Faraday Transactions 94 (1998) 1391.

[93] H.L. Fang, R.L. Swofford, J. Chem. Phys. 72 (1980) 6382.

[94] H.I. Ingvarsdóttir, BS Dissertation (2012).

[95] G.C. Causley, B.R. Russel, J. Chem. Phys. 62 (1975) 848.

[96] P. Chen, J.B. Pallix, W.A. Chupka, S.D. Colson, J. Chem. Phys. 86 (1987) 516.

[97] Y. Chen, J. Jin, L. Pei, X. Ma, C. Chen, Journal of Electron Spectroscopy and Related Phenomena 108 (2000) 221.

[98] Y. Wang, L. Li, W.A. Chupka, Chem. Physi. Lett. 192 (1992) 348.

Appendix

Program codes

2DREMPIV1.2.ipf

```
#pragma rtGlobals=1            // Use modern global access method.
menu "Macros"                  //user-defined macros menu in Igor pro
"Use_cursor"                   // display cursor in the graph, and initiate
variables.
"Add_reference"                //add the known reference masses
"Produce_masssaxis"            //produce a mass axis to assign unknown mass
peak
"REMPI_Integrate"    // integrate specific mass peak for each
wavenumber
end

macro REMPI_Integrate(wavestart,waveend,finallyname)
string wavestart
Prompt wavestart, "Beginning Wavename:", popup,WaveList("*",";","")
string waveend
Prompt waveend, "Ending Wavename:", popup,WaveList("*",";","")
string finallyname
Prompt finallyname, "Wavename:"
```

```
variable startpoint
variable endpoint
variable/G wavenum                //getthe number in  input  wavename  and
global
string wavenameconstant      //set "wave" as a string constant
wavenameconstant="wave"
variable startwave
variable endwave
variable wavedeta
variable eachwaveintegrate
string wavenam
variable x1
variable x2
variable detax
x1=pcsr(A)
x2=pcsr(B)
if (x1<x2)
startpoint=x1
endpoint=x2
else
startpoint=x2
endpoint=x1
endif
detax=endpoint-startpoint
getwavenum(wavestart)             //use "getwavenum" function to get the
number
startwave=wavenum
```

```
getwavenum(waveend)
endwave=wavenum
wavedeta=endwave-startwave+1   //obatin the delta between start wave
and end wave
make/O/N=(wavedeta) $finallyname    //make a new wave, and name as
user defined
variable i
i=0
variable yaveragevalue
do
wavenam=wavenameconstant+num2str(i+startwave)

if (mean($wavenam,startpoint-
2,startpoint+2)<mean($wavenam,endpoint-2,endpoint+2))
yaveragevalue=mean($wavenam,startpoint-2,startpoint+2)
else
yaveragevalue=mean($wavenam,endpoint-2,endpoint+2)
endif
$finallyname[i]=area($wavenam,startpoint,endpoint)-
detax*yaveragevalue
i+=1
while(i<wavedeta)
print " O k !   You get the wave name is: "+finallyname
display $finallyname
killvariables/A
endmacro
```

```
macro Use_cursor()
showinfo
make/n=0/O massreference
make/n=0/O masspoint
endmacro

function getwavenum(wavenam)       //this function is used to find the
number of wave
string wavenam
variable/G wavenum
sscanf wavenam,"wave%f", wavenum
end

macro Add_reference(mass)
variable mass
prompt mass,"Please input its mass:"
variable x1
x1=hcsr(A)
insertpoints 0,1,massreference
insertpoints 0,1,masspoint
massreference[0]=mass
masspoint[0]=x1
endmacro

macro Produce_masssaxis( )  //function to produce mass axis
variable masspoints
string wavenamefromcsr=csrwave(A)
```

```
masspoints=numpnts($wavenamefromcsr)
make/d/n=2/O constants
hideinfo
funcfit /h="00" massfit constants masspoint /x=massreference /d
display masspoint vs massreference
modifygraph mode(masspoint)=3, rgb=(0,0,0)
appendtograph fit_masspoint
make/n=(masspoints)/O massaxis
massaxis=((x-constants[1])/constants[0])^2
if(constants[1]>0)
massaxis[0,constants[1]]=-massaxis[p]
endif

doalert 0, "Ok! You get a mass axis. Its name is 'massaxis' ! Now you can
replace x with new axis :)"
killwaves constants
killwaves W_sigma
endmacro

function massfit(constants, m):FitFunc  // derive a, b constant by fitting
known mass.
wave constants
variable  m
return  constants[0]*m^0.5+constants[1]
end
```

```
ECalibrationV2.1.ipf
#pragma rtGlobals=1            // Use modern global access method.
#pragma rtGlobals=1            // Use modern global access method.
menu "Macros"
submenu "ECalibration"
 "ECalibration"                //To calibrate the spectrum according to power
changing during one scanning.
 "CancelECali"                 //To cancel the last Ecalibration.
 "ChangeScale"                 //Using one standard power to unify all spectra,
eg. power and photons.
end

submenu "Calibrate"
"Calibrate"                    //To connect the ending of the spectrum to the
beginning of next spectrum for two different scannings.
"Back"                         //To cancel the last calibration.
end
end
//you need to use cursor A to get the wave name which you want to
calibrate!!
 macro ECalibration(power_start, power_end,nn)
Variable power_start
Prompt power_start, "Power in the beginning :"
Variable power_end
Prompt power_end, "Power in the end :"
variable nn
prompt nn, "Number of photons :"
```

```
string wavey
string wavex
wavey=CsrWave(A)
wavex=CsrXWave(A)
variable lengthofwave
lengthofwave=numpnts($wavex)
variable kslope
variable valueb
kslope=(power_end-power_start)/($wavex[lengthofwave]-$wavex[0])
valueb=power_start-kslope*$wavex[0]
make/O/N=(lengthofwave) powerline
powerline=valueb+kslope*$wavex
powerline=(1/(powerline^nn))*(power_start^nn)
$wavey=$wavey*powerline
print"-----------------------------------------------------------------"
print "Power at start :",power_start,"mW"
print  "Power at end :",power_end,"mW"
print "Numbers of photons:", nn
print  "Calibrated wave name is :", wavey
print "-----------------------------------------------------------------"
end

macro CancelECali()
doalert 1,"Are you sure you cancel last calibration?"
if (V_flag==1)
string wavey
wavey=CsrWave(A)
```

```
$wavey=$wavey/powerline
killwaves powerline
print "You cancel the last energy calibration"
endif
end

macro ChangeScale(power0)
variable power0
string wavechange
variable apositionvalue
variable bpositionvalue
apositionvalue=vcsr(A)                    // use  cursor A to get the wave
name and determinate Ie value!!
bpositionvalue=vcsr(B)                    // use cursor B to determinate
the value of Io.
wavechange=CsrWave(A)
$wavechange=((2.7/power0)^2)*$wavechange          // Here you can
set the value of the standard power and the number of photons.
print wavechange, "*=(2.7/", power0, ")^2"
end

macro Calibrate()
string wavechange
string wavechangex
variable Io
variable Ie
Ie=vcsr(A)
```

```
Io=vcsr(B)
wavechange=CsrWave(A)
wavechangex=CsrXWave(A)

variable lengthofwave
lengthofwave=numpnts($wavechangex)
make/O/N=(lengthofwave) backupwave
backupwave=$wavechange
variable aa
variable bb
variable nn
variable cc
nn=2  //set the number of photons
cc=($wavechangex[0])^nn
aa=((Ie/Io-1)/(abs((hcsr(A))^nn-cc)))
bb=1-aa*cc
make/O/N=(lengthofwave) tempwave
tempwave=($wavechangex)^nn
$wavechange=$wavechange/(aa*tempwave+bb)
killwaves tempwave
Print "Delta I :", Io-Ie, "    Number of photons :", nn
print "a: ", aa, "      b: ", bb
end

macro Back()
string wavechange
wavechange=CsrWave(A)
```

```
$wavechange=backupwave
killwaves backupwave
print "You cancel the last calibration"
end
```

Deperturbation function

Before a deperturbation calculation, make three waves named “result”, “line” and “*J”* respectively, and input fitting functions provided as below:

Deperturbed0

```
f(JJ,line) = (v1+(B1-B0)*JJ*(JJ+1)-(D1-D0)*(JJ*(JJ+1))^2-line)
```

Deperturbed1:

```
f(JJ,line) = (v1+(B1-B0)*JJ*(JJ+1)-(D1-D0)*(JJ*(JJ+1))^2-line)*(v2+(B2-B0)*JJ*(JJ+1)-(D2-D0)*(JJ*(JJ+1))^2-line)-W^2
```

Deperturbed2:

```
f(JJ,line) = (v1+(B1-B0)*JJ*(JJ+1)-(D1-D0)*(JJ*(JJ+1))^2-line)*(v2+(B2-B0)*JJ*(JJ+1)-(D2-D0)*(JJ*(JJ+1))^2-line)*(v3+(B3-B0)*JJ*(JJ+1)-(D3-D0)*(JJ*(JJ+1))^2-line)-(W^2)*((v2+(B2-B0)*JJ*(JJ+1)-(D2-D0)*(JJ*(JJ+1))^2-line)+(v3+(B3-B0)*JJ*(JJ+1)-(D3-D0)*(JJ*(JJ+1))^2-line))
```

Deperturbed2W

```
f(JJ,line) = (v1+(B1-B0)*JJ*(JJ+1)-(D1-D0)*(JJ*(JJ+1))^2-line)*(v2+(B2-B0)*JJ*(JJ+1)-(D2-D0)*(JJ*(JJ+1))^2-line)*(v3+(B3-
```

B0)*JJ*(JJ+1)-(D3-D0)*(JJ*(JJ+1))^2-line)-(W3^2)*(v2+(B2-B0)*JJ*(JJ+1)-(D2-D0)*(JJ*(JJ+1))^2-line)-(W2^2)*(v3+(B3-B0)*JJ*(JJ+1)-(D3-D0)*(JJ*(JJ+1))^2-line)

Deperturbed1Wheter

f(JJ,line) = (v1+(B1-B0)*JJ*(JJ+1)-(D1-D0)*(JJ*(JJ+1))^2-line)*(v2+(B2-B0)*JJ*(JJ+1)-(D2-D0)*(JJ*(JJ+1))^2-line)*(v3+(B3-B0)*JJ*(JJ+1)-(D3-D0)*(JJ*(JJ+1))^2-line)-(JJ*(JJ+1)*W2^2)*(v2+(B2-B0)*JJ*(JJ+1)-(D2-D0)*(JJ*(JJ+1))^2-line)-(JJ*(JJ+1)*W2^2)*(v3+(B3-B0)*JJ*(JJ+1)-(D3-D0)*(JJ*(JJ+1))^2-line)

Deperturbed2Wheter

f(JJ,line) = (v1+(B1-B0)*JJ*(JJ+1)-(D1-D0)*(JJ*(JJ+1))^2-line)*(v2+(B2-B0)*JJ*(JJ+1)-(D2-D0)*(JJ*(JJ+1))^2-line)*(v3+(B3-B0)*JJ*(JJ+1)-(D3-D0)*(JJ*(JJ+1))^2-line)-(JJ*(JJ+1)*W3^2)*(v2+(B2-B0)*JJ*(JJ+1)-(D2-D0)*(JJ*(JJ+1))^2-line)-(JJ*(JJ+1)*W2^2)*(v3+(B3-B0)*JJ*(JJ+1)-(D3-D0)*(JJ*(JJ+1))^2-line)